2018

An Anisotropic Constitutive Model for Nuclear Grade Graphite

James Christopher
Cleveland State University

AN ANISOTROPIC CONSTITUTIVE MODEL FOR NUCLEAR GRADE GRAPHITE

CHRISTOPHER JAMES

Bachelor of Mechanical Engineering

Cleveland State University

June 1995

submitted in partial fulfillment of requirements for the degree

DOCTOR OF ENGINEERING IN MECHANICAL ENGINEERING

at

CLEVELAND STATE UNIVERSITY

DECEMBER 2018

ACKNOWLEDGMENTS

I would like to thank Dr. Duffy for his guidance and patience in this work. I would like to thank Cleveland State University and the Department of Civil Engineering who made this work possible. Finally I would like to thank the Department of Energy who initially funded this project.

AN ANISOTROPIC CONSTITUTIVE MODEL FOR NUCLEAR GRADE GRAPHITE

CHRISTOPHER JAMES

ABSTRACT

Graphite material is used extensively in nuclear reactors however the material has a limited strain range for elastic behavior. This provides the motivation to derive a constitutive model that captures the inelastic deformations exhibited by this material. This dissertation first presents details of an isotropic constitutive model derived using continuum principles of engineering mechanics that accounts for different inelastic behavior in tension and compression. An inelastic dissipation function was developed using an integrity basis proposed by Green and Mkrtichian (1977) for the isotropic version of the model. This isotropic model was then extended to capture anisotropic stress-strain behavior using directional tensors associated with the material symmetry. In the case of anisotropic graphite the material typically exhibits transversely isotropic behavior. The model parameters were characterized using stress-strain data from several grades of nuclear graphite. Once the model parameter were characterized several benchmark structural components were analyzed with the intent of showing that the model's predictive capability relative to simple component level behavior.

TABLE OF CONTENTS

LIST OF TABLES

LIST OF FIGURES

CHAPTER I

INTRODUCTION

Despite current events associated with the light water reactors in Fukishima, Japan, energy producers continue to look at nuclear power as a viable alternative for power generation. There are several new designs that transcend the older light water reactors that failed to perform safely in Japan. Among the designs for the next generation power plant is the very high temperature reactors (VHTR), molten salt reactors, and super critical water cooled reactors. In addition to generating electricity the VHTR will be able to produce hydrogen without consuming fossil fuels or emitting green house gasses which is a distinct benefit. Emerging technologies often depend on new materials or the innovative use of existing material, and graphite is a key material in the design of several of the next generation nuclear power plants.

Southward et al. (2004) indicates there are two designs for the VHTR. The first design utilizes a prismatic core reactor. The second design is known as a pebble bed reactor. In the prismatic core reactor the nuclear fuel is contained in fuel rods. Hexagonal graphite blocks that hold the fuel rods are used to moderate the nuclear reaction. The cooling gas runs in channels inside the hexagonal prismatic blocks as diagrammed in Figure 1. A prismatic block from the reactor core depicted in Figure 1 is shown in Figure 2. In Figure 2 three rods are shown partially withdrawn from this single hexagonal block. The reactor is comprised of an array of these blocks that accommodate fuel rods, control rods, and cooling channels.

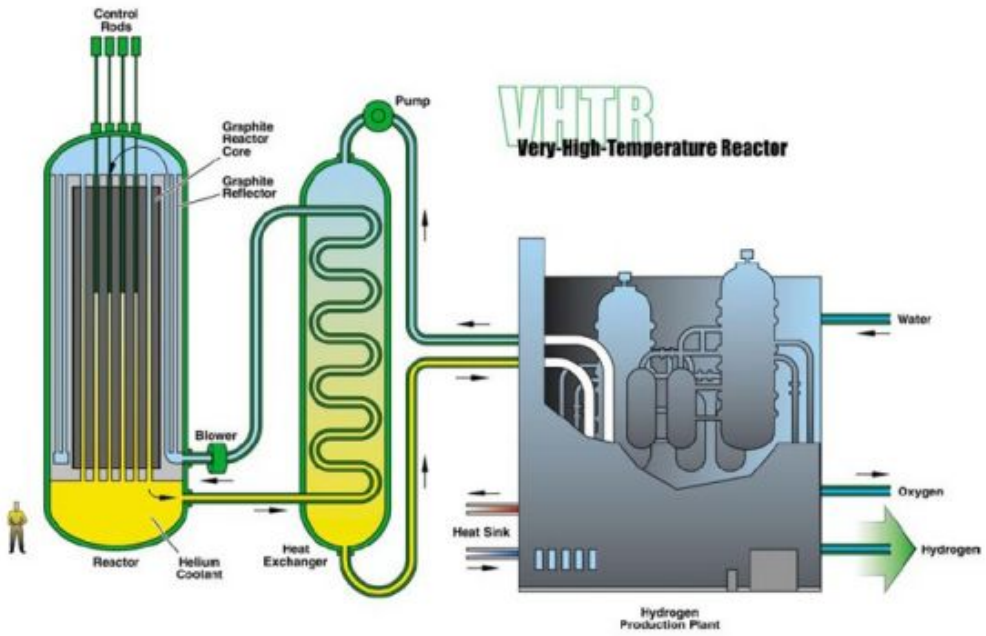

Figure 1: VHTR Schematic – DOE Road map (2002)

Figure 2: VHTR Core Block [1]

Alternatively, in pebble bed reactors the fissile material, the moderator, and a fission product barrier are contained in softball sized pebbles shown in Figure 3. The pebbles are continuously cycled through reactor channels and are removed from the bottom of the reactor. The pebbles are then tested to determine how much nuclear fuel remains. If sufficient fuel remains the pebble is returned to the reactor. Process cooling gas flows around the pebbles as they are cycled through the reactor as shown in Figure 4.

[1] http://www.toyotanso.co.jp/Products/Special_graphite_etc_en.html#01

[2] Image from http://www.euronuclear.org/info/encyclopedia/p/pebble.htm

[3] http://travkin-hspt.com/nuclearen/right.htm

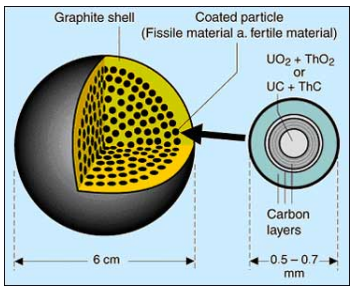

Figure 3: Pebble Schematic [2]

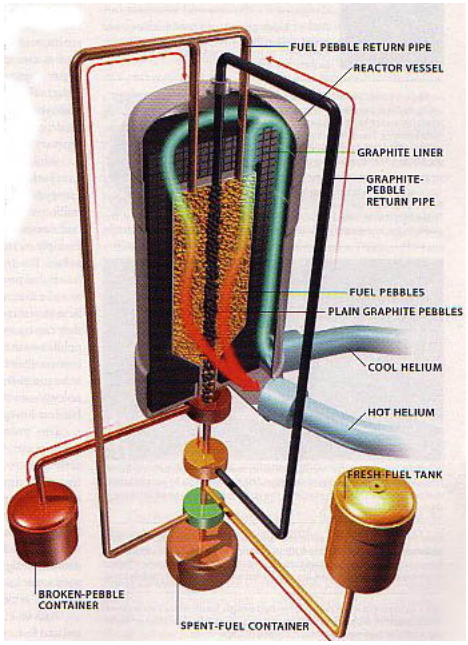

Figure 4: Pebble Bed Reactor Schematic [3]

Prismatic core reactors are designed to reach higher service temperatures than the pebble bed reactor. The initial designs for the prismatic core reactors call for an outlet temperature ranging from $850\ ^{\circ}\mathrm{C}$ to $1000\ ^{\circ}\mathrm{C}$. At these temperature, water can be "cracked" into hydrogen and oxygen in the presence of a catalysis. Thus a virtuous (i.e., clean) process is established that produces electricity, hydrogen feed stocks for the chemical industry, and pure oxygen.

The core components of the VHTR cannot be fabricated from of metals due to radiation levels and operating temperatures. Graphite has long been utilized as a neutron moderator. Several countries including the United States, France, the United Kingdom, Germany,

South Africa, Japan, and China support evolving technologies for nuclear graphite material systems that focus on several aspects of the behavior of graphite in reactor cores. These technologies are key to the VHTR program.

Accurate stress states are a necessity in designing reactor components. The effort here assumes the stress–strain response for nuclear grade graphite can be characterized using an inelastic constitutive model that accounts for different behavior in tension and compression, as well as accounts for material anisotropy. As originally discussed by Seldin (1966) and later by Greenstreet (1970), graphite has a relatively small elastic range. Moreover, Weng (1969) points out that the stress-strain relationship for graphite is for the most part nonlinear. An objective of this thesis is the development of a comprehensive constitutive model that will predict both elastic and inelastic cyclic phenomenological behavior. An appropriate elasticity model is integrated with the proposed inelastic constitutive model when cyclic loading is discussed. In the presence of time dependent phenomenon such as creep, one needs a viscoplastic constitutive model. The time independent inelastic model presented here can be extended to include rate dependent effects in a manner similar to Duffy (1987) and Janosik (1990). This is left for future work.

As was just mentioned one of the fundamental behaviors that must be accounted for in graphite materials is the different behaviors in tension and compression. Graphite is not the only material that behaves differently in tension and compression under mechanical loads. Concrete also exhibits different properties in tension and compression. Inelastic constitutive models exists for concrete, e.g., the phenomenological model developed by William and Warnke (1975), Ottosen (1977), and Hsieh et al. (1952). An effort was made to extend the William and Warnke (1975) model for graphite to include material anisotropy. That effort was unsuccessful. An alternative constitutive model proposed by Green and Mkrtichian (1977) was adopted in this effort. Aspects of this model are thoroughly presented then the model proposed by Green and Mkrtichian (1977) is extended to include anisotropy.

Issues such as neutron radiation damage in graphite, which initially causes an increase

in the modulus of elasticity, and then deteriorates with time, are one of the many topics under current study that will not be addressed in this thesis. Future plans call for modeling this phenomenon by incorporating damage state variables similar to methods proposed by Chow and Yang (1991). Current constitutive models, such as Eason (2008), for graphite that predicts radiation damage are empirically based.

Currently, a fully multi-axial constitutive model does not exist that takes the specific behavior of graphite into account. The model here will take into account that graphite is transversely isotropic and graphite also has different properties in tension and compression. This work begins by assuming the existence of a threshold function, which will also serve as a inelastic potential function. Since the inelastic potential function is scalar valued, tensorial invariant theory is used to construct the function. We include Green and Mkrtichian's (1977) theory that different properties in tension and compression can be modeled by using a piece wise continuous function where the properties are captured through an eigenvector of a principle stress. This threshold function is extended to account for transversely isotropic behavior. Both the isotropic and anisotropic inelastic models are derived based on an associated flow rule and isotropic hardening of the threshold functions. The anisotropic inelastic constitutive model is then exercised with a simple analysis of a structural component later in this thesis. Finally, the thesis concludes by outlining future research avenues to build on this work.

CHAPTER II

ISOTROPIC INELASTIC THRESHOLD FUNCTIONS

It should be pointed out at the beginning of this discussion that the development here of an inelastic stress–strain relationship for graphite is predicated on a phenomenological approach that utilizes the modeling framework of classic metal plasticity. However, the energy dissipation process taking place within the microstructure of graphite is radically different in comparison to the energy dissipation mechanisms that underpin the phenomenological behavior of metal plasticity. Having said that, the phenomenological behavior is mathematically similar between the two, so concepts familiar to metal plasticity are adopted here even though the energy dissipation mechanisms are quite different. The reader is encouraged to keep this in mind throughout this chapter and what follows.

A presumption is made as to the existence of a surface in stress space that encloses a region where the corresponding states of strain are elastic. The region is described by a mathematical function referred to here as a threshold function. This threshold function serves as an inelastic potential function from which an incremental flow law can be derived given certain assumptions as to how graphite "hardens" under thermo-mechanical loads.

Tabeddor (1979) and Vijayakumar, et al.(1987; 1990) emphasize the anisotropic effect that the elongated grain structure of graphite has on the stress-strain relationship for graphite. These authors also discuss how the material behaves differently in tension and in compression. These two properties, i.e., material anisotropy and different behavior in

tension and compression, make formulating a threshold function for graphite challenging.

From a simple mechanical perspective there are two characterizations of differing behavior in tension and compression. The first characterization is referred to as bi-modulus behavior. A bi-modulus material has different elastic stiffness constants in tension and compression. The other characterization captures different elastic behaviors through tensile and compressive threshold stresses that are distinctly different in magnitude. The works of Seldin (1966) and Greenstreet, et al. (1970) show that elastic stiffness properties in tension and compression for virgin graphite do not change. Therefore Young's modulus for graphite is the same for tension and compression. Thus graphite is not a bimodulus material. This thesis defines different properties in tension and compression as a material having different elastic ranges in tension and compression.

Later in this thesis applications of the anisotropic inelasticity model will be discussed and an anisotropic elasticity model is needed. Lekhnitski's (1963) elasticity model is adopted. Lekhnitski's (1963) work can be derived from an elastic potential function, but those details do not add to the discussion here. The rest of this chapter focuses on the threshold function of Green and Mkrtichian (1977). Chapter 3 extends the threshold function developed in this chapter to include transverse isotropy.

2.1 Invariance of the Threshold Function

A phenomenological perspective is adopted to determine the inelastic constitutive model for graphite. The model is based on continuum principles where stress, strain and other engineering properties are defined at a mathematical point. This continuum point needs to be large enough so that the microstructure of the material is homogenous, but small enough to treat stress and strain as a function of position, position being defined as "the point. The assumption is made that a threshold function exists and that the function depends on stress. Since graphite has different properties in tension and compression, the function constructed is dependent on the principle stresses and their eigenvectors. The Cauchy stress tensor, σ_{ij},

is used and a unit direction vector, a_i, is introduced that is associated with a principle stress direction. This gives the following dependence for the threshold function

$$f = f(\sigma_{ij}, a_i a_j) \tag{2.1}$$

The dependence on the direction vector is taken through the direction tensor $a_i a_j$. The sense, i.e. the actual direction, of the principle stress along this line of action is important, but whether a principle stress is tensile or compressive is not accounted for with the direction vector a_i.

The threshold function must be invariant with respect to the coordinate axes. Elements of the stress tensor and elements of the direction vector change with a change of coordinate system. Changes in a coordinate observer, i.e., proper orthogonal transformations in the coordinate axes should leave the scalar value of $f(\sigma_{ij}, a_i a_j)$ unaffected. The issue of form invariance is addressed by using the invariants of the stress tensor, σ_{ij}, and invariants of the direction tensor $a_i a_j$. The invariants are defined through the traces of the stress matrix, the direction matrix and combinations of both. The method of utilizing invariants to construct form invariant scalar functions is described by Rivlin (1969) and Spencer (1971).

A threshold function dependant on stress can be defined in many ways, but it is convenient to construct it as a polynomial of the unique traces of the stress tensors that are quadratic in stress. There are an infinite number of traces of the stress tensor. For an isotropic material that is not dependant on a direction vector, it can be shown that the number of unique traces (the invariants) of the stress tensor reduces to three. The reader is directed to Rivlin (1969) and Spencer (1971) for the rational. All other traces can be written in terms of the first three traces. That means these three traces span the entire stress space in which a threshold function can be constructed. The minimum set of invariants that span the space is called an integrity basis. It is similar in concept with the unit vectors that span Cartesian three space. If one or more of the invariants of the integrity basis is

omitted Tsai and Wu (1971) called this a functional basis. In the next section we will use the functional basis proposed by Green and Mkrtichian (1977) for isotropic materials that behave differently in tension and compression.

2.2 Isotropic Behavior - Functional Dependence

For a scalar valued function with a dependence stipulated by Equation (2.1), Spencer (1971) and Rivlin (1969) show that the integrity basis for that function is

$$I_1 = \sigma_{kk} \tag{2.2}$$

$$I_2 = \sigma_{ij}\sigma_{ji} \tag{2.3}$$

$$I_3 = \sigma_{ij}\sigma_{jk}\sigma_{ki} \tag{2.4}$$

$$I_4 = a_i a_j \sigma_{ji} \tag{2.5}$$

and

$$I_5 = a_i a_j \sigma_{jk}\sigma_{ki} \tag{2.6}$$

Index notation is utilized here and the repeated subscripts indicates summation over the range of one to three. Green and Mkrtichian (1977) omitted invariant I_3 from their threshold function since this invariant is cubic in stress. From a historical perspective ignoring invariants cubic in stress has had precedence in the derivation of constitutive models. In addition, those invariants linear in stress enter the functional dependence as squared terms or as products with another invariant linear in stress. The Green and Mkrtichian (1977)

threshold function has the dependence

$$f(\sigma_{ij}, a_i a_j) = f(I_1, I_2, I_4, I_5) \tag{2.7}$$

Again, the direction of the eigenvector a_i appears through the second order tensor, $a_i a_j$.

The underlying concept is that the response of the material depends on the stress state and whether the principal stresses are tensile or compressive. Principal stresses identified here as σ_1, σ_2, and σ_3 follow the standard convention that they are ordered numerically based on their algebraic value, i.e.,

$$\sigma_1 \geq \sigma_2 \geq \sigma_3 \tag{2.8}$$

The principle stress space is divided into four regions. Following Green and Mkrtichian (1977) the regions and associated threshold functions are listed below. In the first region where all of the principle stresses are tensile, i.e.,

$$\texttt{Region \#1} \quad \sigma_1 \geq \sigma_2 \geq \sigma_3 \geq 0 \qquad f = f_1(\sigma_{ij}) \tag{2.9}$$

a direction vector is unnecessary. A second region is identified where

$$\texttt{Region \#2} \quad \sigma_1 \geq \sigma_2 \geq 0 \geq \sigma_3 \qquad f = f_2(\sigma_{ij}, a_i a_j) \tag{2.10}$$

In region #2 Green and Mkrtichian (1977) associated the direction vector a_i with the compressive principle stress σ_3. Thus for this region

$$a_i = (0, 0, 1) \tag{2.11}$$

This assumes that the principle stress orientations align with the current cartesian coordinate system, i.e., σ_1 is in the direction of x_1, σ_2 is in the direction of x_2, and σ_3 is in the

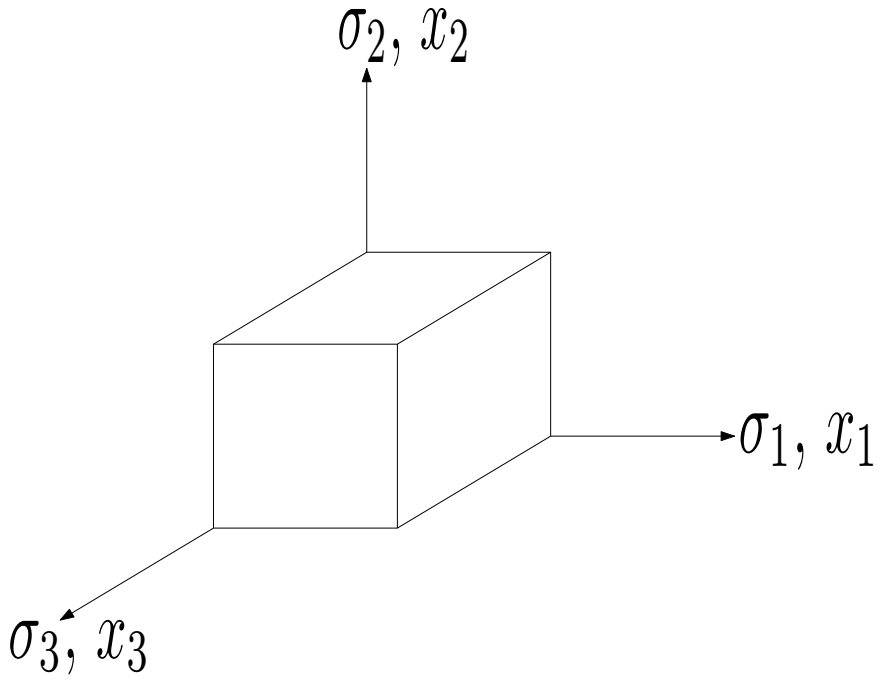

Figure 5: Orientation direction vectors and for the principle stresses

direction of x_3 as shown in Figure 5. A third region is identified where

$$\texttt{Region \#3} \quad \sigma_1 \geq 0 \geq \sigma_2 \geq \sigma_3 \qquad f = f_3(\sigma_{ij}, a_i a_j) \tag{2.12}$$

In region #3 Green and Mkrtichian (1977) associated the direction vector a_i with the tensile principle stress σ_1. Thus

$$a_i = (1, 0, 0) \tag{2.13}$$

Finally, in the fourth region all principle stresses are compressive, i.e.,

$$\texttt{Region \#4} \quad 0 \geq \sigma_1 \geq \sigma_2 \geq \sigma_3 \qquad f = f_4(\sigma_{ij}) \tag{2.14}$$

and a direction vector is once again unnecessary. Moreover, Green and Mkrtichian (1977) define the threshold function for region #1 as

$$f_1 = \frac{1}{2} A_1 I_1^2 + B_1 I_2 - K^2 \tag{2.15}$$

The threshold function for region #2 is defined as

$$f_2 = \frac{1}{2}A_2 I_1^2 + B_2 I_2 + C_2 I_1 I_4 + D_2 I_5 - K^2 \tag{2.16}$$

The threshold function for region #3 is defined as

$$f_3 = \frac{1}{2}A_3 I_1^2 + B_3 I_2 + C_3 I_1 I_4 + D_3 I_5 - K^2 \tag{2.17}$$

and the threshold function for region #4 is defined as

$$f_4 = \frac{1}{2}A_4 I_1^2 + B_4 I_2 - K^2 \tag{2.18}$$

Note that all terms in the last four expressions are quadratic in stress even though I_1 and I_4 are linear in stress. The material constants A_1, A_2, A_3, A_4, B_1, B_2, B_3, B_4, C_2, C_3, D_2, and D_3 are characterized with simple mechanical tests. The parameter K is an inelastic state variable. For a virgin material, the value of this state variable is equal to one. The constants just mentioned will be characterized by initial threshold stresses obtained from the mechanical tests on virgin materials. In the section discussing the inelastic constitutive model the value of K will change according to a specified evolutionary law (see Chapter 4) based on the accumulation of inelastic work under load.

This set of piecewise continuous threshold functions must satisfy two conditions along the boundaries where they meet. The first condition is that the threshold functions must be equal along mutual boundaries. The second condition is that the tangents, the directional derivatives of the threshold functions, must be single valued along a mutual boundary. The second condition dominates the development of the relationships between the twelve constants. In Chapter 4 where an associated flow rule is presented the conditions on the tangents will guarantee that increments in the inelastic strain will be equal at mutual boundaries of the piecewise threshold function. It is noted at this point that region #1 and region

#4 do not share a boundary except at the origin of principle stress space where all regions meet.

The tangents for these functions are calculated by taking the derivative with respect to the Cauchy stress, σ_{ij}. For all four threshold functions the partial derivatives are calculated as follows using the chain rule

$$\frac{\partial f}{\partial \sigma_{ij}}=\frac{\partial f}{\partial I_1}\frac{\partial I_1}{\partial \sigma_{ij}}+\frac{\partial f}{\partial I_2}\frac{\partial I_2}{\partial \sigma_{ij}}+\frac{\partial f}{\partial I_4}\frac{\partial I_4}{\partial \sigma_{ij}}+\frac{\partial f}{\partial I_5}\frac{\partial I_5}{\partial \sigma_{ij}} \tag{2.19}$$

For Equation (2.15)

$$\frac{\partial f_1}{\partial I_1}=A_1 I_1 \tag{2.20}$$

$$\frac{\partial f_1}{\partial I_2}=B_1 \tag{2.21}$$

$$\frac{\partial I_1}{\partial \sigma_{ij}}=\delta_{ij} \tag{2.22}$$

and

$$\frac{\partial I_2}{\partial \sigma_{ij}}=2\sigma_{ij} \tag{2.23}$$

Here δ_{ij} is the Kronecker delta tensor. Thus Equation (2.19) takes the form

$$\frac{\partial f_1}{\partial \sigma_{ij}}=A_1 I_1 \delta_{ij}+2B_1\sigma_{ij} \tag{2.24}$$

in region #1. In a similar fashion for the threshold function f_2

$$\frac{\partial f_2}{\partial I_1}=A_2 I_1+C_2 I_4 \tag{2.25}$$

$$\frac{\partial f_2}{\partial I_2}=B_2 \tag{2.26}$$

$$\frac{\partial f_2}{\partial I_4} = C_2 I_2 \tag{2.27}$$

$$\frac{\partial f_2}{\partial I_5} = D_2 \tag{2.28}$$

$$\frac{\partial I_4}{\partial \sigma_{ij}} = a_i a_j \tag{2.29}$$

and

$$\frac{\partial I_5}{\partial \sigma_{ij}} = a_k a_i \sigma_{jk} + a_j a_m \sigma_{mi} \tag{2.30}$$

Thus in region #2 Equation (2.19) takes the form

$$\frac{\partial f_2}{\partial \sigma_{ij}} = (A_2 I_1 + C_2 I_4)\delta_{ij} + 2B_2 \sigma_{ij} + C_2 I_1 a_i a_j + D_2(a_k a_i \sigma_{jk} + a_j a_m \sigma_{mi}) \tag{2.31}$$

For the threshold function f_3

$$\frac{\partial f_3}{\partial I_1} = A_3 I_1 + C_3 I_4 \tag{2.32}$$

$$\frac{\partial f_3}{\partial I_2} = B_3 \tag{2.33}$$

$$\frac{\partial f_3}{\partial I_4} = C_3 I_2 \tag{2.34}$$

and

$$\frac{\partial f_3}{\partial I_5} = D_3 \tag{2.35}$$

Thus in region #3 Equation (2.19) takes the form

$$\frac{\partial f_3}{\partial \sigma_{ij}} = (A_3 I_1 + C_3 I_4)\delta_{ij} + 2B_3 \sigma_{ij} + C_3 I_1 a_i a_j + D_3(a_k a_i \sigma_{jk} + a_j a_m \sigma_{mi}) \tag{2.36}$$

For the threshold function f_4

$$\frac{\partial f_4}{\partial I_1} = A_4 I_1 \tag{2.37}$$

and

$$\frac{\partial f_4}{\partial I_4} = B_1 \tag{2.38}$$

Thus Equation (2.19) takes the form

$$\frac{\partial f_4}{\partial \sigma_{ij}} = A_4 I_1 \delta_{ij} + 2B_4 \sigma_{ij} \tag{2.39}$$

in region #4

Summarizing

$$\frac{\partial f_1}{\partial \sigma_{ij}} = A_1 I_1 \delta_{ij} + 2B_1 \sigma_{ij} \tag{2.40}$$

$$\frac{\partial f_2}{\partial \sigma_{ij}} = (A_2 I_1 + C_2 I_4)\delta_{ij} + 2B_2 \sigma_{ij} + C_2 I_1 a_i a_j + D_2(a_k a_i \sigma_{jk} + a_j a_m \sigma_{mi}) \tag{2.41}$$

$$\frac{\partial f_3}{\partial \sigma_{ij}} = (A_3 I_1 + C_3 I_4)\delta_{ij} + 2B_3 \sigma_{ij} + C_3 I_1 a_i a_j + D_3(a_k a_i \sigma_{jk} + a_j a_m \sigma_{mi}) \tag{2.42}$$

and

$$\frac{\partial f_4}{\partial \sigma_{ij}} = A_4 I_1 \delta_{ij} + 2B_4 \sigma_{ij} \tag{2.43}$$

Equations (2.40) through (2.43) represent four second order tensor equations in terms of twelve unknowns. In what follows, a sufficient number of scalar expressions embedded in these tensor equations will be extracted in order to define the twelve scalar unknowns. The four second order tensor equations potentially represents thirty-six scalar expressions. Due to the symmetry of the stress tensor the number of scalar equations is reduced to

twenty-four. The pool of available equations is further reduced as directional derivatives are equated along common boundaries. It is noted prior to the development that several constants are not independent.

2.2.1 Relationships Between Coefficients – Uniaxial Tension

In this chapter and in the next chapter threshold stresses are used to define the composite threshold function. These stresses represent the limits of elastic behavior. The elastic range is defined as the point on the stress–strain curve where the curve stops being linear. The tests will be uniaxial tension, uniaxial compression, torsion, and biaxial compression.

- σ_t – uniaxial tensile threshold stress
- σ_c – uniaxial compressive threshold stress
- τ_i – torsional threshold stress
- σ_{bc} – equal biaxial compressive threshold stress

These stress values are obtained from a virgin material. For a virgin material the state variable K is equal to one. For a uniaxial tensile test where the stress applied is equal to the tensile threshold stress, i.e.,

$$\sigma_{ij} = \begin{bmatrix} \sigma_t & 0 & 0 \\ 0 & 0 & 0 \\ 0 & 0 & 0 \end{bmatrix} \tag{2.44}$$

This stress state satisfies the inequalities associated with region #1, region #2, and region #3 since

$$\sigma_1 = \sigma_t \geq \sigma_2 = 0 \geq \sigma_3 = 0 \tag{2.45}$$

The threshold functions along the boundaries of region #1, region #2, and region #3 must satisfy the relationships

$$f_1 = f_2 = f_3 \tag{2.46}$$

for this uniaxial tension test. In addition, the derivatives of the functions along the boundaries of region #1, region #2, and region #3 must satisfy

$$\frac{\partial f_1}{\partial \sigma_{ij}} = \frac{\partial f_2}{\partial \sigma_{ij}} = \frac{\partial f_3}{\partial \sigma_{ij}} \tag{2.47}$$

for the uniaxial tensile test.

Focusing on the derivatives along the boundary between region #1 and region #2 then

$$\frac{\partial f_1}{\partial \sigma_{ij}} = \frac{\partial f_2}{\partial \sigma_{ij}} \tag{2.48}$$

This relationship yields the following tensor expression

$$\begin{aligned} A_1 I_1 \delta_{ij} + 2B_1 \sigma_{ij} = (A_2 I_1 + C_2 I_4)\delta_{ij} + 2B_2 \sigma_{ij} \\ + C_2 I_1 a_i a_j + D_2 (a_k a_i \sigma_{jk} + a_j a_m \sigma_{mi}) \end{aligned} \tag{2.49}$$

For region #1 the function f_1 is not dependent on a principle direction. For region #2 the function f_2 is dependent on the direction vector, a_i, which for this region is defined as

$$a_i = (0, 0, 1) \tag{2.50}$$

The two invariants in Equation (2.49) are

$$I_1 = \sigma_t \tag{2.51}$$

and

$$I_4 = 0 \tag{2.52}$$

Equation (2.49) represents nine scalar equations. Using the symmetry of the Cauchy stress tensor, $\sigma_{ij} = \sigma_{ji}$, the nine scalar equations are reduced to six. The equations where $i \neq j$ yield the scalar identity $0=0$ and no information is gained. For $i = j$ we obtain three scalar relationships.

For Equation (2.49) with $i = j = 2$ yields

$$A_1 = A_2 \tag{2.53}$$

With $i = j = 1$ results in

$$A_1 + 2B_1 = A_2 + 2B_2 \tag{2.54}$$

Substituting (2.53) into Equation (2.54) yields

$$B_1 = B_2 \tag{2.55}$$

With $i = j = 3$ Equation (2.49) yields the following

$$A_1 = A_2 + C_2 \tag{2.56}$$

Substituting Equation (2.53) into Equation (2.56) results in

$$C_2 = 0 \tag{2.57}$$

Next, the argument above is repeated for the derivatives along the shared boundary of region #1 and region #3 where

$$\frac{\partial f_1}{\partial \sigma_{ij}} = \frac{\partial f_3}{\partial \sigma_{ij}} \tag{2.58}$$

for the same uniaxial tension test. This yields the following tensor expression in terms of index notation

$$\begin{aligned} A_1 I_1 \delta_{ij} + 2B_1 \sigma_{ij} = (A_3 I_1 + C_3 I_4)\delta_{ij} + 2B_3 \sigma_{ij} \\ + C_3 I_1 a_i a_j + D_3 (a_k a_i \sigma_{jk} + a_j a_m \sigma_{mi}) \end{aligned} \tag{2.59}$$

In region #3 it was noted earlier that Green and Mkrtichian (1977) took

$$a_i = (1, 0, 0) \tag{2.60}$$

Based on this direction vector and the state of stress the invariants in Equation (2.59) are

$$I_1 = \sigma_t \tag{2.61}$$

and

$$I_4 = \sigma_t \tag{2.62}$$

Once again, Equation (2.59) represents six scalar equations. The equations where $i \neq j$ yields the scalar identity $0 = 0$ and no information is gained. However, three scalar equations are obtained for $i = j$. For $i = j = 1$ Equation (2.59) yields

$$A_1 + 2B_1 = A_3 + 2B_3 + 2C_3 + 2D_3 \tag{2.63}$$

With $i = j = 2$ Equation (2.59) yields

$$A_1 = A_3 + C_3 \tag{2.64}$$

For $i = j = 3$ Equation (2.59) yields the same relationship given in Equation (2.64), and no new information is gained.

2.2.2 Relationships Between Coefficients – Uniaxial Compression

The second test utilized to characterize the twelve constants is a uniaxial compression test. Here the stress applied is equal to the compressive threshold stress, i.e.,

$$\sigma_{ij} = \begin{bmatrix} 0 & 0 & 0 \\ 0 & 0 & 0 \\ 0 & 0 & \sigma_c \end{bmatrix} \tag{2.65}$$

For this stress state we are concerned with region #2, region #3 and region #4 since

$$\sigma_1 = 0 \geq \sigma_2 = 0 \geq \sigma_3 = \sigma_c \tag{2.66}$$

The functions along the boundaries of region #4, region #3, and region #2 must satisfy the relationships

$$f_2 = f_3 = f_4 \tag{2.67}$$

for this uniaxial compression test. In addition, the derivative of the functions along the boundaries of region #4, region #3, and region #2 must satisfy

$$\frac{\partial f_2}{\partial \sigma_{ij}} = \frac{\partial f_3}{\partial \sigma_{ij}} = \frac{\partial f_4}{\partial \sigma_{ij}} \tag{2.68}$$

for the uniaxial compression test.

Focusing on the derivatives along the boundary of region #4 and region #3 gives

$$\frac{\partial f_3}{\partial \sigma_{ij}} = \frac{\partial f_4}{\partial \sigma_{ij}} \tag{2.69}$$

This relationship yields the following tensor expression.

$$\begin{aligned} A_4 I_1 \delta_{ij} + 2B_4 \sigma_{ij} = (A_3 I_1 + C_3 I_4)\delta_{ij} + 2B_3 \sigma_{ij} \\ + C_3 I_1 a_i a_j + D_3 (a_k a_i \sigma_{jk} + a_j a_m \sigma_{mi}) \end{aligned} \tag{2.70}$$

For region #4 the function, f_4, is not dependent on a principle direction. For region #3 the function, f_3, is dependent on the direction vector a_i, which for this region is defined as

$$a_i = (1, 0, 0) \tag{2.71}$$

The invariants in Equation (2.70) are

$$I_1 = \sigma_c \tag{2.72}$$

and

$$I_4 = 0 \tag{2.73}$$

Due to symmetry Equation (2.70) represents six scalar equations. The equations where $i \neq j$ yield the scalar identity $0 = 0$ and no information is gained. For $i = j$ we obtain three scalar relationships. For Equation (2.70) with $i = j = 2$ yields

$$A_4 = A_3 \tag{2.74}$$

With $i = j = 3$ Equation (2.70) yields the following

$$A_4 + 2B_4 = A_3 + 2B_3 \tag{2.75}$$

Substituting Equation (2.74) into Equation (2.75) yields

$$B_4 = B_3 \tag{2.76}$$

Finally, with $i = j = 1$ results in

$$A_4 = A_3 + C_3 \tag{2.77}$$

Substituting Equation (2.74) into Equation (2.77) results in

$$C_3 = 0 \tag{2.78}$$

Substituting Equation (2.78) into Equation (2.64) yields the following

$$A_1 = A_3 \tag{2.79}$$

Therefore

$$A_1 = A_2 = A_3 = A_4 \tag{2.80}$$

and substituting Equations (2.78) and (2.80) into (2.63) results in

$$B_1 = B_3 + D_3 \tag{2.81}$$

Next, along the shared boundary of region #4 and region #2

$$\frac{\partial f_4}{\partial \sigma_{ij}} = \frac{\partial f_2}{\partial \sigma_{ij}} \tag{2.82}$$

for uniaxial compression. This yields the following tensor expression

$$\begin{aligned} A_4 I_1 \delta_{ij} + 2B_4 \sigma_{ij} = (A_2 I_1 + C_2 I_4)\delta_{ij} + 2B_2 \sigma_{ij} \\ + C_2 I_1 a_i a_j + D_2 (a_k a_i \sigma_{jk} + a_j a_m \sigma_{mi}) \end{aligned} \tag{2.83}$$

In region #2 it was noted earlier that the a_i vector points in the direction of the principle

compression stress. Thus a_i is defined as

$$a_i = (0, 0, 1) \tag{2.84}$$

The invariants of Equation (2.83) are

$$I_1 = \sigma_c \tag{2.85}$$

and

$$I_4 = \sigma_c \tag{2.86}$$

Once again, due to symmetry Equation (2.83) represents six scalar equation. The equations where $i \neq j$ yield $0 = 0$ and no information is gained. Three scalar equations are obtained for $i = j$. Substituting Equations (2.57) and (2.80) into Equation (2.83) yields the following tensor equation

$$2B_4\sigma_{ij} = 2B_2\sigma_{ij} + D_2(a_k a_i \sigma_{jk} + a_j a_m \sigma_{mi}) \tag{2.87}$$

For $i = j = 3$ Equation (2.87) yields

$$B_4 = B_2 + D_2 \tag{2.88}$$

Substituting Equation (2.55) into Equation (2.81) yields

$$B_2 = B_3 + D_3 \tag{2.89}$$

Substituting Equation (2.76) into Equation (2.88) yields

$$B_3 = B_2 + D_2 \tag{2.90}$$

Substituting Equation (2.89) into Equation (2.90) yields

$$B_2 = B_2 + D_2 + D_3 \tag{2.91}$$

Simplifying Equation (2.91) yields

$$D_2 = -D_3 \tag{2.92}$$

Thus the relationship between all of the constants have been defined.

2.3 Independent Functional Constants for Isotropy

The following relationships between the functional constants were derived in the previous two sections

$$A_1 = A_2 = A_3 = A_4 \tag{2.93}$$

$$B_1 = B_2 \tag{2.94}$$

$$B_3 = B_4 \tag{2.95}$$

$$B_1 = B_4 + D_3 \tag{2.96}$$

$$B_4 = B_1 + D_2 \tag{2.97}$$

$$C_2 = C_3 = 0 \tag{2.98}$$

and

$$D_2 = -D_3 \tag{2.99}$$

These relationships can be found in Green and Mkrtichian (1977). There are three independent constants in the expressions above. The independent constants are A_1, B_1, and D_2. The next step is to characterize these constants in terms of threshold stresses associated with simple mechanical tests.

The threshold functions are rewritten in terms of these three independent constants as follows:

$$f_1 = \frac{1}{2}A_1 I_1^2 + B_1 I_2 - K^2 \tag{2.100}$$

$$f_2 = \frac{1}{2}A_1 I_1^2 + B_1 I_2 + D_2 I_5 - K^2 \tag{2.101}$$

$$f_3 = \frac{1}{2}A_1 I_1^2 + (B_1 + D_2) I_2 + (-D_2) I_5 - K^2 \tag{2.102}$$

and

$$f_4 = \frac{1}{2}A_1 I_1^2 + (B_1 + D_2) I_2 - K^2 \tag{2.103}$$

The mechanical tests needed to define the three independent constants were identified earlier. They are a uniaxial tensile test (σ_t), a uniaxial compreession test (σ_c), and a torsion test (τ_i).

For a uniaxial tensile test where the stress applied is equal to the tensile threshold stress

$$\sigma_{ij} = \begin{bmatrix} \sigma_t & 0 & 0 \\ 0 & 0 & 0 \\ 0 & 0 & 0 \end{bmatrix} \tag{2.104}$$

Using Equation (2.100) the invariants are

$$I_1 = \sigma_t \tag{2.105}$$

and

$$I_2 = \sigma_t^2 \tag{2.106}$$

Substituting these quantities into Equation (2.100) with K equal to one yields

$$\frac{1}{2}A_1\sigma_t^2 + B_1\sigma_t^2 - 1 = 0 \tag{2.107}$$

Rearranging this equation yields

$$\frac{1}{2}A_1 + B_1 = \frac{1}{\sigma_t^2} \tag{2.108}$$

The next test utilized in identifying the unknown constants is a uniaxial compression test where the applied stress is equal to the compressive threshold stress. Hence,

$$\sigma_{ij} = \begin{bmatrix} \sigma_c & 0 & 0 \\ 0 & 0 & 0 \\ 0 & 0 & 0 \end{bmatrix} \tag{2.109}$$

Using Equation (2.103) the invariants are

$$I_1 = \sigma_c \tag{2.110}$$

and

$$I_2 = \sigma_c^2 \tag{2.111}$$

Substituting these quantities into Equation (2.103) with K equal to one yields

$$\frac{1}{2}A_1\sigma_c^2 + (B_1 + D_2)\sigma_c^2 - 1 = 0 \tag{2.112}$$

Rearranging this equation yields

$$\frac{1}{2}A_1 + B_1 + D_2 = \frac{1}{\sigma_c^2} \tag{2.113}$$

The last test is a torsion test where

$$\sigma_{ij} = \begin{bmatrix} 0 & \tau_i & 0 \\ \tau_i & 0 & 0 \\ 0 & 0 & 0 \end{bmatrix} \tag{2.114}$$

Using Equation (2.101) the invariants are

$$I_1 = 0 \tag{2.115}$$

$$I_2 = 2\tau_i^2 \tag{2.116}$$

and

$$I_5 = \tau_i^2 \tag{2.117}$$

Substituting these quantities into Equation (2.101) with K equal to one yields

$$2B_1\tau_i^2 + D_2\tau_i^2 - 1 = 0 \tag{2.118}$$

Rearranging this equation yields

$$2B_1 + D_2 = \frac{1}{\tau_i^2} \tag{2.119}$$

Equations (2.108), (2.113), and (2.119) are three equations in three unknowns. Solving these equations for A_1, B_1, and D_2 yields

$$A_1 = \frac{1}{\sigma_c^2} + \frac{1}{\sigma_t^2} - \frac{1}{\tau_i^2} \tag{2.120}$$

$$B_1 = \frac{1}{2\sigma_t^2} - \frac{1}{2\sigma_c^2} + \frac{1}{2\tau_i^2} \tag{2.121}$$

and

$$D_2 = \frac{1}{\sigma_c^2} - \frac{1}{\sigma_t^2} \tag{2.122}$$

With these constant defined in terms of inelastic flow stresses a map of the threshold surface can be constructed. Graphically it is convenient to plot the function in Haigh-Westergaard (principal) stress state. In the Haigh-Westergaard stress space the six components of the stress tensor are represented by the principle stress vector $(\sigma_1, \sigma_2, \sigma_3)$. In the Haigh-Westergaard stress space a given state of stress can be decomposed into hydrostatic and deviatoric components. Figure 6 depicts this decomposition. The line d in figure 6 represents the hydrostatic axis where $\sigma_1 = \sigma_2 = \sigma_3$. Planes normal to the hydrostatic stress are called deviatoric planes. Point P (σ_1,σ_2,σ_3) is an arbitrary state of stress. This state of stress can be described in terms of its hydrostatic component, vector ON, and its deviatoric componet, vector NP. This yeids several graphical schemes to present threshold functions. They are

- a principle stress plane ($\sigma_1 - \sigma_2$ plane)
- a deviatoric plane presented in the Haigh-Westergaard stress space, or

- a meridian plane perpendicular to the deviatoric plane (defined by the coordinat axes in figure 6 as $\xi - r$)

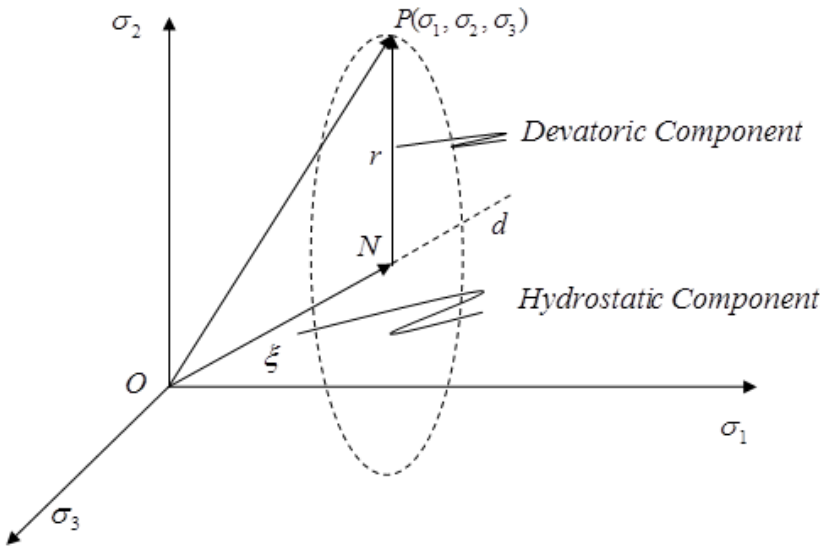

Figure 6: Haigh-Westergaard (principal) stress space

Figure 7 depicts a threshold surface projected onto the $\sigma_1 - \sigma_2$ stress plane. For this figure the three threshold stresses discussed above were arbitrarily set at $\sigma_t = 1.1\ MPa$, $\sigma_c = 5.0\ MPa$, and $\tau_i = 1.04\ MPa$ and are identified in the figure 7. Stress states within the surface represent elastic states of stress. These values are better depicted using a different set of axis as shown in Figure 8. This figure represents the same threshold function, but the σ_2 axis is replaced by a shear stress axis, τ_i.

Figure 9 depicts a series of nested surfaces associated with different values of the state variable K. The inside surface has a K value of one. The middle surface has a K value of two. The outside surface has a K value of three. As the inelastic work is accumulated and the graphite material hardens the inelastic state variable increases, values for the threshold stresses σ_t, σ_c, and τ_i increase accordingly. The values of the threshold stress will change

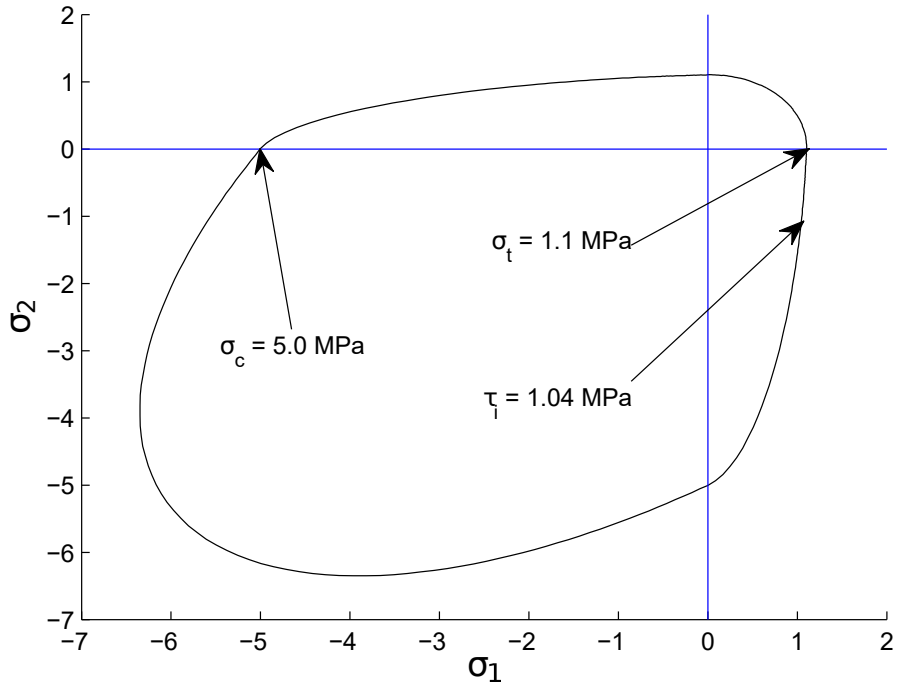

Figure 7: Green and Mkrtichian threshold surface with $\sigma_t = 1.1\ MPa$, $\sigma_c = 5.0\ MPa$, and $\tau_i = 1.04\ MPa$ with $K = 1$

according to the evolutionary laws presented in Chapter 4. This nesting of surfaces will be revisited in that section of this work.

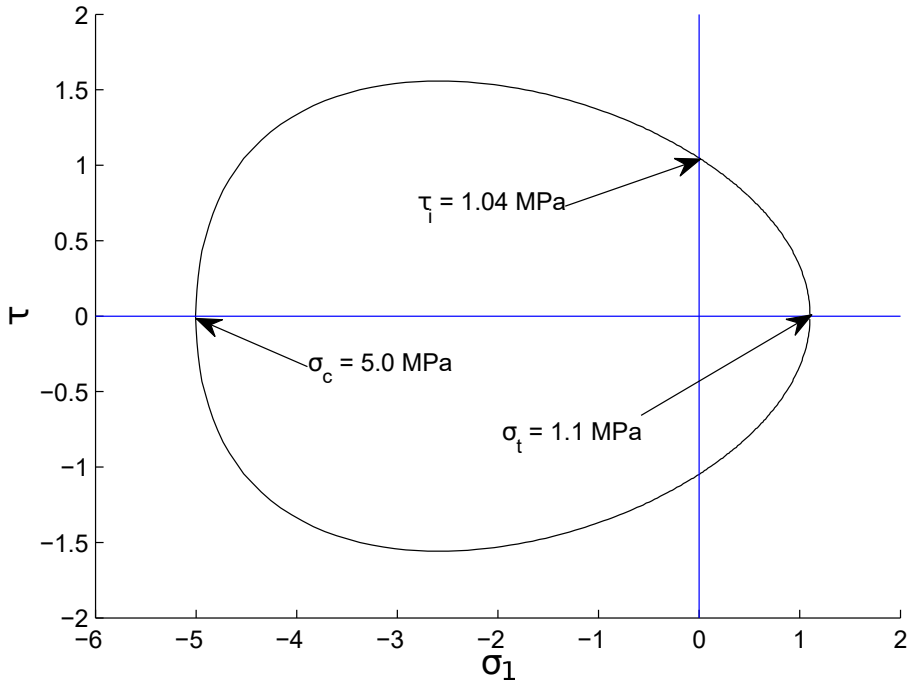

Figure 8: Green and Mkrtichian threshold surface with $\sigma_t = 1.1\ MPa$, $\sigma_c = 5.0\ MPa$, and $\tau_i = 1.04\ MPa$ with $K = 1$

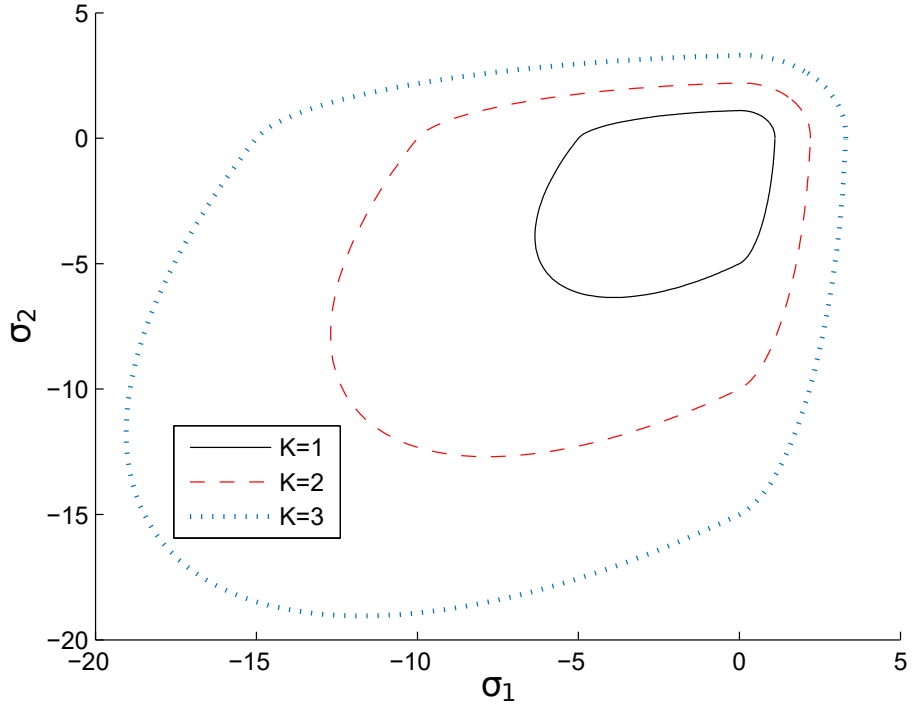

Figure 9: Nested threshold surfaces corresponding to $K = 1, 2, 3$

CHAPTER III

ANISOTROPIC INELASTIC THRESHOLD FUNCTION

3.1 Formulation of an Anisotropic Threshold Function

Burchell (2007) and others have indicated over the years that certain types of graphite exhibit anisotropic behavior. In this chapter the isotropic threshold function from the last chapter is extended to incorporate anisotropy, specifically transverse isotropy. A transversely isotropic material is characterized by a plane where the material properties are isotropic, and a preferred material direction perpendicular to this plane of isotropy where the material has different properties. Jones and Dudley (1976) described in detail the transversely isotropic deformation behavior of ATJ-S graphite. This type of graphite is fabricated from coke splinters that align themselves along the molding direction. As a result a billet exhibits the transversely isotropic directional dependence alluded to in Figure (1) of Jones and Dudley (1976)

To include transversely isotropy behavior in the current inelastic deformation model the threshold function must be constructed to include a dependence on a preferred material direction. This preferred material direction is designated through a second direction vector identified here as d_i. Since one can not distinguish between the preferred material direction and its reflection then the dependence of d_i appears through the second order tensor, $d_i d_j$. Now dependence of the threshold function presented in the previous chapter is extended

such that

$$f = f(\sigma_{ij}, a_i a_j, d_i d_j) \tag{3.1}$$

The definition of the unit vector a_i is the same as in the previous chapter. Spencer (1971) and Rivlin (1969) show that for a scalar valued function with the dependence stipulated by Equation (3.1) the integrity basis for this threshold function is

$$I_1 = \sigma_{kk} \tag{3.2}$$

$$I_2 = \sigma_{ij}\sigma_{ji} \tag{3.3}$$

$$I_3 = \sigma_{ij}\sigma_{jk}\sigma_{ki} \tag{3.4}$$

$$I_4 = a_i a_j \sigma_{ji} \tag{3.5}$$

$$I_5 = a_i a_j \sigma_{jk}\sigma_{ki} \tag{3.6}$$

$$I_6 = d_i d_j \sigma_{ji} \tag{3.7}$$

$$I_7 = d_i d_j \sigma_{jk}\sigma_{ki} \tag{3.8}$$

$$I_8 = a_i a_j d_j d_k \sigma_{ki} \tag{3.9}$$

and

$$I_9 = a_i a_j d_j d_k \sigma_{km}\sigma_{mi} \tag{3.10}$$

This effort requires a modification to the invariant I_9 as defined in Equation (3.10). This updated version for the I_9 invariant is

$$I_9 = \frac{1}{2}(a_i a_j d_j d_k \sigma_{km} \sigma_{mi} + a_k a_j d_j d_i \sigma_{km} \sigma_{mi}) \tag{3.11}$$

The details for the equivalence between these two versions of I_9 are presented in the Appendix. For use in the inelastic model shown in Chapter 4 a requirement for these invariants is that these derivatives with respect to the Cauchy stress must result in a symmetric second order tensor. This derivative with respect to the Cauchy stress for the original I_9 invariant results in a non-symmetric second order tensor, but by using the update version of I_9 this derivative results in a symmetric second order tensor.

The invariant I_3 is omitted again since this invariant is cubic in stress. Moreover, I_8 will never enter into the threshold function because when the polynomial function for f is constructed in terms of the above invariants, the coefficients associated with I_8 are zero. The invariant I_8 is carried along in the derivation that follows until it is apparent that it needs to be removed, whereas the invariant I_3 is omitted immediately. As will be seen shortly the invariants linear in stress enter the functional dependence as squared terms or as products with another invariant linear in stress. Therefore the transversely isotropic threshold function is quadratic in stress and has the following dependence

$$f(\sigma_{ij}, a_i a_j, d_i d_j) = f(I_1, I_2, I_4, I_5, I_6, I_7, I_8, I_9) \tag{3.12}$$

The underlying concept is that the response of the material depends on the stress state, the preferred material direction, and whether the principal stresses are tensile or compressive. Once again principle stresses follow the standard convention where they are ordered numerically based on their algebraic value, i.e.,

$$\sigma_1 \geq \sigma_2 \geq \sigma_3 \tag{3.13}$$

The principle stress space is divided into four regions and developing the functional form of the anisotropic threshold function proceeds in a manner similar to the isotropic threshold function. The regions and associated threshold functions are listed below.

In the first region where all of the principle stresses are tensile, i.e.,

$$\text{Region \#1} \quad \sigma_1 \geq \sigma_2 \geq \sigma_3 \geq 0 \qquad f = f_1(\sigma_{ij}, d_i d_j) \tag{3.14}$$

and a direction vector for the principle stress direction is unnecessary. A second region is identified where

$$\text{Region \#2} \quad \sigma_1 \geq \sigma_2 \geq 0 \geq \sigma_3 \qquad f = f_2(\sigma_{ij}, a_i a_j, d_i d_j) \tag{3.15}$$

In region #2 the direction vector a_i is associated with the compressive principle stress σ_3. Thus for this region

$$a_i = (0, 0, 1) \tag{3.16}$$

Again the Cartesian coordinate system is aligned with the principle stress coordinate system, which is depicted in Figure 5. A third region is identified where

$$\text{Region \#3} \quad \sigma_1 \geq 0 \geq \sigma_2 \geq \sigma_3 \qquad f = f_3(\sigma_{ij}, a_i a_j, d_i d_j) \tag{3.17}$$

In region #3 the direction vector a_i is associated with the tensile principle stress direction σ_1. Thus for this region

$$a_i = (1, 0, 0) \tag{3.18}$$

Finally, in the fourth region all principle stresses are compressive, i.e.,

$$\text{Region \#4} \quad 0 \geq \sigma_1 \geq \sigma_2 \geq \sigma_3 \qquad f = f_4(\sigma_{ij}, d_i d_j) \tag{3.19}$$

and a direction vector for the principle stress direction is unnecessary.

Building on the original form of the Green-Mkrtichian (1977) model through the use of the invariants that include d_i, the threshold function in region #1 is defined as

$$f_1 = \frac{1}{2}A_1 I_1^2 + B_1 I_2 + E_1 I_1 I_6 + F_1 I_7 - K^2 \tag{3.20}$$

The threshold function in region #2 is defined as

$$\begin{aligned} f_2 = \frac{1}{2}A_2 I_1^2 + B_2 I_2 + C_2 I_1 I_4 + D_2 I_5 + E_2 I_1 I_6 \\ + F_2 I_7 + G_2 I_1 I_8 + H_2 I_9 - K^2 \end{aligned} \tag{3.21}$$

The threshold function in region #3 is defined as

$$\begin{aligned} f_3 = \frac{1}{2}A_3 I_1^2 + B_3 I_2 + C_3 I_1 I_4 + D_3 I_5 + E_3 I_1 I_6 \\ + F_3 I_7 + G_3 I_1 I_8 + H_3 I_9 - K^2 \end{aligned} \tag{3.22}$$

and the threshold function in region #4 is defined as

$$f_4 = \frac{1}{2}A_4 I_1^2 + B_4 I_2 + E_4 I_1 I_6 + F_4 I_7 - K^2 \tag{3.23}$$

These four functions represent polynomial forms in terms of invariant quantities quadratic in stress. Historically this has precedence. Other forms such as rational formulations or transcendental functions could be studied. This effort leaves those types of functions for others to explore. The forms presented here for the threshold functions simplify to the threshold functions developed by Green and Mkrtichian (1977) for isotropic materials presented in the previous chapter. This is demonstrated later in this chapter after the polynomial coefficients A_1, A_2, A_3, A_4, B_1, B_2, B_3, B_4, C_2, C_3, D_2, D_3, E_1, E_2, E_3, E_4, F_1, F_2, F_3, F_4, G_2, G_3, H_2, and H_3 are characterized with simple mechanical tests. Thus isotropy is a special case of the formulation above.

The simple mechanical tests are identified by the states of stress they produce. These

stress states represent the limits of elastic behavior. As a material hardens with accumulated deformation, the threshold functions defining the elastic region of the stress space will change. Fundamentally, the elastic range is defined as the point on the stress–strain curve where permanent deformations are not accumulated after unloading. This is typically the point where the stress-strain curve becomes non-linear. The eight tests identified are uniaxial tension in the plane of isotropy, uniaxial compression in the plane of isotropy, biaxial compression in the plane of isotropy, torsional test in the plane of isotropy, uniaxial tension in the preferred material direction, uniaxial compression in the preferred material direction, mixed biaxial compression in the preferred material direction and in the plane of isotropy, and a torsional test across the plane of isotropy. The following notation is adopted to identify the threshold stresses:

- σ_t – uniaxial tensile threshold stress in the plane of isotropy
- σ_c – uniaxial compressive threshold stress in the plane of isotropy
- σ_{bc} – equal biaxial compressive threshold stress in the plane of isotropy
- τ_i – torsional stress in the plane of isotropy
- σ_{st} – uniaxial tensile threshold stress along the strong direction
- σ_{sc} – uniaxial compressive threshold stress along the strong direction
- σ_{mbc} – equal biaxial compressive threshold stress along the strong direction and in the plane of isotropy
- τ_s – torsional stress across the plane of isotropy

The parameter K in the equations above is an inelastic state variable associated with isotropic hardening. For a virgin material, the value of this state variable is equal to one. Similarly, the polynomial coefficients just mentioned will be characterized by mechanical

tests on virgin materials. In the section discussing the inelastic constitutive model the value of K will change according to a specified evolutionary law (see Chapter 4).

3.2 Relationships Between Functional Coefficients

The set of piecewise continuous threshold functions identified in the previous section must satisfy two conditions along the boundaries where they meet. The first condition is that the threshold functions must be equal along mutual boundaries. The second condition is that the tangents, the directional derivatives of the threshold functions, must be single valued everywhere but especially along a mutual boundary. The second condition dominates the development of relationships between the twenty-four polynomial coefficients. In the next chapter where an associated flow rule is presented the conditions on the tangents will guarantee that increments in the inelastic strain will be equal at mutual boundaries of the piecewise threshold function. It is noted at this point that region #1 and region #4 do not share a boundary except at the origin of principle stress space where all regions meet. The first condition, i.e., the threshold functions must be equal along the boundaries help in establishing the value of the coefficients in terms of the simple mechanical tests mentioned above. This is discussed in Section 3.3

The tangents for these four functions are calculated by taking the derivatives with respect to the Cauchy stress, σ_{ij}. For all four threshold functions the partial derivatives are calculated using the chain rule

$$\begin{aligned}\frac{\partial f}{\partial \sigma_{ij}} = &\frac{\partial f}{\partial I_1}\frac{\partial I_1}{\partial \sigma_{ij}} + \frac{\partial f}{\partial I_2}\frac{\partial I_2}{\partial \sigma_{ij}} + \frac{\partial f}{\partial I_4}\frac{\partial I_4}{\partial \sigma_{ij}} + \frac{\partial f}{\partial I_5}\frac{\partial I_5}{\partial \sigma_{ij}} \\ &+ \frac{\partial f}{\partial I_6}\frac{\partial I_6}{\partial \sigma_{ij}} + \frac{\partial f}{\partial I_7}\frac{\partial I_7}{\partial \sigma_{ij}} + \frac{\partial f}{\partial I_8}\frac{\partial I_8}{\partial \sigma_{ij}} + \frac{\partial f}{\partial I_9}\frac{\partial I_9}{\partial \sigma_{ij}}\end{aligned} \tag{3.24}$$

For the threshold function f_1 the partial derivatives on the right hand side of Equation (3.24) are

$$\frac{\partial f_1}{\partial I_1} = A_1 I_1 + E_1 I_6 \tag{3.25}$$

$$\frac{\partial f_1}{\partial I_2} = B_1 \tag{3.26}$$

$$\frac{\partial f_1}{\partial I_6} = E_1 I_1 \tag{3.27}$$

$$\frac{\partial f_1}{\partial I_7} = F_1 \tag{3.28}$$

$$\frac{\partial I_1}{\partial \sigma_{ij}} = \delta_{ij} \tag{3.29}$$

$$\frac{\partial I_2}{\partial \sigma_{ij}} = 2\sigma_{ij} \tag{3.30}$$

$$\frac{\partial I_6}{\partial \sigma_{ij}} = d_i d_j \tag{3.31}$$

and

$$\frac{\partial I_7}{\partial \sigma_{ij}} = d_k d_i \sigma_{jk} + d_j d_m \sigma_{mi} \tag{3.32}$$

Thus Equation (3.24) for f_1 takes the form

$$\begin{aligned} \frac{\partial f_1}{\partial \sigma_{ij}} =& (A_1 I_1 + E_1 I_6)\delta_{ij} + 2B_1 \sigma_{ij} + \\ & E_1 I_1 d_i d_j + F_1 (d_k d_i \sigma_{jk} + d_j d_m \sigma_{mi}) \end{aligned} \tag{3.33}$$

in the first region of the principle stress space.

In a similar fashion for the threshold function f_2

$$\frac{\partial f_2}{\partial I_1} = A_2 I_1 + C_2 I_4 + E_2 I_6 + G_2 I_8 \tag{3.34}$$

$$\frac{\partial f_2}{\partial I_2} = B_2 \tag{3.35}$$

$$\frac{\partial f_2}{\partial I_4} = C_2 I_1 \tag{3.36}$$

$$\frac{\partial f_2}{\partial I_5} = D_2 \tag{3.37}$$

$$\frac{\partial f_2}{\partial I_6} = E_2 I_1 \tag{3.38}$$

$$\frac{\partial f_2}{\partial I_7} = F_2 \tag{3.39}$$

$$\frac{\partial f_2}{\partial I_8} = G_2 I_1 \tag{3.40}$$

$$\frac{\partial f_2}{\partial I_9} = H_2 \tag{3.41}$$

$$\frac{\partial I_4}{\partial \sigma_{ij}} = a_i a_j \tag{3.42}$$

$$\frac{\partial I_5}{\partial \sigma_{ij}} = a_k a_i \sigma_{jk} + a_j a_m \sigma_{mi} \tag{3.43}$$

$$\frac{\partial I_8}{\partial \sigma_{ij}} = a_j a_q d_q d_i \tag{3.44}$$

and

$$\frac{\partial I_9}{\partial \sigma_{ij}} = \frac{1}{2}(a_m a_n d_n d_i \sigma_{jm} + a_j a_n d_n d_k \sigma_{ki} + a_i a_n d_n d_m \sigma_{jm} + a_k a_n d_n d_j \sigma_{ki}) \tag{3.45}$$

Thus Equation (3.24) for f_2 takes the form

$$\begin{aligned}\frac{\partial f_2}{\partial \sigma_{ij}} =&(A_2 I_1 + C_2 I_4 + E_2 I_6 + G_2 I_8)\delta_{ij} + 2B_2\sigma_{ij} + C_2 I_1 a_i a_j + \\ &D_2(a_k a_i \sigma_{jk} + a_j a_m \sigma_{mi}) + E_2 I_1 d_i d_j + F_2(d_k d_i \sigma_{jk} + d_j d_m \sigma_{mi}) + \\ &G_2 I_1 a_j a_q d_q d_i + H_2\Big(\frac{1}{2}(a_m a_n d_n d_i \sigma_{jm} + a_j a_n d_n d_k \sigma_{ki} + \\ &a_i a_n d_n d_m \sigma_{jm} + a_k a_n d_n d_j \sigma_{ki})\Big)\end{aligned} \tag{3.46}$$

in the second region of the principle stress space.

For the threshold function f_3

$$\frac{\partial f_3}{\partial I_1} = A_3 I_1 + C_3 I_4 + E_3 I_6 + G_3 I_8 \tag{3.47}$$

$$\frac{\partial f_3}{\partial I_2} = B_3 \tag{3.48}$$

$$\frac{\partial f_3}{\partial I_4} = C_3 I_1 \tag{3.49}$$

$$\frac{\partial f_3}{\partial I_5} = D_3 \tag{3.50}$$

$$\frac{\partial f_3}{\partial I_6} = E_3 I_1 \tag{3.51}$$

$$\frac{\partial f_3}{\partial I_7} = F_3 \tag{3.52}$$

$$\frac{\partial f_3}{\partial I_8} = G_3 I_1 \tag{3.53}$$

and

$$\frac{\partial f_3}{\partial I_9} = H_3 \tag{3.54}$$

Equation (3.24) takes the form

$$\begin{aligned}\frac{\partial f_3}{\partial \sigma_{ij}} =&(A_3 I_1 + C_3 I_4 + E_3 I_6 + G_3 I_8)\delta_{ij} + 2B_3\sigma_{ij} + C_3 I_1 a_i a_j + \\ & D_3(a_k a_i \sigma_{jk} + a_j a_m \sigma_{mi}) + E_3 I_1 d_i d_j + F_3(d_k d_i \sigma_{jk} + d_j d_m \sigma_{mi}) + \\ & G_3 I_1 a_j a_q d_q d_i + H_3\Big(\frac{1}{2}(a_m a_n d_n d_i \sigma_{jm} + a_j a_n d_n d_k \sigma_{ki} + \\ & a_i a_n d_n d_m \sigma_{jm} + a_k a_n d_n d_j \sigma_{ki})\Big)\end{aligned} \tag{3.55}$$

in the third region of the principle stress space.

For the threshold function f_4

$$\frac{\partial f_4}{\partial I_1} = A_4 I_1 + E_4 I_6 \tag{3.56}$$

$$\frac{\partial f_4}{\partial I_2} = B_4 \tag{3.57}$$

$$\frac{\partial f_4}{\partial I_6} = E_4 I_1 \tag{3.58}$$

and

$$\frac{\partial f_4}{\partial I_7} = F_4 \tag{3.59}$$

Thus Equation (3.24) takes the form

$$\begin{aligned}\frac{\partial f_4}{\sigma_{ij}} =&(A_4 I_1 + E_4 I_6)\delta_{ij} + 2B_4\sigma_{ij} + \\ & E_4 I_1 d_i d_j + F_4(d_k d_i \sigma_{jk} + d_j d_m \sigma_{mi})\end{aligned} \tag{3.60}$$

in the fourth region of the principle stress space.

Summarizing

$$\frac{\partial f_1}{\partial \sigma_{ij}} = (A_1 I_1 + E_1 I_6)\delta_{ij} + 2B_1\sigma_{ij} + E_1 I_1 d_i d_j + F_1(d_k d_i \sigma_{jk} + d_j d_m \sigma_{mi}) \tag{3.61}$$

$$\begin{aligned}\frac{\partial f_2}{\partial \sigma_{ij}} = {} & (A_2 I_1 + C_2 I_4 + E_2 I_6 + G_2 I_8)\delta_{ij} + 2B_2\sigma_{ij} + C_2 I_1 a_i a_j + \\ & D_2(a_k a_i \sigma_{jk} + a_j a_m \sigma_{mi}) + E_2 I_1 d_i d_j + F_2(d_k d_i \sigma_{jk} + d_j d_m \sigma_{mi}) + \\ & G_2 I_1 a_j a_q d_q d_i + H_2\Big(\frac{1}{2}(a_m a_n d_n d_i \sigma_{jm} + a_j a_n d_n d_k \sigma_{ki} + \\ & a_i a_n d_n d_m \sigma_{jm} + a_k a_n d_n d_j \sigma_{ki})\Big)\end{aligned} \tag{3.62}$$

$$\begin{aligned}\frac{\partial f_3}{\partial \sigma_{ij}} = {} & (A_3 I_1 + C_3 I_4 + E_3 I_6 + G_3 I_8)\delta_{ij} + 2B_3\sigma_{ij} + C_3 I_1 a_i a_j + \\ & D_3(a_k a_i \sigma_{jk} + a_j a_m \sigma_{mi}) + E_3 I_1 d_i d_j + F_3(d_k d_i \sigma_{jk} + d_j d_m \sigma_{mi}) + \\ & G_3 I_1 a_j a_q d_q d_i + H_3\Big(\frac{1}{2}(a_m a_n d_n d_i \sigma_{jm} + a_j a_n d_n d_k \sigma_{ki} + \\ & a_i a_n d_n d_m \sigma_{jm} + a_k a_n d_n d_j \sigma_{ki})\Big)\end{aligned} \tag{3.63}$$

and

$$\frac{\partial f_4}{\partial \sigma_{ij}} = (A_1 I_1 + E_1 I_6)\delta_{ij} + 2B_1\sigma_{ij} + E_1 I_1 d_i d_j + F_1(d_k d_i \sigma_{jk} + d_j d_m \sigma_{mi}) \tag{3.64}$$

Equations (3.61) through (3.64) represent four symmetric second order tensor equations in terms of twenty–four unknowns. In what follows, a sufficient number of scalar expression embedded in these tensor equation will be extracted in order to define relationships between the twenty–four polynomial coefficients. It is noted prior to the development that several coefficients are not independent.

3.2.1 Relationships Between Coefficients – Uniaxial Tension in the Plane of Isotropy

For a uniaxial tensile test in the plane of isotropy where the stress applied is equal to the tensile threshold stress of the material, the Cauchy stress tensor has the form

$$\sigma_{ij} = \begin{bmatrix} \sigma_t & 0 & 0 \\ 0 & 0 & 0 \\ 0 & 0 & 0 \end{bmatrix} \tag{3.65}$$

This stress state satisfies the inequalities associated with region #1, region #2, and region #3 since

$$\sigma_1 = \sigma_t \geq \sigma_2 = 0 \geq \sigma_3 = 0 \tag{3.66}$$

The threshold functions along the shared boundaries of region #1,region #2, and region #3 must satisfy the relationships

$$f_1 = f_2 = f_3 \tag{3.67}$$

for this state of stress. In addition, the derivatives of the functions along the shared boundaries of region #1, region #2, and region #3 must satisfy

$$\frac{\partial f_1}{\partial \sigma_{ij}} = \frac{\partial f_2}{\partial \sigma_{ij}} = \frac{\partial f_3}{\partial \sigma_{ij}} \tag{3.68}$$

for this state of stress.

Focusing on the derivatives along the boundary of region #1 and region #2 then

$$\frac{\partial f_1}{\partial \sigma_{ij}} = \frac{\partial f_2}{\partial \sigma_{ij}} \tag{3.69}$$

This relationship yields the following tensor expression

$$
\begin{aligned}
&(A_1 I_1 + E_1 I_6)\delta_{ij} + 2B_1\sigma_{ij} + E_1 I_1 d_i d_j + F_1(d_k d_i \sigma_{jk} + d_j d_m \sigma_{mi}) = \\
&\quad (A_2 I_1 + C_2 I_4 + E_2 I_6 + G_2 I_8)\delta_{ij} + 2B_2\sigma_{ij} + C_2 I_1 a_i a_j + \\
&\quad D_2(a_k a_i \sigma_{jk} + a_j a_m \sigma_{mi}) + E_2 I_1 d_i d_j + F_2(d_k d_i \sigma_{jk} + d_j d_m \sigma_{mi}) + \\
&\quad G_2 I_1 a_j a_q d_q d_i + H_2\Big(\frac{1}{2}(a_m a_n d_n d_i \sigma_{jm} + a_j a_n d_n d_k \sigma_{ki} + \\
&\qquad a_i a_n d_n d_m \sigma_{jm} + a_k a_n d_n d_j \sigma_{ki})\Big)
\end{aligned}
\tag{3.70}
$$

For region #1 the function f_1 does not depend on a principle direction. In region #2 the function f_2 does depend on the direction vector a_i. Just as in the isotropic case the compressive stress which is assumed to be σ_3 is tracked in Region #2 (even though it is zero) and the vector a_i is defined as

$$a_i = (0, 0, 1) \tag{3.71}$$

For a tensile test in the plane of isotropy the tensile stress direction must be orthogonal to the preferred material direction vector d_i. Here the preferred material direction vector d_i is assumed coincident with the principle compressive stress direction a_i. Thus

$$d_i = (0, 0, 1) \tag{3.72}$$

The state of stress and material orientation are depicted in Figure 10. With this information the invariants from the transversely isotropic integrity basis are

$$I_1 = \sigma_t \tag{3.73}$$

$$I_6 = 0 \tag{3.74}$$

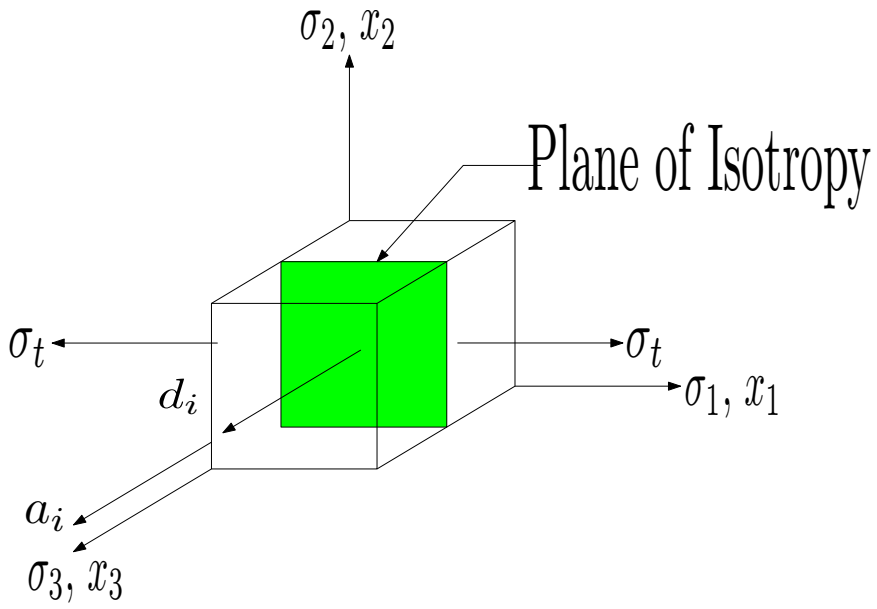

Figure 10: First Tensile Test in the Plane of Isotropy

$$I_4 = 0 \tag{3.75}$$

and

$$I_8 = 0 \tag{3.76}$$

Since Equation (3.70) is a partial derivative of two of the threshold functions this equation is a composite function of clearly defined invariants (scalar constants) and second order tensors. Equation (3.70) represents nine scalar equations. Using the symmetry of the Cauchy stress tensor, i.e. $\sigma_{ij} = \sigma_{ji}$, the nine scalar equations are reduced to six. The equations where $i \neq j$ yield the scalar identity $0 = 0$ and no information is gained. With $i = j$ we obtain three scalar relationships that are presented momentarily.

With $i = j = 2$ the tangent relationships for f_1 and f_2 expressed in Equation (3.70) simplifies to

$$A_1 = A_2 \tag{3.77}$$

With $i = j = 1$ Equation (3.70) yields

$$A_1 + 2B_1 = A_2 + 2B_2 \tag{3.78}$$

Substituting Equation (3.77) into Equation (3.78) yields

$$B_1 = B_2 \tag{3.79}$$

With $i = j = 3$ Equation (3.70) yields the following

$$A_1 + E_1 = A_2 + E_2 + C_2 + G_2 \tag{3.80}$$

Substituting Equation (3.77) into Equation (3.80) yields

$$E_1 = E_2 + C_2 + G_2 \tag{3.81}$$

More relationships between the coefficients can be obtained from the tangent relationship between threshold functions f_1 and f_2. Equation (3.70) must also be satisfied when the preferred material direction is along the same direction as principle stress direction for σ_2. For this case the material direction vector d_i is defined as

$$d_i = (0, 1, 0) \tag{3.82}$$

The applied uniaxial stress defined by the stress tensor in Equation (3.65) is still in the plane of isotropy, which can be seen in Figure 11. Note that the vector a_i remains unchanged for an applied stress of σ_t in the σ_1 principle stress direction. For this stress state and material direction the four invariants (I_1, I_4, I_6, and I_8) in Equation (3.70) remain the same values identified in Equations (3.73) through (3.76). With $i = j = 1$ Equation (3.70) gives the same result that was identified in Equation (3.78) is obtained and no new information is

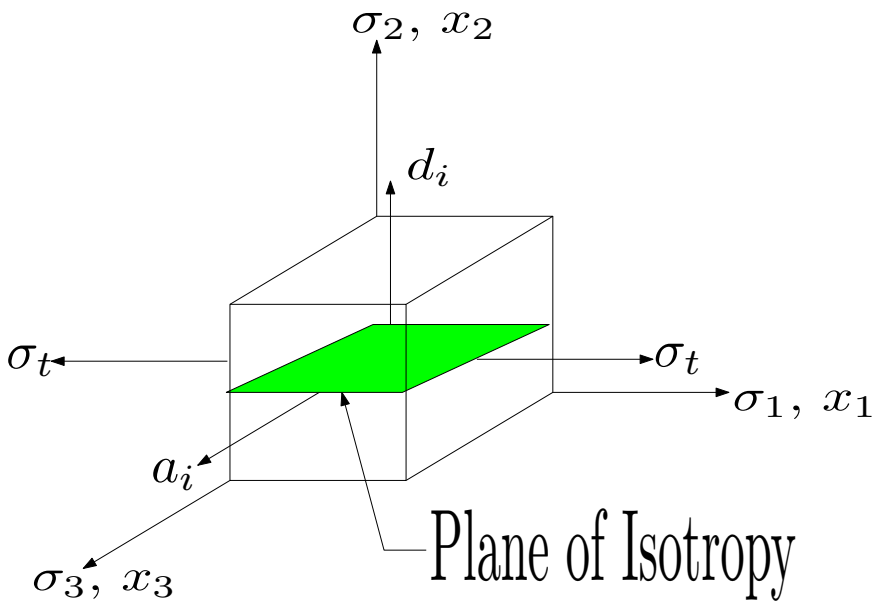

Figure 11: Second Tensile Test in the Plane of Isotropy

gained. However with $i = j = 2$ Equation (3.70) yields

$$A_1 + E_1 = A_2 + E_2 \tag{3.83}$$

Substituting Equation (3.77) into Equation (3.83) yields

$$E_1 = E_2 \tag{3.84}$$

For $i = j = 3$ Equation (3.70) yields

$$A_1 = A_2 + C_2 \tag{3.85}$$

Substituting Equation (3.77) into Equation (3.85) yields

$$C_2 = 0 \tag{3.86}$$

Finally, substituting Equations (3.86) and (3.84) into (3.81) yields

$$G_2 = 0 \tag{3.87}$$

Note that G_2 is associated with I_8. If G_3 is found to be equal to zero then the threshold functions loose all dependence on I_8.

Next the argument above is repeated for the derivatives along the shared boundary between region #1 and region #3 where

$$\frac{\partial f_1}{\partial \sigma_{ij}} = \frac{\partial f_3}{\partial \sigma_{ij}} \tag{3.88}$$

This yields the following tensor expression in terms of index notation

$$\begin{aligned}
&(A_1 I_1 + E_1 I_6)\delta_{ij} + 2B_1\sigma_{ij} + E_1 I_1 d_i d_j + F_1(d_k d_i \sigma_{jk} + d_j d_m \sigma_{mi}) = \\
&\quad (A_3 I_1 + C_3 I_4 + E_3 I_6 + G_3 I_8)\delta_{ij} + 2B_3\sigma_{ij} + C_3 I_1 a_i a_j + \\
&\quad D_3(a_k a_i \sigma_{jk} + a_j a_m \sigma_{mi}) + E_3 I_1 d_i d_j + F_3(d_k d_i \sigma_{jk} + d_j d_m \sigma_{mi}) + \\
&\quad G_3 I_1 a_j a_q d_q d_i + H_3\Big(\frac{1}{2}(a_m a_n d_n d_i \sigma_{jm} + a_j a_n d_n d_k \sigma_{ki} + \\
&\qquad a_i a_n d_n d_m \sigma_{jm} + a_k a_n d_n d_j \sigma_{ki})\Big)
\end{aligned} \tag{3.89}$$

In region #3 the a_i vector is defined as

$$a_i = (1, 0, 0) \tag{3.90}$$

With the plane of isotropy coinciding with the $\sigma_1 - \sigma_2$ plane (see Figure 12) the d_i vector is defined as

$$d_i = (0, 0, 1) \tag{3.91}$$

Once again uniaxial tensile stress σ_t is applied in the σ_1 principle stress direction. Based on the direction vectors and the state of stress the invariants in Equation (3.89) are

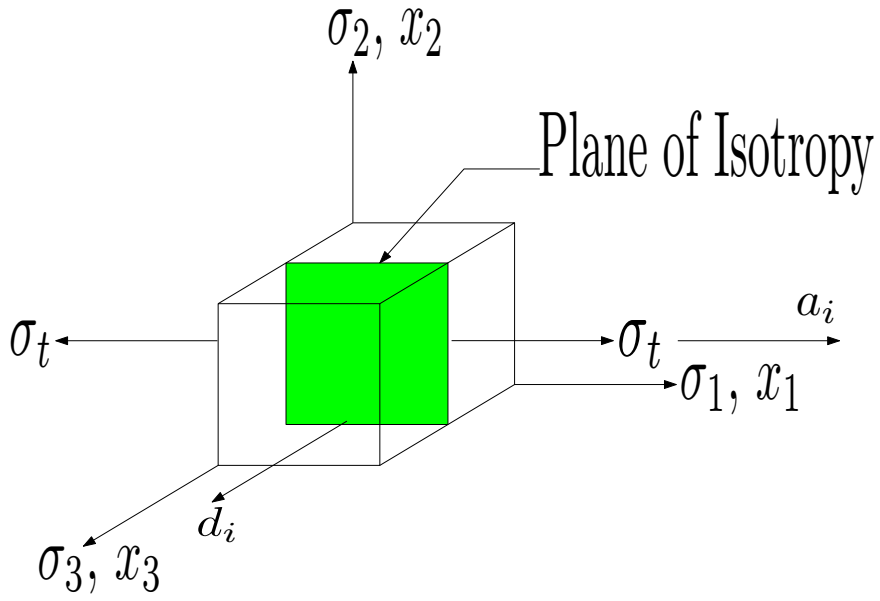

Figure 12: Third Tensile Test in the Plane of Isotropy

$$I_1 = \sigma_t \tag{3.92}$$

$$I_4 = \sigma_t \tag{3.93}$$

$$I_6 = 0 \tag{3.94}$$

and

$$I_8 = 0 \tag{3.95}$$

Again this is a second order tensor function that is explicitly dependent on certain invariants. Due to the symmetry of the Cauchy stress tensor Equation (3.89) represents six scalar equations. The equations where $i \neq j$ yields the scalar identity $0 = 0$ and no information is gained. Three non-zero scalar equations are obtained for $i = j$.

For $i = j = 1$ Equation (3.89) yields

$$A_1 + 2B_1 = A_3 + 2B_3 + 2C_3 + 2D_3 \tag{3.96}$$

With $i = j = 2$ Equation (3.89) yields

$$A_1 = A_3 + C_3 \tag{3.97}$$

and finally with $i = j = 3$ Equation (3.89) yields

$$A_1 + E_1 = A_3 + C_3 + E_3 \tag{3.98}$$

3.2.2 Relationships Between Coefficients – Uniaxial Compression in the Plane of Isotropy

The second test utilized to characterize the twenty-four polynomial coefficients is a uniaxial compression test in the plane of isotropy. Here the stress applied is equal to the compressive threshold stress, i.e.,

$$\sigma_{ij} = \begin{bmatrix} 0 & 0 & 0 \\ 0 & 0 & 0 \\ 0 & 0 & \sigma_c \end{bmatrix} \tag{3.99}$$

This stress state is valid in region #2, region #3, and region #4 since

$$\sigma_1 = 0 \geq \sigma_2 = 0 \geq \sigma_3 = \sigma_c \tag{3.100}$$

The functions along the shared boundaries of these regions satisfy the relationships

$$f_2 = f_3 = f_4 \tag{3.101}$$

for this uniaxial compression test. In addition, the derivative of the functions along the boundaries of region #2, region #3, and region #4 must satisfy

$$\frac{\partial f_2}{\partial \sigma_{ij}} = \frac{\partial f_3}{\partial \sigma_{ij}} = \frac{\partial f_4}{\partial \sigma_{ij}} \tag{3.102}$$

for the uniaxial compression test.

Focusing on the derivatives along the boundary between region #3 and region #4 then

$$\frac{\partial f_3}{\partial \sigma_{ij}} = \frac{\partial f_4}{\partial \sigma_{ij}} \tag{3.103}$$

This relationship yields the following tensor expression

$$\begin{aligned}
&(A_4 I_1 + E_4 I_6)\delta_{ij} + 2B_4\sigma_{ij} + E_4 I_1 d_i d_j + F_4(d_k d_i \sigma_{jk} + d_j d_m \sigma_{mi}) = \\
&\quad (A_3 I_1 + C_3 I_4 + E_3 I_6 + G_3 I_8)\delta_{ij} + 2B_3\sigma_{ij} + C_3 I_1 a_i a_j + \\
&\quad D_3(a_k a_i \sigma_{jk} + a_j a_m \sigma_{mi}) + E_3 I_1 d_i d_j + F_3(d_k d_i \sigma_{jk} + d_j d_m \sigma_{mi}) + \\
&\quad G_3 I_1 a_j a_q d_q d_i + H_3\Big(\frac{1}{2}(a_m a_n d_n d_i \sigma_{jm} + a_j a_n d_n d_k \sigma_{ki} + \\
&\qquad a_i a_n d_n d_m \sigma_{jm} + a_k a_n d_n d_j \sigma_{ki})\Big)
\end{aligned} \tag{3.104}$$

For region #4 the function f_4 does not depend on a principle direction. However, the function f_3 does depend on the direction vector a_i, which in region #3 is defined as

$$a_i = (1, 0, 0) \tag{3.105}$$

The plane of isotropy is identified as the $\sigma_2 - \sigma_3$ plane, thus the d_i vector is defined as

$$d_i = (1, 0, 0) \tag{3.106}$$

The state of stress and material orientation are depicted in Figure 13. With this information the invariants from the transversely isotropic integrity basis are

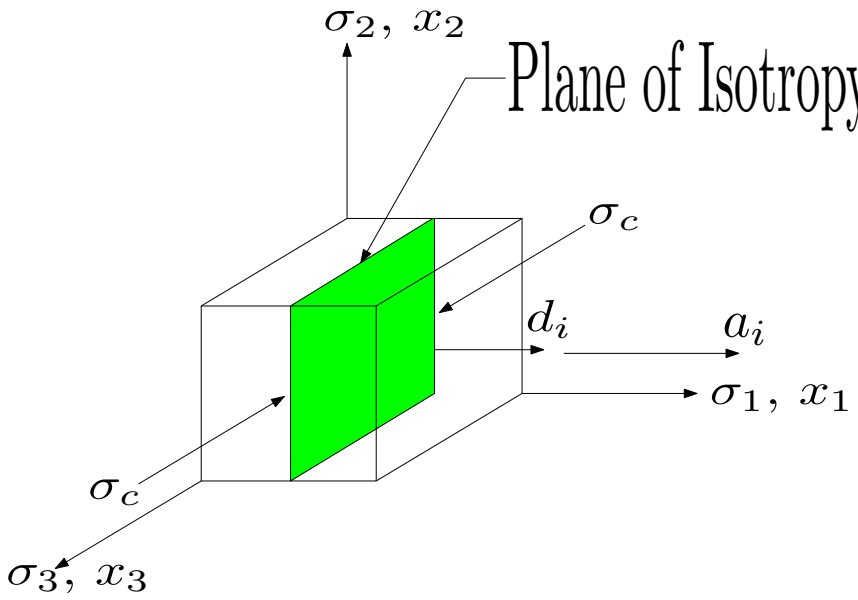

Figure 13: First Compression Test in the Plane of Isotropy

$$I_1 = \sigma_c \tag{3.107}$$

$$I_4 = 0 \tag{3.108}$$

$$I_6 = 0 \tag{3.109}$$

and

$$I_8 = 0 \tag{3.110}$$

Again this is a second order tensor function that is explicitly dependent on certain invariants. Due to symmetry of the stress tensor Equation (3.104) represents six scalar equations. Again when $i \neq j$ three scalar identities of $0 = 0$ are obtained and no information is gained. For $i = j$ we obtain three non-zero scalar relationships. These relationships are explored next.

For $i = j = 2$ Equation (3.104) yields

$$A_4 = A_3 \tag{3.111}$$

With $i = j = 3$ Equation (3.104) yields

$$A_4 + 2B_4 = A_3 + 2B_3 \tag{3.112}$$

Substituting Equation (3.111) into Equation (3.112) yields

$$B_4 = B_3 \tag{3.113}$$

and for $i = j = 1$ Equation (3.104) yields

$$A_4 + E_4 = A_3 + E_3 + C_3 + G_3 \tag{3.114}$$

Substituting Equation (3.111) into Equation (3.114) yields

$$E_4 = E_3 + C_3 + G_3 \tag{3.115}$$

For this state of stress Equation (3.104) must still be satisfied if the plane of isotropy is $\sigma_1 - \sigma_3$ plane, and for this orientation of the plane of isotropy the d_i vector is defined as

$$d_i = (0, 1, 0) \tag{3.116}$$

Since the state of stress remains the same, the vector a_i is unchanged. The applied compressive stress, the a_i vector, and the d_i vector are shown in Figure 14. With this information the invariants from the transversely isotropic integrity basis are

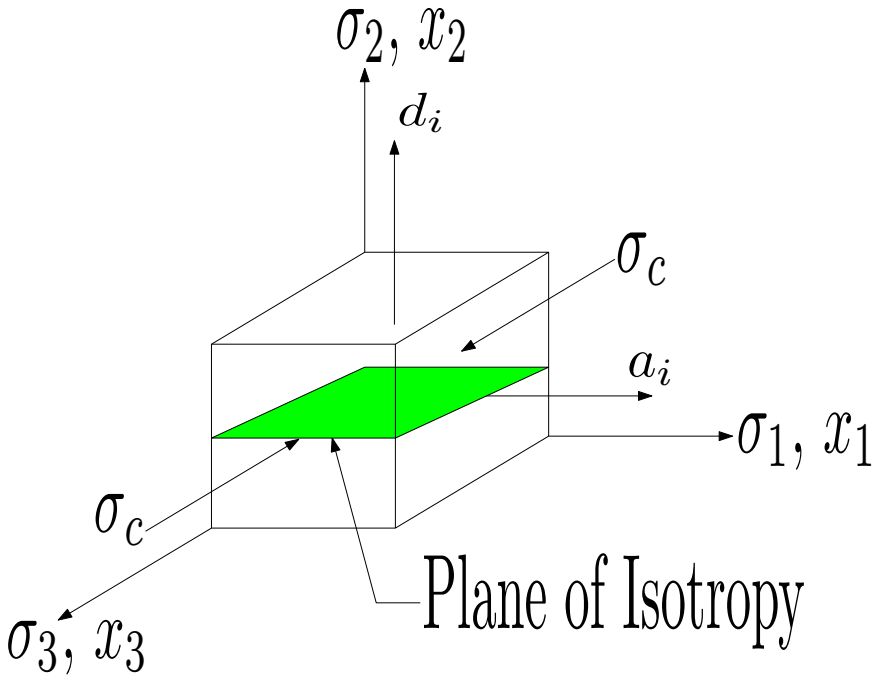

Figure 14: Second Compression Test in the Plane of Isotropy

$$I_1 = \sigma_c \tag{3.117}$$

$$I_4 = 0 \tag{3.118}$$

$$I_6 = 0 \tag{3.119}$$

and

$$I_8 = 0 \tag{3.120}$$

With $i = j = 3$ Equation (3.104) yields the same Equation as (3.112) and no new information is gained. With $i = j = 2$ Equation (3.104) yields

$$A_4 + E_4 = A_3 + E_3 \tag{3.121}$$

Substituting Equation (3.111) into Equation (3.121) yields

$$E_4 = E_3 \tag{3.122}$$

For Equation (3.104) $i = j = 1$ results in

$$A_4 = A_3 + C_3 \tag{3.123}$$

Substituting Equation (3.111) into Equation (3.123) yields

$$C_3 = 0 \tag{3.124}$$

Substituting Equation (3.124) and (3.122) into Equation (3.115) yields

$$G_3 = 0 \tag{3.125}$$

At this point I_8 can be removed from the integrity basis since G_2 and G_3 have been shown to be zero.

Continuing on, substituting Equation (3.124) into Equation (3.97) yields

$$A_1 = A_3 \tag{3.126}$$

Thus

$$A_1 = A_2 = A_3 = A_4 \tag{3.127}$$

Substituting Equation (3.124) and (3.126) into Equation (3.98) yields

$$E_1 = E_3 \tag{3.128}$$

Thus

$$E_1 = E_2 = E_3 = E_4 \tag{3.129}$$

Substituting Equation (3.124) and (3.127) into Equation (3.96) yields

$$B_1 = B_3 + D_3 \tag{3.130}$$

Finally for this state of stress, the derivatives along the shared boundary of region #4 and region #2 must satisfy

$$\frac{\partial f_4}{\partial \sigma_{ij}} = \frac{\partial f_2}{\partial \sigma_{ij}} \tag{3.131}$$

for the uniaxial compression test in the plane of isotropy identified in Figure 14. This yields the following tensor expression

$$\begin{aligned}
&(A_4 I_1 + E_3 I_6)\delta_{ij} + 2B_4\sigma_{ij} + E_4 I_1 d_i d_j + F_4(d_k d_i \sigma_{jk} + d_j d_m \sigma_{mi}) = \\
&\quad (A_2 I_1 + C_2 I_4 + E_2 I_6 + G_2 I_8)\delta_{ij} + 2B_2\sigma_{ij} + C_2 I_1 a_i a_j + \\
&\quad D_2(a_k a_i \sigma_{jk} + a_j a_m \sigma_{mi}) + E_2 I_1 d_i d_j + F_2(d_k d_i \sigma_{jk} + d_j d_m \sigma_{mi}) + \\
&\quad G_2 I_1 a_j a_q d_q d_i + H_2\Big(\frac{1}{2}(a_m a_n d_n d_i \sigma_{jm} + a_j a_n d_n d_k \sigma_{ki} + \\
&\qquad a_i a_n d_n d_m \sigma_{jm} + a_k a_n d_n d_j \sigma_{ki})\Big)
\end{aligned} \tag{3.132}$$

Equation (3.132) can be simplified using Equations (3.127), (3.129), (3.86), and (3.87) yielding

$$\begin{aligned}
&2B_4\sigma_{ij} + F_4(d_k d_i \sigma_{jk} + d_j d_m \sigma_{mi}) = 2B_2\sigma_{ij} + D_2(a_k a_i \sigma_{jk} + a_j a_m \sigma_{mi}) \\
&\quad + F_2(d_k d_i \sigma_{jk} + d_j d_m \sigma_{mi}) + H_2\Big(\frac{1}{2}(a_m a_n d_n d_i \sigma_{jm} + a_j a_n d_n d_k \sigma_{ki} + \\
&\qquad a_i a_n d_n d_m \sigma_{jm} + a_k a_n d_n d_j \sigma_{ki})\Big)
\end{aligned} \tag{3.133}$$

In region #2 it was noted earlier that the a_i vector points in the direction of the principle

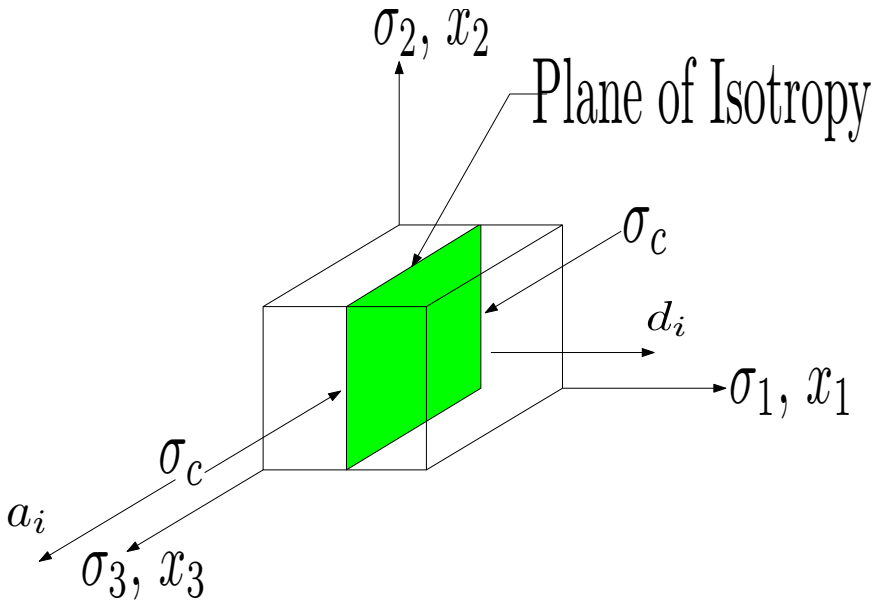

Figure 15: Third Compression Test in the Plane of Isotropy

compressive stress. Thus a_i is defined as

$$a_i = (0, 0, 1) \tag{3.134}$$

The preferred material direction vector is defined by taking the plane of isotropy to coincide with the $\sigma_2 - \sigma_3$ plane. Thus

$$d_i = (1, 0, 0) \tag{3.135}$$

Once again Equation (3.133) is a second order tensor function that is explicitly dependent on cerain invariants and represents six scalar equations. The equations where $i \neq j$ yield $0=0$ and no information is gained. Three scalar equations are obtained for $i = j$.

Solving Equation (3.133) with $i = j = 1$ and $i = j = 2$ yield the scalar identity $0=0$ in both cases and no information is gained. However, for $i = j = 3$ Equation (3.133) yields

$$B_4 = B_2 + D_2 \tag{3.136}$$

Substituting Equation (3.79) into Equation (3.130) yields

$$B_2 = B_3 + D_3 \tag{3.137}$$

Substituting Equation (3.113) into Equation (3.136) yields

$$B_3 = B_2 + D_2 \tag{3.138}$$

Substituting Equation (3.137) into Equation (3.138) yields

$$D_2 = -D_3 \tag{3.139}$$

3.2.3 Relationships Between Coefficients – Uniaxial Tension in the Preferred Material Direction

Before the deriving the relationships between the polynomial coefficients using material tests conducted in the preferred material direction, the threshold functions and their derivatives are simplified. These threshold equations and their derivatives are simplified through the use of Equations (3.86), (3.87), (3.124), and (3.125). Using these four relationships yields

$$f_1 = \frac{1}{2}A_1 I_1^2 + B_1 I_2 + E_1 I_1 I_6 + F_1 I_7 - K^2 \tag{3.140}$$

$$f_2 = \frac{1}{2}A_2 I_1^2 + B_2 I_2 + D_2 I_5 + E_2 I_1 I_6 + F_2 I_7 + H_2 I_9 - K^2 \tag{3.141}$$

$$f_3 = \frac{1}{2}A_3 I_1^2 + B_3 I_2 + D_3 I_5 + E_3 I_1 I_6 + F_3 I_7 + H_3 I_9 - K^2 \tag{3.142}$$

and

$$f_4 = \frac{1}{2}A_4 I_1^2 + B_4 I_2 + E_4 I_1 I_6 + F_4 I_7 - K^2 \tag{3.143}$$

The coresponding tangents to these threshold surfaces are as follows

$$\begin{aligned}\frac{\partial f_1}{\partial \sigma_{ij}} &= (A_1 I_1 + E_1 I_6)\delta_{ij} + 2B_1\sigma_{ij} \\ &\quad + E_1 I_1 d_i d_j + F_1(d_k d_i \sigma_{jk} + d_j d_m \sigma_{mi})\end{aligned} \tag{3.144}$$

$$\begin{aligned}\frac{\partial f_2}{\partial \sigma_{ij}} &= (A_2 I_1 + E_2 I_6)\delta_{ij} + 2B_2\sigma_{ij} + D_2(a_k a_i \sigma_{jk} + a_j a_m \sigma_{mi}) + \\ &\quad E_2 I_1 d_i d_j + F_2(d_k d_i \sigma_{jk} + d_j d_m \sigma_{mi}) + H_2\Big(\frac{1}{2}(a_m a_n d_n d_i \sigma_{jm} + \\ &\quad a_j a_n d_n d_k \sigma_{ki} + a_i a_n d_n d_m \sigma_{jm} + a_k a_n d_n d_j \sigma_{ki})\Big)\end{aligned} \tag{3.145}$$

$$\begin{aligned}\frac{\partial f_3}{\partial \sigma_{ij}} &= (A_3 I_1 + E_3 I_6)\delta_{ij} + 2B_3\sigma_{ij} + D_3(a_k a_i \sigma_{jk} + a_j a_m \sigma_{mi}) + \\ &\quad E_3 I_1 d_i d_j + F_3(d_k d_i \sigma_{jk} + d_j d_m \sigma_{mi}) + H_3\Big(\frac{1}{2}(a_m a_n d_n d_i \sigma_{jm} + \\ &\quad a_j a_n d_n d_k \sigma_{ki} + a_i a_n d_n d_m \sigma_{jm} + a_k a_n d_n d_j \sigma_{ki})\Big)\end{aligned} \tag{3.146}$$

and

$$\begin{aligned}\frac{\partial f_4}{\partial \sigma_{ij}} &= (A_4 I_1 + E_4 I_6)\delta_{ij} + 2B_4\sigma_{ij} \\ &\quad + E_4 I_1 d_i d_j + F_4(d_k d_i \sigma_{jk} + d_j d_m \sigma_{mi})\end{aligned} \tag{3.147}$$

The next test considered is a uniaxial tension test in the preferred material direction. For a uniaxial tensile test in the preferred material direction where the applied stress is equal to the threshold stress, i.e.,

$$\sigma_{ij} = \begin{bmatrix} \sigma_{st} & 0 & 0 \\ 0 & 0 & 0 \\ 0 & 0 & 0 \end{bmatrix} \tag{3.148}$$

This stress state satisfies inequalities associated with region #1, region #2, and region #3

since

$$\sigma_1 = \sigma_{st} \geq \sigma_2 = 0 \geq \sigma_3 = 0 \tag{3.149}$$

The threshold function along the boundaries of region #1, region #2, and region #3 must satisfy the relationships

$$f_1 = f_2 = f_3 \tag{3.150}$$

for this uniaxial tension test. In addition the derivatives of the function along the boundaries of region #1, region #2, and region #3 must satisfy

$$\frac{\partial f_1}{\partial \sigma_{ij}} = \frac{\partial f_2}{\partial \sigma_{ij}} = \frac{\partial f_3}{\partial \sigma_{ij}} \tag{3.151}$$

for the uniaxial tensile test in the preferred material direction.

Focusing on the derivatives along the boundary between region #1 and region #2 then

$$\frac{\partial f_1}{\partial \sigma_{ij}} = \frac{\partial f_2}{\partial \sigma_{ij}} \tag{3.152}$$

This relationship yields the following tensor expression

$$\begin{aligned}
&(A_1 I_1 + E_1 I_6)\delta_{ij} + 2B_1\sigma_{ij} + E_1 I_1 d_i d_j + F_1(d_k d_i \sigma_{jk} + d_j d_m \sigma_{mi}) = \\
&\quad A_2 I_1 + E_2 I_6)\delta_{ij} + 2B_2\sigma_{ij} + D_2(a_k a_i \sigma_{jk} + a_j a_j \sigma_{mi}) + E_2 I_1 d_i d_j \\
&\quad + F_2(d_k d_i \sigma_{jk} + d_j d_m \sigma_{mi}) + H_2\Big(\frac{1}{2}(a_m a_n d_n d_i \sigma_{jm} + a_j a_n d_n d_k \sigma_{ki} + \\
&\qquad a_i a_n d_n d_m \sigma_{jm} + a_k a_n d_n d_j \sigma_{ki})\Big)
\end{aligned} \tag{3.153}$$

For region #1 the function, f_1, does not depend on a principle direction. For region #2 the function, f_2 does depend on the direction vector a_i which is defined as

$$a_i = (0, 0, 1) \tag{3.154}$$

The vector, d_i which points in the preferred material direction is will be taken in the direc-

tion of the applied stress in this section, i.e.,

$$d_i = (1, 0, 0) \tag{3.155}$$

Equation (3.153) is a second order tensor function that is explicitly on certain invariants and represents six scalar equation. The equations where $i \neq j$ yield the scalar identity $0=0$ and no information is gained. For $i = j$ we obtain three scalar relationships.

The state of stress and the material direction are depicted in Figure 16. Simplifying Equation (3.153) using Equations (3.79), (3.77), and (3.84) yields

$$\begin{aligned} F_1(d_k d_i \sigma_{jk} + d_j d_m \sigma_{mi}) = D_2(a_k a_i \sigma_{jk} + a_j a_m \sigma_{mi}) + \\ F_2(d_k d_i \sigma_{jk} + d_j d_m \sigma_{mi}) + H_2\Big(\frac{1}{2}(a_m a_n d_n d_i \sigma_{jm} + a_j a_n d_n d_k \sigma_{ki} + \\ a_i a_n d_n d_m \sigma_{jm} + a_k a_n d_n d_j \sigma_{ki})\Big) \end{aligned} \tag{3.156}$$

For Equation (3.156) $i = j = 1$ results in

$$F_1 = F_2 \tag{3.157}$$

With $i = j = 2$ and $i = j = 3$ Equation (3.156) yields the scalar identity $0 = 0$ and no information is gained.

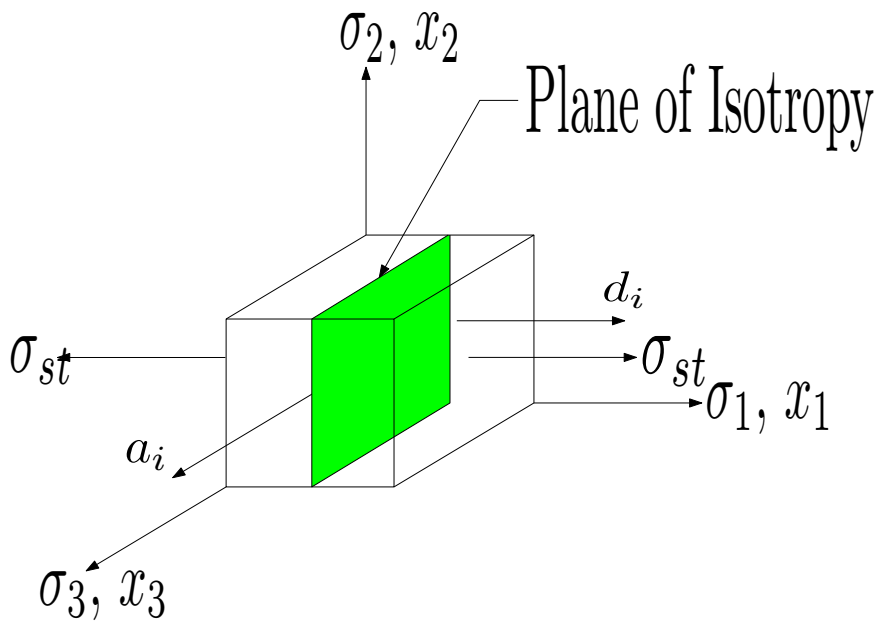

Figure 16: Tensile Test in the Preferred Material Direction

Next, the argument above is repeated for the derivatives along the shared boundary of region #1 and region #3 where

$$\frac{\partial f_1}{\partial \sigma_{ij}} = \frac{\partial f_3}{\partial \sigma_{ij}} \tag{3.158}$$

for the same uniaxial tension test in the preferred material direction. This yields the following tensor expression

$$\begin{aligned}(A_1 I_1 + E_1 I_6)\delta_{ij} + 2B_1\sigma_{ij} + E_1 I_1 d_i d_j + F_1(d_k d_i \sigma_{jk} + d_j d_m \sigma_{mi}) = \\ (A_3 I_1 + E_3 I_6)\delta_{ij} + 2B_3\sigma_{ij} + D_3(a_k a_i \sigma_{jk} + a_j a_j \sigma_{mi}) + E_3 I_1 d_i d_j \\ + F_3(d_k d_i \sigma_{jk} + d_j d_m \sigma_{mi}) + H_3\Big(\frac{1}{2}(a_m a_n d_n d_i \sigma_{jm} + a_j a_n d_n d_k \sigma_{ki} + \\ a_i a_n d_n d_m \sigma_{jm} + a_k a_n d_n d_j \sigma_{ki})\Big)\end{aligned} \tag{3.159}$$

Equation (3.159) is simplified by using Equations (3.126) and (3.128) yielding the follow-

ing tensor expression

$$2B_1\sigma_{ij}+F_1(d_kd_i\sigma_{jk}+d_jd_m\sigma_{mi}) = 2B_3\sigma_{ij}+D_3(a_ka_i\sigma_{jk}+a_ja_m\sigma_{mi})+ F_3(d_kd_i\sigma_{jk}+d_jd_m\sigma_{mi})+H_3\Big(\frac{1}{2}(a_ma_nd_nd_i\sigma_{jm}+a_ja_nd_nd_k\sigma_{ki}+ a_ia_nd_nd_m\sigma_{jm}+a_ka_nd_nd_j\sigma_{ki})\Big) \tag{3.160}$$

In region #3 it was noted earlier that the vector a_i is defined as

$$a_i = (1,0,0) \tag{3.161}$$

Due to the symmetry of the second order tensors that appear in this expression Equation (3.160) represents six scalar equations. The equations where $i \neq j$ yield the scalar identity $0=0$ and no information is gained. Three scalar equations are obtained when $i = j$.

For $i = j = 1$ Equation (3.160) yields

$$B_1 + F_1 = B_3 + D_3 + F_3 + H_3 \tag{3.162}$$

Substituting Equation (3.130) into Equation (3.162) yields

$$F_1 = F_3 + H_3 \tag{3.163}$$

With $i = j = 2$ and $i = j = 3$ Equation (3.160) simplifies to the scalar identity $0=0$ and no information is gained.

3.2.4 Relationships Between Coefficients – Uniaxial Compression in the Preferred Material Direction

The next test considered is a uniaxial compression test in the preferred material direction. When the applied stress is equal to the threshold stress the Cauchy stress tensor take the

form

$$\sigma_{ij} = \begin{bmatrix} 0 & 0 & 0 \\ 0 & 0 & 0 \\ 0 & 0 & \sigma_{sc} \end{bmatrix} \tag{3.164}$$

This stress state satisfies the inequalities associated with region #2, region #3, and region #4 since

$$\sigma_1 = 0 \geq \sigma_2 = 0 \geq \sigma_3 = \sigma_{sc} \tag{3.165}$$

The threshold function along the boundaries of region #2, region #3, and region #4 must satisfy the relationships

$$f_2 = f_3 = f_4 \tag{3.166}$$

for a uniaxial compression test in the preferred material direction. In addition the derivatives of the functions along the boundaries between region #2, region #3, and region #4 must satisfy

$$\frac{\partial f_2}{\partial \sigma_{ij}} = \frac{\partial f_3}{\partial \sigma_{ij}} = \frac{\partial f_4}{\partial \sigma_{ij}} \tag{3.167}$$

for a uniaxial tensile test in the preferred material direction.

Focusing on the derivatives along the boundary between region #4 and region #3 then

$$\frac{\partial f_3}{\partial \sigma_{ij}} = \frac{\partial f_4}{\partial \sigma_{ij}} \tag{3.168}$$

This relationship yields the following tensor expression

$$\begin{aligned} &(A_4 I_1 + E_4 I_6)\delta_{ij} + 2B_4\sigma_{ij} + E_4 I_1 d_i d_j + F_4(d_k d_i \sigma_{jk} + d_j d_m \sigma_{mi}) = \\ &\quad (A_3 I_1 + E_3 I_6)\delta_{ij} + 2B_3\sigma_{ij} + D_3(a_k a_i \sigma_{jk} + a_j a_j \sigma_{mi}) + E_3 I_1 d_i d_j + \\ &\quad F_3(d_k d_i \sigma_{jk} + d_j d_m \sigma_{mi}) + H_3\Big(\frac{1}{2}(a_m a_n d_n d_i \sigma_{jm} + a_j a_n d_n d_k \sigma_{ki} + \\ &\qquad a_i a_n d_n d_m \sigma_{jm} + a_k a_n d_n d_j \sigma_{ki})\Big) \end{aligned} \tag{3.169}$$

Which simplifies to

$$F_4(d_k d_i \sigma_{jk} + d_j d_m \sigma_{mi}) = D_3(a_k a_i \sigma_{jk} + a_j a_m \sigma_{mi}) + F_3(d_k d_i \sigma_{jk} + d_j d_m \sigma_{mi}) + H_3\Big(\frac{1}{2}(a_m a_n d_n d_i \sigma_{jm} + a_j a_n d_n d_k \sigma_{ki} + a_i a_n d_n d_m \sigma_{jm} + a_k a_n d_n d_j \sigma_{ki})\Big) \tag{3.170}$$

by substituting Equations (3.111), (3.113), and (3.122) into Equation (3.169). For region #4 the function, f_4, does not depend on a principle direction. In region #3 the function, f_3 does depend on the direction vector a_i which is defined as

$$a_i = (1, 0, 0) \tag{3.171}$$

In this section the vector d_i is taken in the direction of the applied stress, i.e.,

$$d_i = (0, 0, 1) \tag{3.172}$$

Due to symmetry of the second order stress tensors that appear in this expression Equation (3.169) represents six scalar equations. The equations where $i \neq j$ yield the scalar identity $0=0$ and no information is gained. For $i = j$ we obtain three scalar relationships.

The state of stress and material direction are depicted in Figure 17 With $i = j = 1$ and $i = j = 2$ Equation (3.170) reduces to the scalar identity $0=0$ and no information is gained. For $i = j = 3$ Equation (3.170) yields

$$F_4 = F_3 \tag{3.173}$$

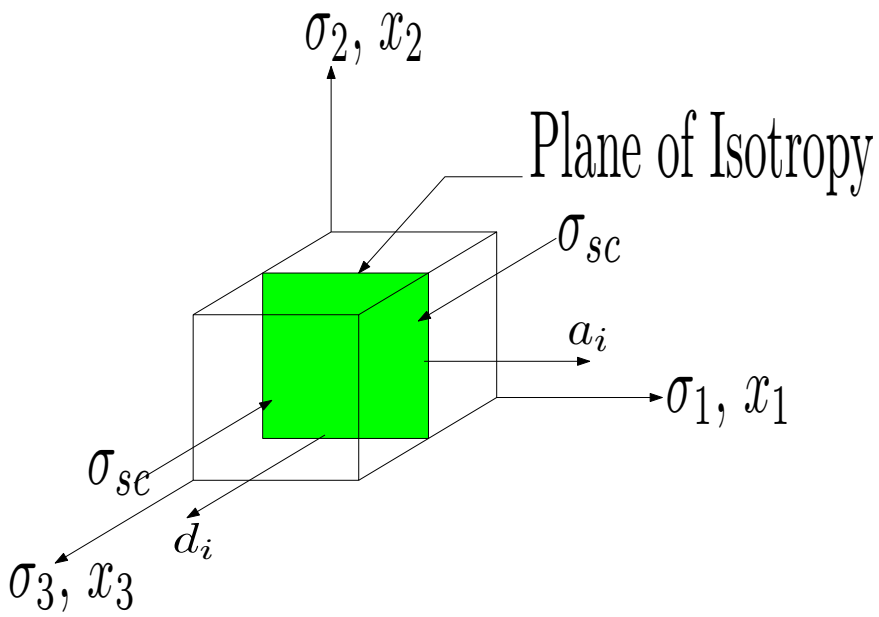

Figure 17: Compression Test in the Preferred Material Direction

Next, the argument above is repeated for the derivatives along the shared boundary between region #4 and region #2 where

$$\frac{\partial f_2}{\partial \sigma_{ij}} = \frac{\partial f_4}{\partial \sigma_{ij}} \tag{3.174}$$

for the same uniaxial compression test in the preferred material direction. This yields the following tensor expression

$$\begin{aligned}
&(A_4 I_1 + E_4 I_6)\delta_{ij} + 2B_4\sigma_{ij} + E_4 I_1 d_i d_j + F_4(d_k d_i \sigma_{jk} + d_j d_m \sigma_{mi}) = \\
&\quad (A_2 I_1 + E_2 I_6)\delta_{ij} + 2B_2\sigma_{ij} + D_2(a_k a_i \sigma_{jk} + a_j a_j \sigma_{mi}) + E_2 I_1 d_i d_j + \\
&\quad F_2(d_k d_i \sigma_{jk} + d_j d_m \sigma_{mi}) + H_2\Big(\frac{1}{2}(a_m a_n d_n d_i \sigma_{jm} + a_j a_n d_n d_k \sigma_{ki} + \\
&\qquad a_i a_n d_n d_m \sigma_{jm} + a_k a_n d_n d_j \sigma_{ki})\Big)
\end{aligned} \tag{3.175}$$

This tensor equation can be simplified using Equations (3.126) and (3.128) yielding

$$\begin{aligned} 2B_4\sigma_{ij} + F_4(d_k d_i \sigma_{jk} + d_j d_m \sigma_{mi}) = 2B_2\sigma_{ij} + D_2(a_k a_i \sigma_{jk} + a_j a_m \sigma_{mi}) + \\ F_2(d_k d_i \sigma_{jk} + d_j d_m \sigma_{mi}) + H_2\Big(\frac{1}{2}(a_m a_n d_n d_i \sigma_{jm} + a_j a_n d_n d_k \sigma_{ki} + \\ a_i a_n d_n d_m \sigma_{jm} + a_k a_n d_n d_j \sigma_{ki})\Big) \end{aligned} \tag{3.176}$$

Due to the symmetry of the second order tensors appearing in this expression Equation (3.176) represents six scalar equations. The equations where $i \neq j$ yield the scalar identity $0=0$ and no information is gained. However, three scalar equations are obtained for $i = j$.

For $i = j = 1$ and $i = j = 2$ Equation (3.176) yields the scalar identity $0=0$ and no information is gained. For $i = j = 3$ Equation (3.176) yields

$$B_4 + F_4 = B_2 + D_2 + F_2 + H_2 \tag{3.177}$$

Substituting Equation (3.136) into Equation (3.177) yields

$$F_4 = F_2 + H_2 \tag{3.178}$$

Substituting Equations (3.157), (3.163), and (3.173) into Equation (3.178) yields

$$H_2 = -H_3 \tag{3.179}$$

This expression represents the last relationship involving the unknown polynomial coefficients of the threshold function. In this section the number of coefficients have been reduced and it was shown that the coefficients were not independent of one another. The six polynomial coefficients that are independant are identified in the next section and they are expressed in terms of the simple mechanical tests identified earlier.

3.3 Functional Coefficients in Terms of Mechanical Tests

The following relationships between the functional constants were developed in the previous sections

$$A_1 = A_2 = A_3 = A_4 \tag{3.180}$$

$$B_1 = B_2 \tag{3.181}$$

$$B_1 = B_3 + D_3 \tag{3.182}$$

$$B_3 = B_4 \tag{3.183}$$

$$B_4 = B_2 + D_2 \tag{3.184}$$

$$C_2 = C_3 = G_2 = G_3 = 0 \tag{3.185}$$

$$D_2 = -D_3 \tag{3.186}$$

$$E_1 = E_2 = E_3 = E_4 \tag{3.187}$$

$$F_1 = F_2 \tag{3.188}$$

$$F_1 = F_3 + H_3 \tag{3.189}$$

$$F_3 = F_4 \tag{3.190}$$

$$F_4 = F_2 + H_2 \tag{3.191}$$

and

$$H_2 = -H_3 \tag{3.192}$$

Note that G_2 and G_3, the leading coefficients for the I_8 invariant in the threshold function are both zero. Hence I_8 never enters into the functional dependence.

With the relationships among the functional constants determined in the previous section and summarized in Equations (3.180) through (3.192), the threshold function are be expressed as

$$f_1 = \frac{1}{2}A_1 I_1^2 + B_1 I_2 + E_1 I_1 I_6 + F_1 I_7 - 1 \tag{3.193}$$

$$f_2 = \frac{1}{2}A_1 I_1^2 + B_1 I_2 + E_1 I_1 I_6 + F_1 I_7 + D_2 I_5 + H_2 I_9 - 1 \tag{3.194}$$

$$\begin{aligned} f_3 = \frac{1}{2}A_1 I_1^2 + (B_1 + D_2) I_2 + E_1 I_1 I_6 + (F_1 + H_2) I_7 \\ + (-D_2) I_5 + (-H_2) I_9 - 1 \end{aligned} \tag{3.195}$$

and

$$f_4 = \frac{1}{2}A_1 I_1^2 + (B_1 + D_2) I_2 + E_1 I_1 I_6 + (F_1 + H_2) I_7 - 1 \tag{3.196}$$

From these last four equations we see that only six polynomial coefficients, i.e., A_1, B_1, D_2, E_1, F_1, and H_2 require characterization in terms of mechanical tests.

As can be discerned from Equations (3.180) through (3.192) these polynomial coefficients are not related to one another. The six mechanical tests needed to define the six

independent coefficients were identified earlier. The mechanical tests are uniaxial tension in the plane of isotropy (σ_t), uniaxial tension in the preferred material direction (σ_{st}), uniaxial compression in the plane of isotropy (σ_c), uniaxial compression in the preferred material direction (σ_{sc}), torsion in the plane on isotropy (τ_i), and torsion across the plane of isotropy (τ_s). These tests are assumed to be performed on a virgin material. For a virgin material the state variable K is equal to one.

For a uniaxial tensile in the plane of isotropy where the stress applied is equal to the tensile threshold stress

$$\sigma_{ij} = \begin{bmatrix} \sigma_t & 0 & 0 \\ 0 & 0 & 0 \\ 0 & 0 & 0 \end{bmatrix} \tag{3.197}$$

For this test the plane of isotropy will be the $\sigma_1 - \sigma_2$ plane. Thus the d_i vector is defined as

$$d_i = (0, 0, 1) \tag{3.198}$$

For a uniaxial tensile test the a_i is defined as

$$a_i = (0, 0, 1) \tag{3.199}$$

The state of stress and material orientation were depicted earlier in Figure 10. With this information the invariant from the transversely isotropic integrity basis are

$$I_1 = \sigma_t \tag{3.200}$$

$$I_2 = \sigma_t^2 \tag{3.201}$$

$$I_6 = 0 \tag{3.202}$$

and

$$I_7 = 0 \tag{3.203}$$

Setting Equation (3.193) equal to zero with K equal to one yields

$$\begin{aligned} f_1 &= \frac{1}{2}A_1\sigma_t^2 + B_1\sigma_t^2 - 1 \\ &= 0 \end{aligned} \tag{3.204}$$

Rearranging this equation yields

$$\frac{1}{2}A_1 + B_1 = \frac{1}{\sigma_t^2} \tag{3.205}$$

The next test utilized in identifying the unknown constants is a uniaxial compression test in the plane of isotropy where the applied stress is equal to the compressive threshold stress. Hence,

$$\sigma_{ij} = \begin{bmatrix} \sigma_c & 0 & 0 \\ 0 & 0 & 0 \\ 0 & 0 & 0 \end{bmatrix} \tag{3.206}$$

For this test the plane of isotropy will be the $\sigma_1 - \sigma_2$ plane. Thus the d_i vector is defined as

$$d_i = (0, 0, 1) \tag{3.207}$$

For a uniaxial compression test in the σ_1 direction the a_i vector is defined as

$$a_i = (0, 0, 1) \tag{3.208}$$

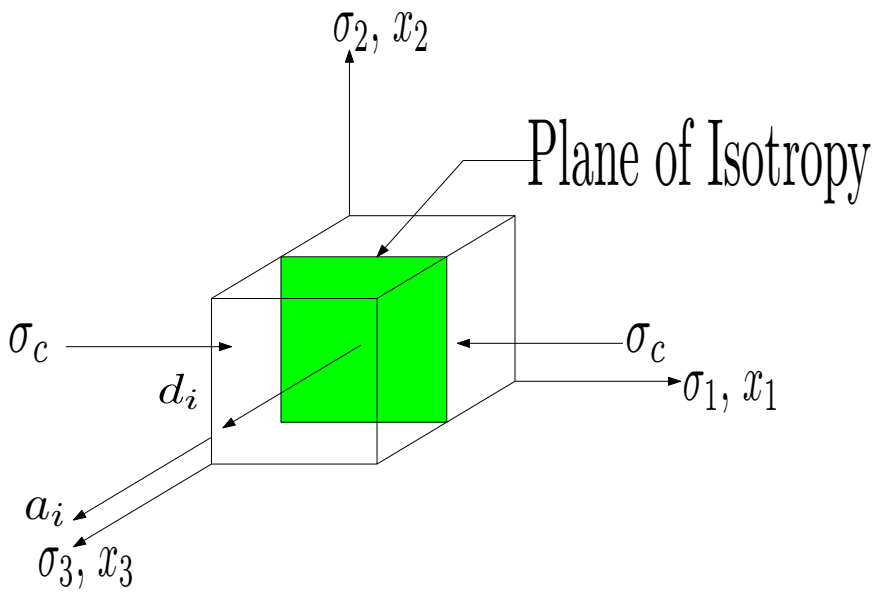

Figure 18: Compression Test in the Plane of Isotropy

The state of stress and material orientation are depicted in Figure 18. With this information the invariants from the transversely isotropic integrity bases are

$$I_1 = \sigma_c \tag{3.209}$$

$$I_2 = \sigma_c^2 \tag{3.210}$$

$$I_6 = 0 \tag{3.211}$$

and

$$I_7 = 0 \tag{3.212}$$

Setting Equation (3.196) equal to zero with K equal to one yields

$$\begin{aligned} f_4 &= \frac{1}{2}A_1\sigma_c^2 + (B_1 + D_2)\sigma_c^2 - 1 \\ &= 0 \end{aligned} \tag{3.213}$$

Rewriting this equation yields

$$\frac{1}{2}A_1 + B_1 + D_2 = \frac{1}{\sigma_c^2} \tag{3.214}$$

The next test is a torsion test in the plane of isotropy where the applied stress is equal to the threshold stress. Where,

$$\sigma_{ij} = \begin{bmatrix} 0 & \tau_i & 0 \\ \tau_i & 0 & 0 \\ 0 & 0 & 0 \end{bmatrix} \tag{3.215}$$

For this test the plane of isotropy will be the $\sigma_1 - \sigma_2$ plane. Thus the d_i vector is defined as

$$d_i = (0, 0, 1) \tag{3.216}$$

For biaxial compression the a_i vector is defined as

$$a_i = (-\frac{\sqrt{2}}{2}, \frac{\sqrt{2}}{2}, 0) \tag{3.217}$$

The state of stress and material orientation are depicted in Figure **??**. With this information the invariants from the transversely isotropic integrity basis are

$$I_1 = 0 \tag{3.218}$$

$$I_2 = 2\tau_i^2 \tag{3.219}$$

$$I_5 = \tau_i^2 \tag{3.220}$$

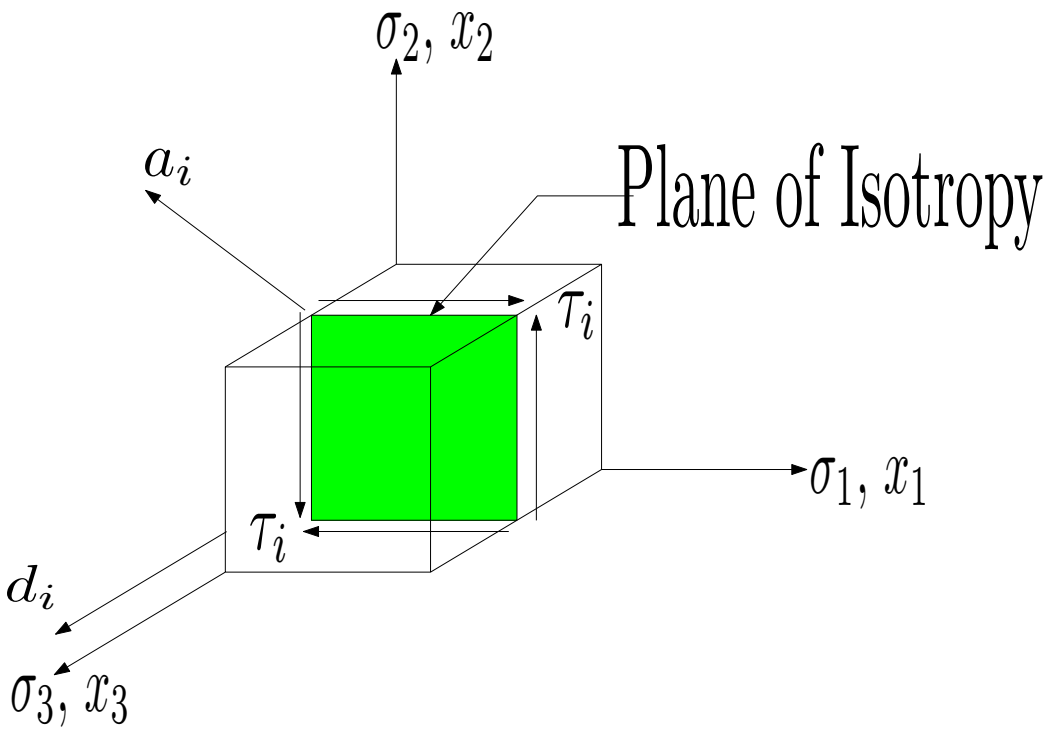

Figure 19: Torsion Test in the Plane of Isotropy

$$I_6 = 0 \tag{3.221}$$

and

$$I_7 = 0 \tag{3.222}$$

$$I_9 = 0 \tag{3.223}$$

Setting Equation (3.196) equal to zero with K equal to one yields

$$\begin{aligned} f_2 &= 2B_1\tau_i^2 + D_2\tau_i^2 - 1 \\ &= 0 \end{aligned} \tag{3.224}$$

Rewriting this equation yield

$$2B_1 + D_2 = \frac{1}{\tau_i^2} \tag{3.225}$$

Equations (3.205), (3.214), and (3.225) are the same equations obtained in the previous chapter. This is reasonable since all applied stresses are contained in the plane of isotropy. As before solving these three equation simultaneously yields.

$$A_1 = \frac{1}{\sigma_c^2} + \frac{1}{\sigma_t^2} - \frac{1}{\tau_i^2} \tag{3.226}$$

$$B_1 = \frac{1}{2\sigma_t^2} - \frac{1}{2\sigma_c^2} + \frac{1}{2\tau_i^2} \tag{3.227}$$

and

$$D_2 = \frac{1}{\sigma_c^2} - \frac{1}{\sigma_t^2} \tag{3.228}$$

The polynomial coefficients, A_1, B_1, and D_2, are equal to their respective polynomial coefficients developed in the isotropic derivation found in the previous chapter.

The next material test is a uniaxial tensile test in the preferred direction where the applied stress is equal to the threshold stress. Here the Cauchy stress tensor takes the form

$$\sigma_{ij} = \begin{bmatrix} \sigma_{st} & 0 & 0 \\ 0 & 0 & 0 \\ 0 & 0 & 0 \end{bmatrix} \tag{3.229}$$

Since this material test is in the preferred material direction, the d_i vector is defined as

$$d_i = (1, 0, 0) \tag{3.230}$$

For a uniaxial tensile test in the σ_1 direction the a_i vector is defined as

$$a_i = (0, 0, 1) \tag{3.231}$$

The state of stress and material orientation are depicted in Figure 20. With this information

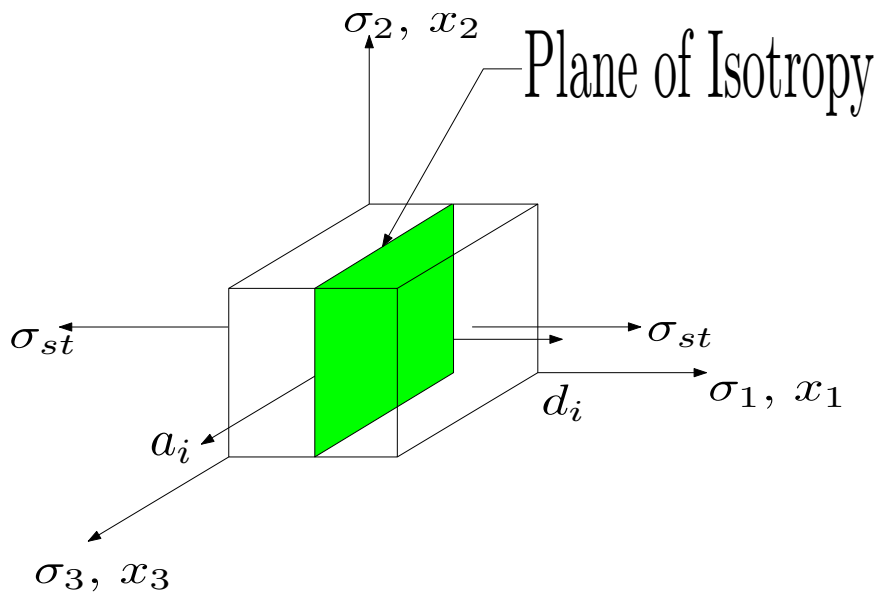

Figure 20: Tensile Test in the Preferred Material Direction

the invariants from the transversely isotropic integrity basis are

$$I_1 = \sigma_{st} \tag{3.232}$$

$$I_2 = \sigma_{st}^2 \tag{3.233}$$

$$I_6 = \sigma_{st} \tag{3.234}$$

and

$$I_7 = \sigma_{st}^2 \tag{3.235}$$

Setting Equation (3.193) equal to zero with K equal to one yields

$$\begin{aligned} f_1 &= \frac{1}{2}A_1\sigma_{st}^2 + B_1\sigma_{st}^2 + E_1\sigma_{st}^2 + F_1\sigma_{st}^2 - 1 \\ &= 0 \end{aligned} \tag{3.236}$$

Rewriting this equation yields

$$\frac{1}{2}A_1 + B_1 + E_1 + F_1 = \frac{1}{\sigma_{st}^2} \tag{3.237}$$

Next consider a material test where uniaxial compression is applied in the preferred direction. Here the Cauchy stress tensor is

$$\sigma_{ij} = \begin{bmatrix} \sigma_{sc} & 0 & 0 \\ 0 & 0 & 0 \\ 0 & 0 & 0 \end{bmatrix} \tag{3.238}$$

Since this material test is in the preferred material direction the d_i vector is defined as

$$d_i = (1, 0, 0) \tag{3.239}$$

For a compression test in the σ_1 direction the a_i vector is defined as

$$a_i = (0, 0, 1) \tag{3.240}$$

The state of stress and material orientation are depicted in Figure 21. With this information the invariants for the transversely isotropic integrity basis are

$$I_1 = \sigma_{sc} \tag{3.241}$$

$$I_2 = \sigma_{sc}^2 \tag{3.242}$$

$$I_6 = \sigma_{sc} \tag{3.243}$$

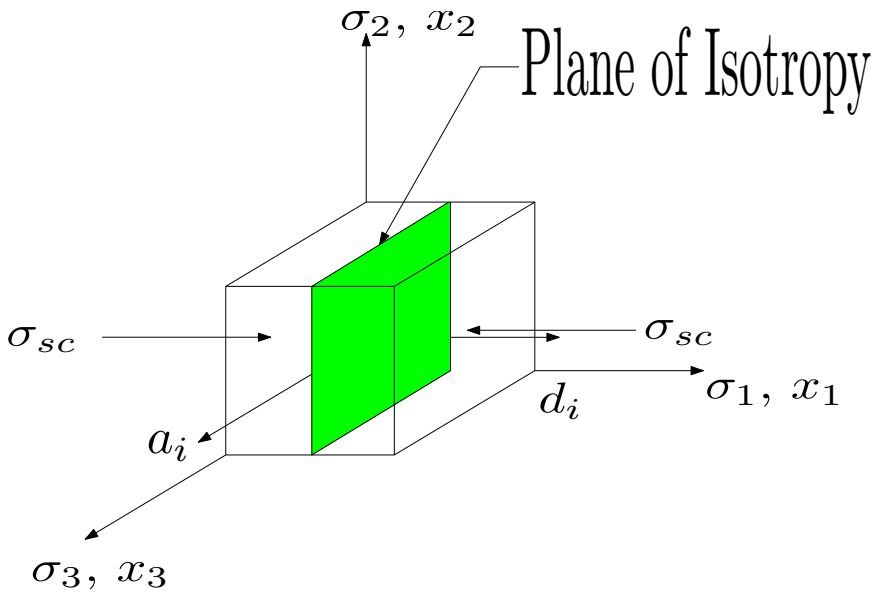

Figure 21: Compression Test in the Preferred Material Direction

and

$$I_7 = \sigma_{sc}^2 \tag{3.244}$$

Setting Equation (3.196) equal to zero with K equal to one yields

$$\begin{aligned} f_4 &= \frac{1}{2}A_1\sigma_{sc}^2 + (B_1 + D_2)\sigma_{sc}^2 + E_1\sigma_{sc}^2 + (F_1 + H_2)\sigma_{sc}^2 - 1 \\ &= 0 \end{aligned} \tag{3.245}$$

Rearranging this equation yields

$$\frac{1}{2}A_1 + B_1 + D_2 + E_1 + F_1 + H_2 = \frac{1}{\sigma_{sc}^2} \tag{3.246}$$

Finally, consider a torsion test where the torque is applied across the plane of isotropy. Here the Cauchy stress tensor is

$$\sigma_{ij} = \begin{bmatrix} 0 & \tau_s & 0 \\ \tau_s & 0 & 0 \\ 0 & 0 & 0 \end{bmatrix} \tag{3.247}$$

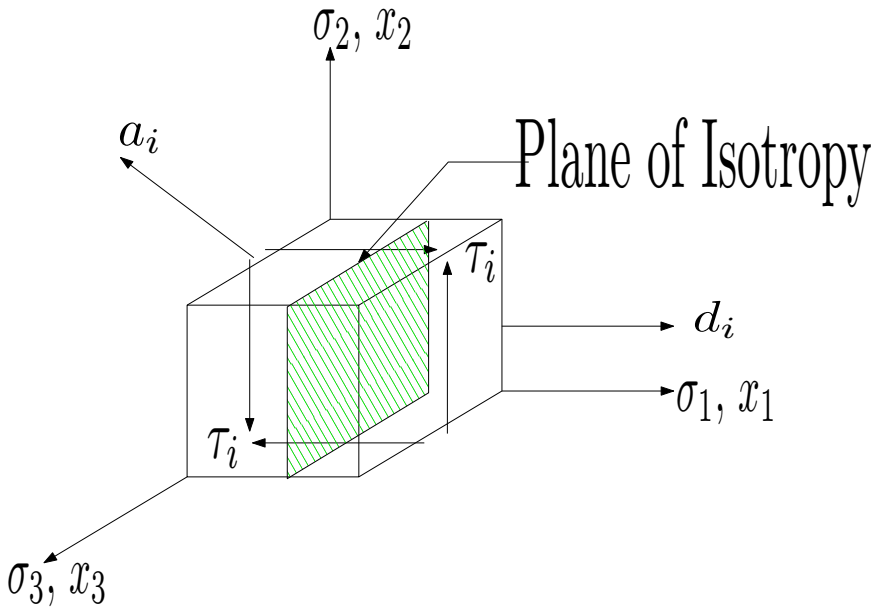

Figure 22: Torsion Test across the Plane of Isotropy

With

$$d_i = (1, 0, 0) \tag{3.248}$$

and for this last test the a_i vector is defined as

$$a_i = (-\frac{\sqrt{2}}{2}, \frac{\sqrt{2}}{2}, 0) \tag{3.249}$$

The state of stress and material orientation are depicted in Figure 22. With this information the invariants for the transversely isotropic integrity basis are

$$I_1 = 0 \tag{3.250}$$

$$I_2 = 2\tau_s^2 \tag{3.251}$$

$$I_5 = \tau_s^2 \tag{3.252}$$

$$I_6 = 0 \tag{3.253}$$

$$I_7 = \tau_s^2 \tag{3.254}$$

and

$$I_9 = \frac{1}{2}\tau_s^2 \tag{3.255}$$

Setting Equation (3.196) equal to zero with K equal to one yields

$$\begin{aligned} f_2 &= 2B_1\tau_s^2 + D_2\tau_s^2 + F_1\tau_s^2 + \frac{1}{2}H_2\tau_s^2 - 1 \\ &= 0 \end{aligned} \tag{3.256}$$

Rearranging this equation yields

$$2B_1 + D_2 + F_1 + \frac{1}{2}H_2 = \frac{1}{\tau_s^2} \tag{3.257}$$

Solving Equations (3.237), (3.246), and (3.257) simultaneously results in

$$E_1 = \frac{1}{2\sigma_{sc}^2} - \frac{1}{2\sigma_c^2} + \frac{1}{2\sigma_{st}^2} - \frac{1}{2\sigma_t^2} + \frac{1}{\tau_i^2} - \frac{1}{\tau_s^2} \tag{3.258}$$

$$F_1 = \frac{1}{2\sigma_c^2} - \frac{1}{2\sigma_{sc}^2} + \frac{1}{2\sigma_{st}^2} - \frac{1}{2\sigma_t^2} - \frac{1}{\tau_i^2} + \frac{1}{\tau_s^2} \tag{3.259}$$

and

$$H_2 = \frac{1}{\sigma_{sc}^2} - \frac{1}{\sigma_c^2} - \frac{1}{\sigma_{st}^2} + \frac{1}{\sigma_t^2} \tag{3.260}$$

Summarizing

$$A_1 = \frac{1}{\sigma_c^2} + \frac{1}{\sigma_t^2} - \frac{1}{\tau_i^2} \tag{3.261}$$

$$B_1 = \frac{1}{2}\left(\frac{1}{\sigma_t^2} - \frac{1}{\sigma_c^2} + \frac{1}{\tau_i^2}\right) \tag{3.262}$$

$$D_2 = \frac{1}{\sigma_c^2} - \frac{1}{\sigma_t^2} \tag{3.263}$$

$$E_1 = \frac{1}{2\sigma_{sc}^2} - \frac{1}{2\sigma_c^2} + \frac{1}{2\sigma_{st}^2} - \frac{1}{2\sigma_t^2} + \frac{1}{\tau_i^2} - \frac{1}{\tau_s^2} \tag{3.264}$$

$$F_1 = \frac{1}{2\sigma_c^2} - \frac{1}{2\sigma_{sc}^2} + \frac{1}{2\sigma_{st}^2} - \frac{1}{2\sigma_t^2} - \frac{1}{\tau_i^2} + \frac{1}{\tau_s^2} \tag{3.265}$$

and

$$H_2 = \frac{1}{\sigma_{sc}^2} - \frac{1}{\sigma_c^2} - \frac{1}{\sigma_{st}^2} + \frac{1}{\sigma_t^2} \tag{3.266}$$

The next set of figures use the following material parameters. The material parameters are $\sigma_t = 1.048$, $\sigma_c = 3.5$, $\tau_i = 1.0$, $\sigma_{st} = 1.593$, $\sigma_{sc} = 5.293$, and $\tau_s = 1.15$. These values for the different material tests are for H451 graphite as estimated from Burchell (2007). Figure 23 shows the threshold surface with the material direction set to $d_i = (1, 0, 0)$. In Figure 23, it is shown that the tensile and compressive threshold stresses intersect at the principle stress axis. Figure 24 shows the threshold surface in the σ_{11}, σ_{12} plane with the material direction set to $d_i = (1, 0, 0)$. In this figure the values cross the axis at the threshold stresses. Figure 25 shows the threshold surface in the σ_{22}, σ_{23} plane with the material directcion set to $d_i = (1, 0, 0)$. In this figure the values cross the axis at the threshold stresses. Figure 26 shows the effect on the threshold surface of varying the direction of the d_i vector. The directions for the material direction vectors in the $\sigma_1 - \sigma_2$ plane are d_i, are 0^o, 45^o, and 90^o as measured from the σ_1 direction. Also shown in Figure 26 is a threshold surface in the plane of isotropy.

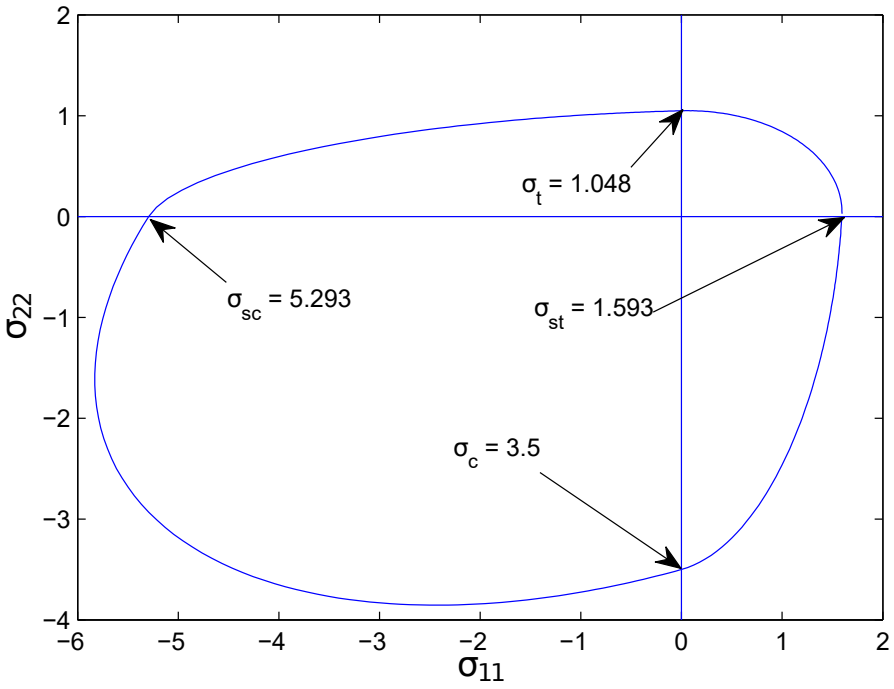

Figure 23: Anisotropic threshold surfaces in the σ_1, σ_2 stress space with $d_i = (1, 0, 0)$

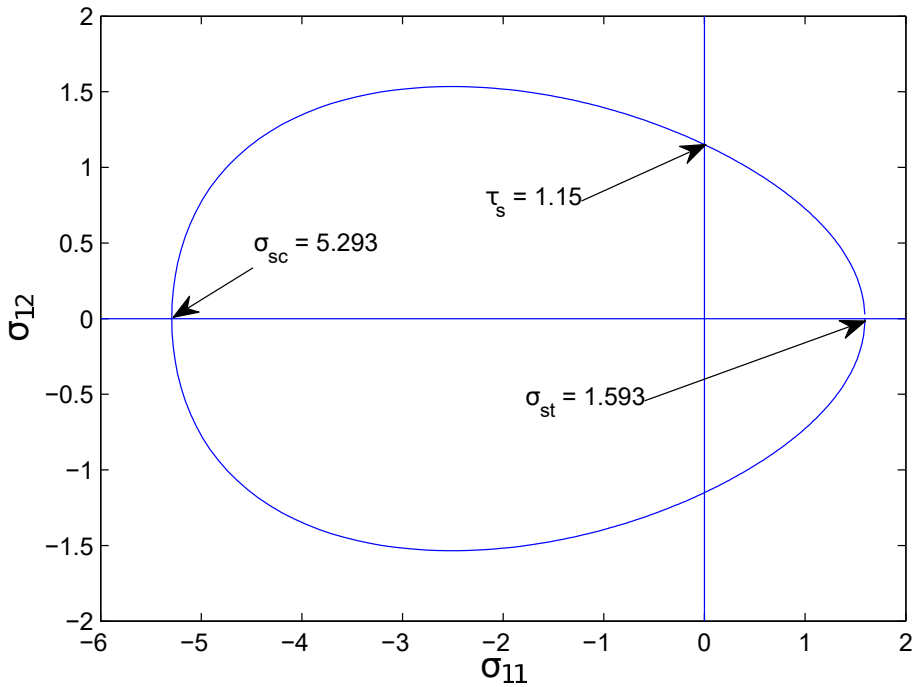

Figure 24: Anisotropic threshold surfacesin the σ_{11}, σ_{12} stress space with $d_i = (1, 0, 0)$

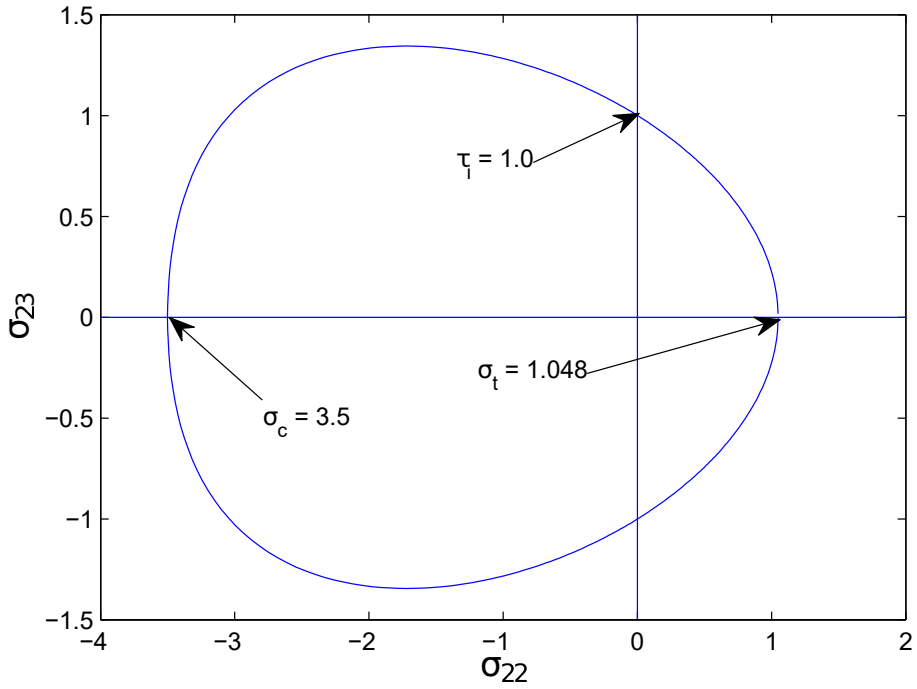

Figure 25: Anisotropic threshold surfacesin the σ_{22}, σ_{23} stress space with $d_i = (1, 0, 0)$

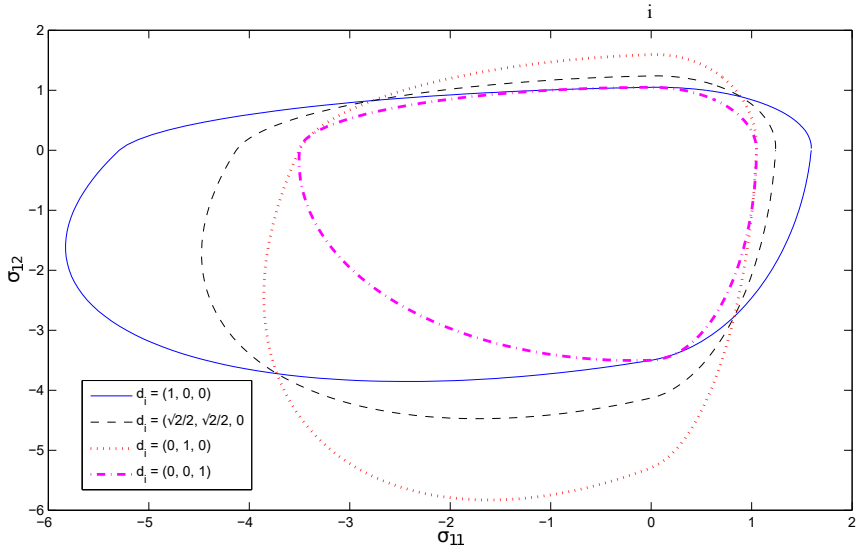

Figure 26: Anisotropic threshold surfaces with different preferred material directions

3.4 Isotropy as a Special Case

The isotropic threshold function is a special case of this anisotropic threshold function. To see that equate the tensile threshold stess in the plane of isotropy with the tensile threshold stess in the preferred material direction.

$$\sigma_{st} = \sigma_t \tag{3.267}$$

Also equate the compression threshold stress in the plane of isotropy with the compression threshold stress in the preferred material direction.

$$\sigma_{sc} = \sigma_c \tag{3.268}$$

Finally equate the biaxial compressive threshold stress in the plane of isotropy with the mixed biaxial threshold stress across the plane of isotropy.

$$\tau_s = \tau_i \tag{3.269}$$

Substituting these equations into the equation for the constant E_1 yields

$$E_1 = \frac{1}{2\sigma_{sc}^2} - \frac{1}{2\sigma_c^2} + \frac{1}{2\sigma_{st}^2} - \frac{1}{2\sigma_t^2} + \frac{1}{\tau_i^2} - \frac{1}{\tau_s^2} \tag{3.270}$$

Therefore

$$E_1 = 0 \tag{3.271}$$

Repeating this process for the constant F_1

$$F_1 = \frac{1}{2\sigma_c^2} - \frac{1}{2\sigma_{sc}^2} + \frac{1}{2\sigma_{st}^2} - \frac{1}{2\sigma_t^2} - \frac{1}{\tau_i^2} + \frac{1}{\tau_s^2} \tag{3.272}$$

Thus

$$F_1 = 0 \tag{3.273}$$

Finally, repeating this process for the constant H_2

$$H_2 = \frac{1}{\sigma_c^2} - \frac{1}{\sigma_c^2} - \frac{1}{\sigma_t^2} + \frac{1}{\sigma_t^2} \tag{3.274}$$

Thus

$$H_2 = 0 \tag{3.275}$$

Since the terms relating to anisotropy become zero the anisotropic threshold functions reduce to the isotropic threshold functions derived in the previous chapter.

CHAPTER IV

Inelastic Constitutive Law

4.1 Preliminary Concepts - Basic Ingredients

An incremental modeling approach is presented here as a first step in capturing multi-axial non-linear constitutive behavior for graphite. This approach ignores the effects from exposure to radiation, which can be modeled through the use of continuum damage mechanics. The incremental non-linear inelastic constitutive model also ignores rate effects and assumes that any time dependent phenomenon exhibited by nuclear graphite used in high temperature service conditions can be captured using other modeling techniques. The reader is directed to the viscoplastic models of Robinson (1978), Chaboche (1977), and Bodner (1975) for rate dependent modeling techniques.

There are three fundamental components necessary for an incremental inelastic constitutive law based on the work hardening concepts. First is a threshold function. An isotropic threshold function was presented in Chapter II and an anisotropic extension of the isotropic function was presented in Chapter III. The second component is a hardening rule - also known as an evolutionary law. A hardening rule provides a mathematical description of how a threshold function evolves (i.e., how a material "hardens") as inelastic deformations accumulate. The third component is a flow rule. Chen and Han (1995) as well as Mendelsohn (1968) outlined how a flow rule relates incremental strain and the state of stress with predefined inelastic state variables. Their approach with modifications is followed here.

Two types of flow rules dominate inelastic modeling. The first is referred to as an associated flow rule. With an associated flow rule the threshold function serves as a potential function. Inelastic constitutive models for ductile metals historically have been modeled using associated flow rules. The second type is known as a non-associated flow rule. Constitutive relationships for soils that follow a Drucker-Prager threshold function typically utilize a non-associated flow rule. With nuclear graphite an associated flow rule is adopted.

Consider a graphite test specimen that is uniaxially loaded and then unloaded under tension. Tensile stress-strain data obtained from Bratton (2009) for H-451 graphite is depicted in Figure (27). In this figure ϵ_I represents the permanent strain that remains after unloading, ϵ_E represents elastic, or recoverable strain, and σ^* is the maximum total stress applied over the load cycle. From the figure the total strain is

$$\epsilon_t = \epsilon_I + \epsilon_E \tag{4.1}$$

Casting this expression into an incremental form leads to

$$d\epsilon_t = d\epsilon_I + d\epsilon_E \tag{4.2}$$

The key is quantifying the incremental inelastic strain, $d\epsilon_I$. The model that quantifies this mathematically is known as the flow rule which is the primary topic of this chapter.

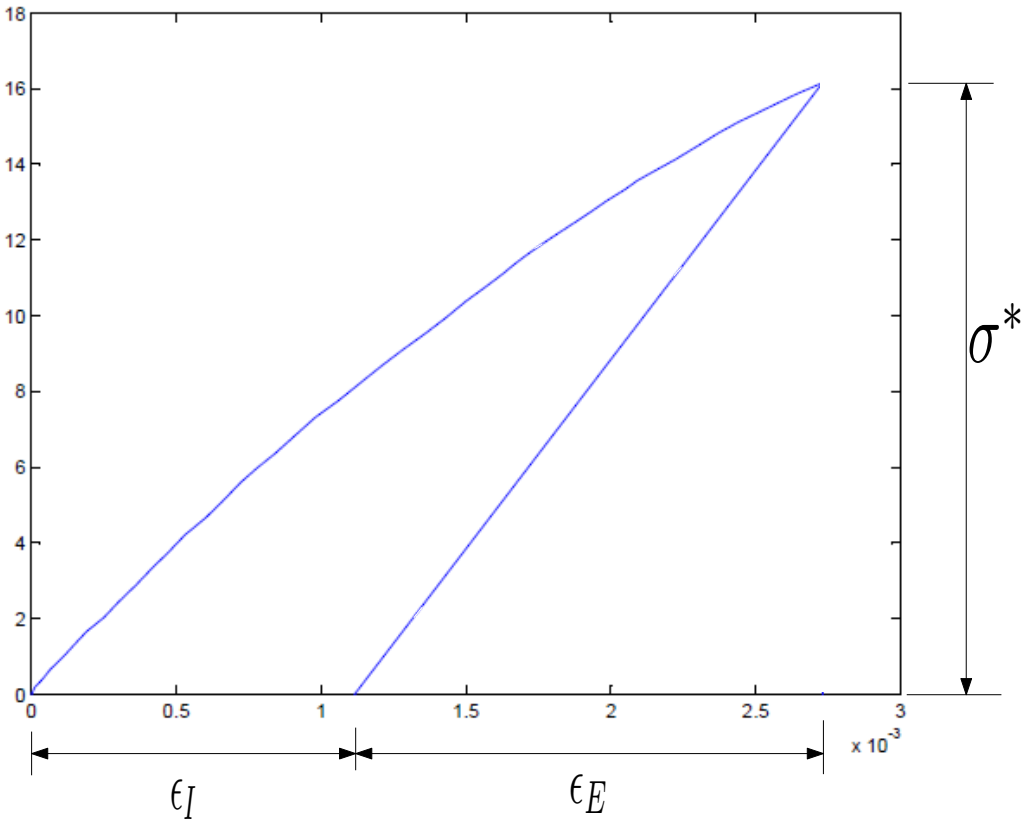

Figure 27: Uniaxial tension test Data from Bratton (2009)

A loading rule must be established before inelastic strains can be quantified. The loading rule determines whether or not inelastic strains occur along a load path. As noted throughout the first several chapters the boundary of the threshold function defines elastic states of stress. Stress states outside of the surface of the threshold function are mathematically inaccessible. States of stress within the threshold surface are elastic states of stress. The inaccessible states of stress can be subsequently embedded within the surface by evolving the threshold function. This evolution process incorporates stress states along the functional boundary first and then eventually migrates the functional boundary sufficiently so that stress states beyond the boundary are assimilated. The threshold-potential function therefore must be dependent on stress as well as on a number of inelastic state

variables that are grouped and defined by the vector H_α, i.e.,

$$f = f(\sigma_{ij}, H_\alpha) \qquad \alpha = 1, 2, 3, \cdots, n \tag{4.3}$$

How a material hardens influences the number of state variables that comprise the vector H_α. Isotropic hardening and kinematic hardening are the two classic evolutionary schemes. Isotropic hardening requires one state variable, kinematic hardening requires a second order tensor of state variables with six distinct components. Both types of hardening schemes are captured in the stress-strain curves presented in Figure (28) and Figure (29). Uniaxial stress is increased beyond the initial threshold stress and the stress-strain curve becomes progressively nonlinear. Unloading and subsequent reloading of the material produces a larger threshold stress than found in the virgin material. The difference between the initial threshold stress and subsequent threshold stress values stresses indicates the material is hardening. This behavior can be modeled by the surface of the threshold potential function expanding equally in all direction. An equally expansive threshold potential function in all directions is indicative of isotropic hardening.

One can unload uniaxially from tension and reload into the compressive region of the stress space as shown in Figure (29). A material may respond with a lower magnitude of the threshold stress in compression than in tension. This is the so-called Bauschinger effect that is associated with kinematic hardening. Kinematic hardening will not be addressed here although the model framework could accommodate this type of hardening. The reader should be mindful that for graphite the virgin threshold stress in compression is larger than the virgin threshold stress in tension. For this reason this effort fucuses on isotropic modeling in order to track the different behavior of graphite in tension and compression. Details on specific aspects of the evolutionary law for isotropic hardening appear in a later section.

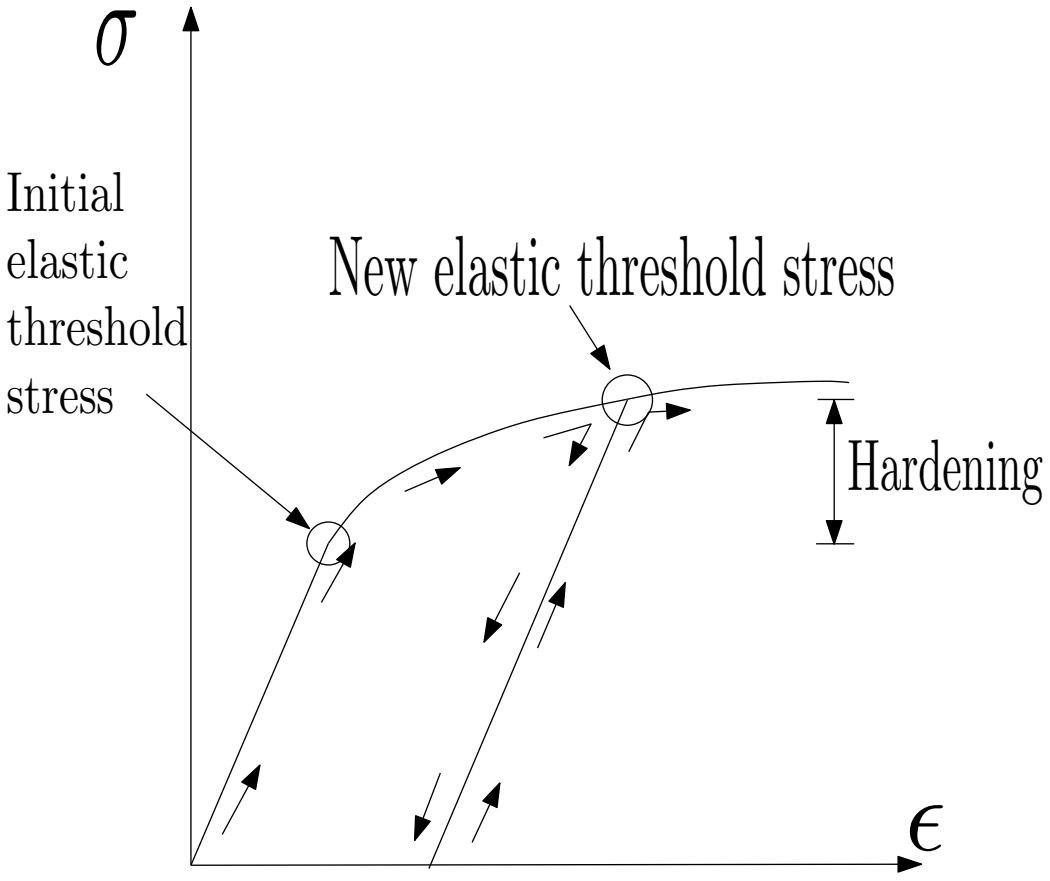

Figure 28: Notion of Hardening Chaboche (1977)

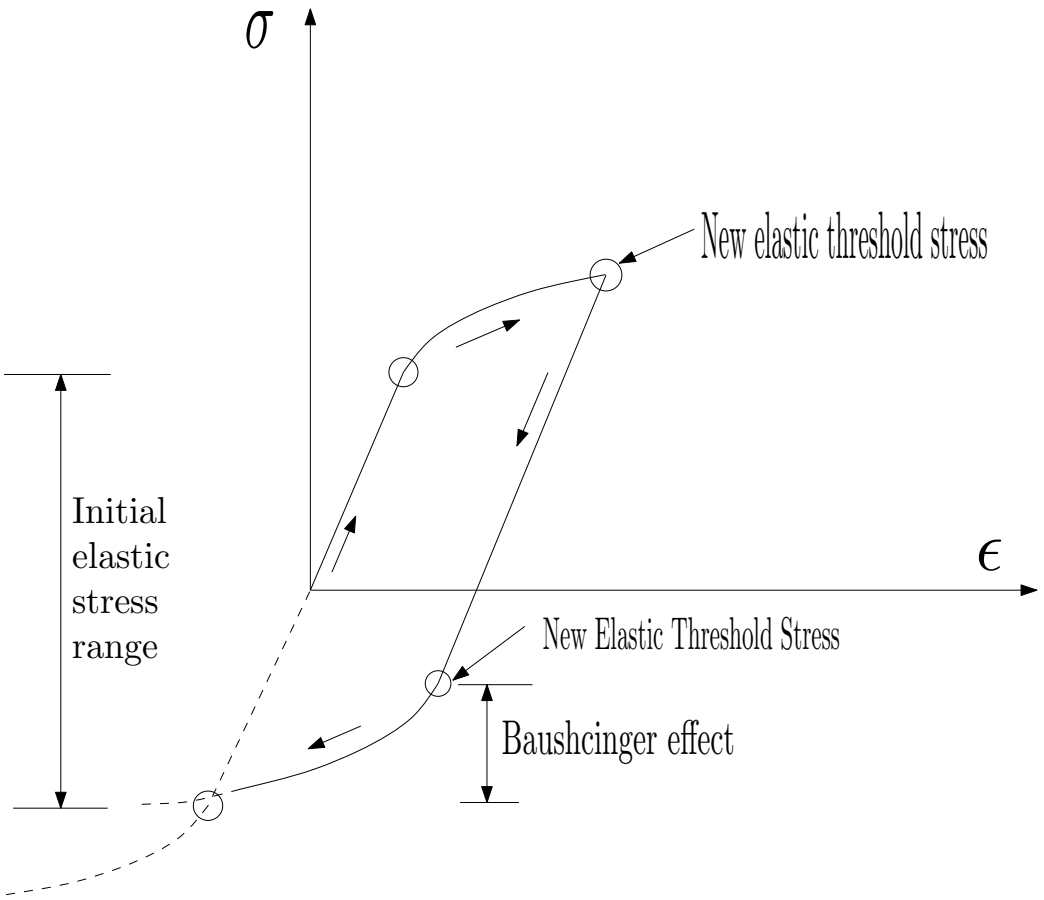

Figure 29: Kinematic Hardening and Bauschinger Effects Chaboche (1977)

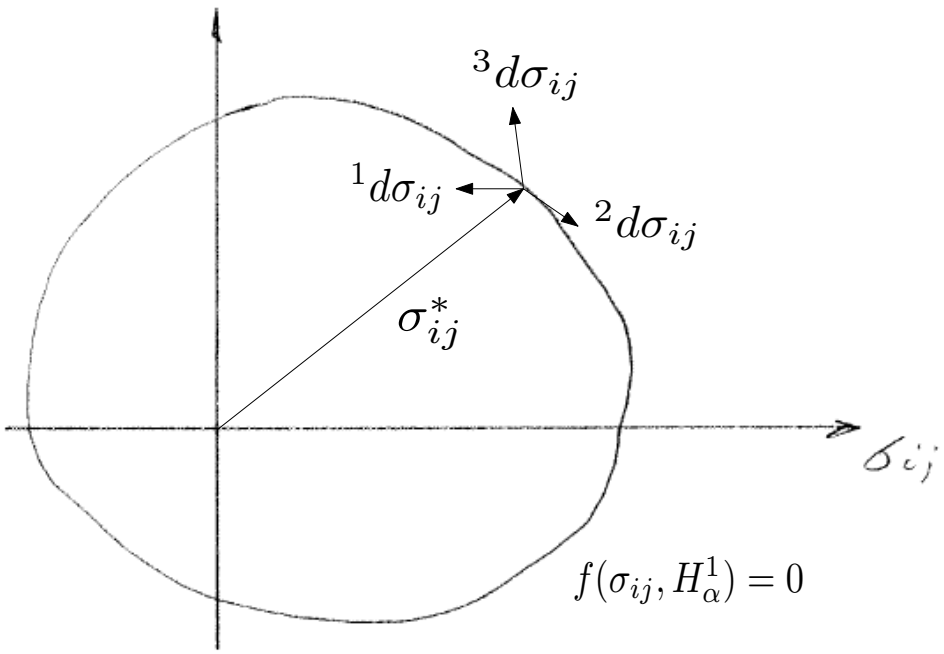

Figure 30: Possible directions for the stress increment $d\sigma_{ij}$

4.2 Loading Rule

In Figure (30) an initial stress state (σ^*_{ij}) is depicted that lies on the threshold surface and several possible increments in stress, denoted as $\mathrm{d}\sigma_{ij}$, are shown. In general a stress increment can be directed to the inside of the threshold-potential function ($^1d\sigma_{ij}$), tangent to the threshold-potential function ($^2d\sigma_{ij}$), or in an outward direction to the threshold-potential function ($^3d\sigma_{ij}$). A load path that lies completely inside or traverses along the surface of the threshold function will accrue elastic strains. Inelastic strains occur when the stress increment is an outward normal vector ($^3d\sigma_{ij}$) to the threshold surface. The stress state σ^*_{ij} on the surface of a threshold function such that

$$f(\sigma^*_{ij}, H^1_\alpha) = 0 \tag{4.4}$$

A change in the stress state that does not change the inelastic state variable H^1_α corresponds to unloading into the elastic stress region. As unloading takes place the value of the scalar

threshold function is less than zero for elastic states of stress i.e.,

$$f(\sigma_{ij}^{*} + {}^{1}d\sigma_{ij}, H_{\alpha}^{1}) < 0 \tag{4.5}$$

Correspondingly the differential change in the threshold function is negative, i.e.,

$$df < 0 \tag{4.6}$$

With

$$df = \frac{\partial f}{\partial \sigma_{ij}} \, {}^{1}d\sigma_{ij} + \frac{\partial f}{\partial H_{\alpha}} dH_{\alpha} \tag{4.7}$$

and the fact that the inelastic state does not change, i.e.,

$$dH_{\alpha} \equiv 0 \tag{4.8}$$

then

$$\begin{aligned} df &= \left\{ \frac{\partial f}{\partial \sigma_{ij}} \bigg|_{\sigma_{ij}^{*}} \right\} {}^{1}d\sigma_{ij} \\ &< 0 \end{aligned} \tag{4.9}$$

The inner product on the right hand side of Equation (4.9) can be interpreted graphically from the general schematic in Figure 30. If the incremental load vector is directed inwards the angle between the incremental load vector and the gradient to the threshold surface is greater than 90°, and this corresponds to unloading.

However, if

$$dH_{\alpha} \neq 0 \tag{4.10}$$

and the inelastic state changes from H_{α}^{1} to H_{α}^{2}, which is indicated in figure 31, then the new

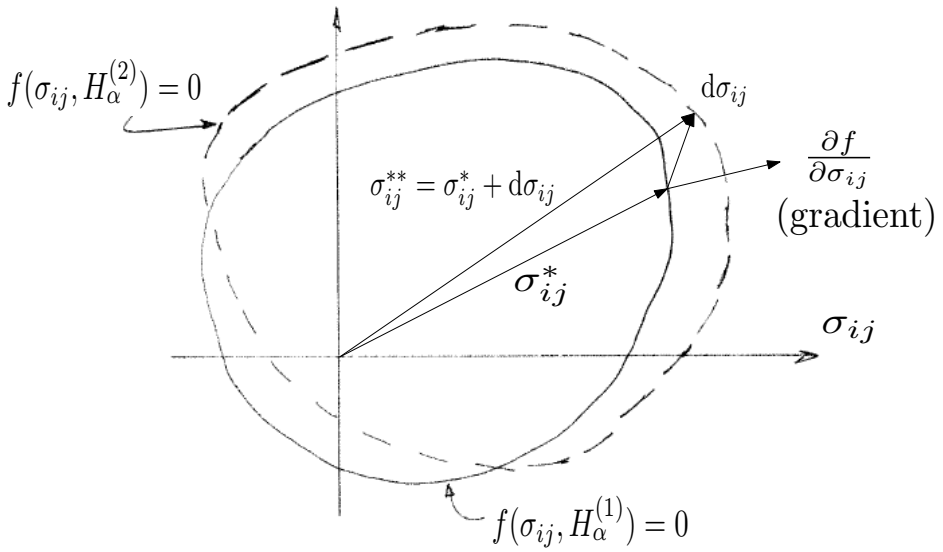

Figure 31: Inelastic Loading

threshold surface can be characterized as

$$f(\sigma_{ij}^{*} + {}^{3}d\sigma_{ij}\ , H_\alpha^1 + dH_\alpha) = f(\sigma_{ij}^{*} + {}^{3}d\sigma_{ij}\ , H_\alpha^2) \tag{4.11}$$

and inelastic strains accrue, i.e.,

$$d\epsilon^I \neq 0 \tag{4.12}$$

The interpretation of the inner product of the gradient to the threshold function and the increment in the stress vector mathematically leads to

$$\left\{ \left. \frac{\partial f}{\partial \sigma_{ij}} \right|_{\sigma_{ij}^{*}} \right\} \quad {}^{3}\mathrm{d}\sigma_{ij} \geq 0 \tag{4.13}$$

for a change in inelastic state. Here the angle between the incremental load vector and the gradient to the threshold function is less than 90°.

If an increment in stress is imposed such that inelastic strains accrue, and the inelastic state of the material changes, then subsequent stress states must still lie on the surface of an evolved threshold-potential function as shown in Figure 31. This requirement is known as the consistency condition, i.e., the current state of stress must consistently lie on the surface

of the function for inelastic strains to occur. The consistency condition can be described mathematically in a simple manner by realizing that taking the differential of

$$f = 0 \tag{4.14}$$

leads to

$$\begin{aligned} d(f = 0) \\ df &= d(0) \\ &= 0 \end{aligned} \tag{4.15}$$

Thus Equation (4.7) can be set equal to zero, i.e.,

$$\begin{aligned} \mathrm{d}f &= \frac{\partial f}{\partial \sigma_{ij}} \mathrm{d}\sigma_{ij} + \frac{\partial f}{\partial H_\alpha} \mathrm{d}H_\alpha \\ &= 0 \end{aligned} \tag{4.16}$$

and this last expression is the mathematical description of the consistency condition. The consistency condition is introduced here as a part of the discussion of a loading rule for convenience. It is used later to quantify the amount of inelastic strain given an increment in the stress state.

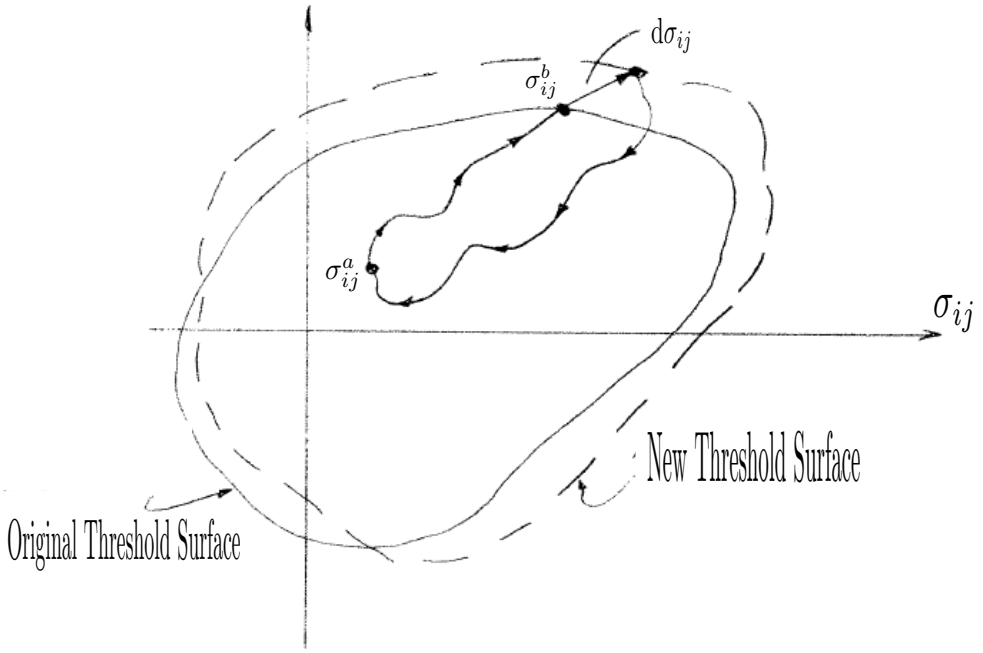

Figure 32: Inelastic Loading

Figure (32) shows a loading path that starts at an elastic state of stress identified as σ^a_{ij}. The material is then loaded to a level of stress identified as σ^b_{ij} which lies on the threshold surface, and then an incremental load $\mathrm{d}\sigma_{ij}$ is applied. The increment in stress gives rise to an increment in inelastic strain and changes the inelastic state of the material. This change of inelastic state impacts the stress-strain curve since the material hardens. The presence of inelastic strains can be detected through the nonlinear behavior of the stress-strain curve or by unloading the material and noting the permanent strains. The incremental stress $\mathrm{d}\sigma_{ij}$ shown in this figure evolves the threshold function. After $d\sigma_{ij}$ is applied the material is then unloaded to the original stress state σ^a_{ij}. Since the stress states along the path from σ^a_{ij} to σ^b_{ij} are all located within the threshold surface, the material responds in an elastic manner along this segment of the load path. The inelastic behavior of the material along this multiaxial stress cycle, i.e., from σ^a_{ij} to σ^b_{ij}, to $\sigma^b_{ij} + d\sigma_{ij}$ and finally back to σ^a_{ij} is best

described mathematically by

$$\left.\begin{matrix} \mathrm{d}\epsilon_{ij}^{I} \neq 0 \\ \mathrm{d}H_{\alpha} \neq 0 \end{matrix}\right\} \begin{cases} f(\sigma_{ij}, H_{\alpha}) = 0 \\ \text{and} \\ \dfrac{\partial f}{\partial \sigma_{ij}} \mathrm{d}\sigma_{ij} > 0 \end{cases} \tag{4.17}$$

or

$$\left.\begin{matrix} \mathrm{d}\epsilon_{ij}^{I} = 0 \\ \mathrm{d}H_{\alpha} = 0 \end{matrix}\right\} \begin{cases} f(\sigma_{ij} + \mathrm{d}\sigma_{ij}, H_{\alpha}) < 0 \\ \text{or} \\ f(\sigma_{ij}, H_{\alpha}) = 0 \text{ and} \\ \dfrac{\partial f}{\partial \sigma_{ij}} \mathrm{d}\sigma_{ij} < 0 \end{cases} \tag{4.18}$$

Equations (4.17) and (4.18) define the loading rule in general terms. The inelastic history of the material is tracked by the changes in the state variables H_{α} that subsequently impose changes to the threshold function. The increment of elastic strain due to an increment in stress and the evolutions in the inelastic state variable for an isotropic material with different behavior in tension and compression are mathematically described and quantified in the next section.

4.3 Incremental Evolutionary Law

It has been implied throughout that incremental changes in inelastic strain are accompanied by changes in the inelastic state variable. Mathematically the link between inelastic strain and the change in the state variable can be simply expressed as

$$d\epsilon_{ij}^{I} = Q_{ij\alpha} dH_{\alpha} \tag{4.19}$$

or after inverting Equation (4.19)

$$dH_{\alpha} = F_{ij\alpha} d\epsilon_{ij}^{I} \tag{4.20}$$

where

$$F_{ij\alpha} = Q^{-1}_{ij\alpha} \tag{4.21}$$

The tensor functions $Q_{ij\alpha}$, or $F_{ij\alpha}$, are dependant on the current stress state and the current inelastic state of the material, i.e.,

$$F_{ij\alpha} = F_{ij\alpha}(\sigma_{ij}, H_\alpha) \tag{4.22}$$

If isotropic hardening is assumed then the state variable vector H_α is represented by a scalar variable K.

$$H_{(\alpha=1)} = K \tag{4.23}$$

Taking the differential of both sides leads to

$$dH_{(\alpha=1)} = dK \tag{4.24}$$

and

$$dK = F_{ij}(\sigma_{mn}, K) d\epsilon^I_{ij} \tag{4.25}$$

The right hand side of this last equation is a scalar quantity where the tensor function F_{ij} depends on the state of stress and the current inelastic state. Equation (4.25) states that if there are no inelastic strains then there is no change in the state variable, i.e., if

$$\mathrm{d}\epsilon^I_{ij} = 0 \tag{4.26}$$

then

$$\mathrm{d}K = 0 \tag{4.27}$$

A simple assumption is made at this point for the form of F_{ij} in Equation (4.25). Let

$$F_{ij}(\sigma_{mn}, K) = \mathscr{F}(K)\sigma_{ij} \tag{4.28}$$

so that the tensor function F_{ij} is a scalar multiple of the applied stress state. Here an assumption is made that the dependence on K emerges through the scalar function $\mathscr{F}$. A simple interpretation of the scalar multiplier $\mathscr{F}$ is presented in section 4.5, i.e., the dependence of the scalar multiplier function $\mathscr{F}$ will be based on the current tangent of the stress-strain curve. Inserting Equation (4.28) into Equation (4.20) leads to

$$dK = [\mathscr{F}(K)]\, \sigma_{ij} d\epsilon_{ij}^{I} \tag{4.29}$$

4.4 Isotropic Flow Rule

The flow law, the inelastic stress-strain relationship, is derived using the partial derivatives of the threshold-potential functions, i.e.,

$$\begin{aligned} d\epsilon_{ij}^{I} &= d\lambda \, \frac{\partial f}{\partial \sigma_{ij}} \\ &= \mathrm{d}\lambda \, \frac{\partial f(\sigma_{ij}, a_i, K)}{\partial \sigma_{ij}} \end{aligned} \tag{4.30}$$

Recall that a_i is a vector associated with the direction of the principle stresses. Equation (4.30) represents a flow rule that embodies the potential-morality concept, and by using the threshold function in this equation an associated flow rule is explicitly adopted. The gradient defines the direction of the increment of the inelastic strain vector and $d\lambda$ defines the length.

Making use of the isotropic threshold function from Section 2.2, recall that there are four functional forms of f and there are four partial derivatives of the function. Explicit formulations of these partial derivatives are given in Equations (2.40), (2.41), (2.42), and (2.43). So the derivatives in Equation (4.30) have been defined earlier. However, the scalar multiplier $d\lambda$ needs defined and this is accomplished by developing an evolutionary law for the inelastic state variable. The evolutionary law is combined with the consistency

condition to produce a mathematical expression for $d\lambda$. Recall that

$$\begin{aligned} \mathrm{d}f &= \frac{\partial f}{\partial \sigma_{ij}}\,\mathrm{d}\sigma_{ij} + \frac{\partial f}{\partial K} dK \\ &= 0 \end{aligned} \tag{4.31}$$

Substituting Equation (4.29) into Equation (4.31) and solving for $\mathrm{d}\lambda$ yields

$$\mathrm{d}\lambda = -\left[\frac{\partial f}{\partial K}\frac{\partial f}{\partial \sigma_{ij}} F_{ij}\right]^{-1} \frac{\partial f}{\partial \sigma_{km}}\,\mathrm{d}\sigma_{km} \tag{4.32}$$

Substitution of Equation (4.32) into Equation (4.30) yields

$$\mathrm{d}\epsilon^{I}_{ij} = -\left[\frac{\partial f}{\partial K}\frac{\partial f}{\partial \sigma_{pq}} F_{pq}\right]^{-1} \frac{\partial f}{\partial \sigma_{km}}\frac{\partial f}{\partial \sigma_{ij}}\,\mathrm{d}\sigma_{km} \tag{4.33}$$

Now define the bracketed scalar quantity above as

$$G = -\left[\frac{\partial f}{\partial K}\frac{\partial f}{\partial \sigma_{pq}} F_{pq}\right]^{-1} \tag{4.34}$$

then

$$\mathrm{d}\epsilon^{I}_{ij} = G\frac{\partial f}{\partial \sigma_{km}}\frac{\partial f}{\partial \sigma_{ij}}\,\mathrm{d}\sigma_{km} \tag{4.35}$$

where

$$d\lambda = G\frac{\partial f}{\partial \sigma_{km}} d\sigma_{km} \tag{4.36}$$

What remains are the details associated with the substitution of the partial derivatives of the threshold potential function and the particular form for G.

We now derive the specifics for the inelasticity model using the isotropic Green and Mkrtichian (1977) threshold function. This form for the threshold functions account for material behavior where tensile stress states produced a different response than compressive stress states. Green and Mkrtichian (1977) divided the threshold surface into four piecewise

continuous functions based on principle stresses as follows

$$\texttt{Region \#1} \quad \sigma_1 \geq \sigma_2 \geq \sigma_3 \geq 0 \tag{4.37}$$

$$\texttt{Region \#2} \quad \sigma_1 \geq \sigma_2 \geq 0 \geq \sigma_3 \tag{4.38}$$

$$\texttt{Region \#3} \quad \sigma_1 \geq 0 \geq \sigma_2 \geq \sigma_3 \tag{4.39}$$

$$\texttt{Region \#4} \quad 0 \geq \sigma_1 \geq \sigma_2 \geq \sigma_3 \tag{4.40}$$

The subscripts on the functions below denote in which region of the stress space the function is valid. Recall for region #1

$$f_1 = \frac{1}{2}A_1 I_1^2 + B_1 I_2 - K^2 \tag{4.41}$$

The threshold function for region #2 was defined earlier as

$$f_2 = \frac{1}{2}A_2 I_1^2 + B_2 I_2 + D_2 I_5 - K^2 \tag{4.42}$$

The threshold function for region #3 was defined earlier as

$$f_3 = \frac{1}{2}A_3 I_1^2 + B_3 I_2 + D_3 I_5 - K^2 \tag{4.43}$$

and the threshold function for region #4 was defined earlier as

$$f_4 = \frac{1}{2}A_4 I_1^2 + B_4 I_2 - K^2 \tag{4.44}$$

Previously only virgin threshold potential function were considered where K was taken equal to one. Now K is allowed to vary since it is an inelastic state variable. The derivative of the threshold function in region #1 with respect to the inelastic state variable is

$$\frac{\partial f_1}{\partial K} = -2K \tag{4.45}$$

Since isotropic hardening was assumed then similar derivatives with respect to K for region #2, region #3, and region #4 are obtained, i.e.,

$$\frac{\partial f_2}{\partial K} = -2K \tag{4.46}$$

$$\frac{\partial f_3}{\partial K} = -2K \tag{4.47}$$

and

$$\frac{\partial f_4}{\partial K} = -2K \tag{4.48}$$

respectively.

Keeping in mind that $\mathscr{F} = \mathscr{F}(K)$ and this function is scalar valued, then substituting Equations (2.40), (4.28), and (4.45) into Equation (4.34) yields the following for region #1

$$G_1 = \left[\mathscr{F} 2K(A_1 I_1^2 + 2B_1 I_2)\right]^{-1} \tag{4.49}$$

Substituting Equations (2.41),(4.28), and (4.46) into Equation (4.34) yields the following for region #2

$$G_2 = \left[\mathscr{F} 2K(A_2 I_1^2 + 2B_2 I_2 + 2D_2 I_5)\right]^{-1} \tag{4.50}$$

Substituting Equations (2.42), (4.28), and (4.47) into Equation (4.34) yields the following for region #3

$$G_3 = \left[\mathscr{F} 2K(A_3 I_1^2 + 2B_3 I_2 + 2D_3 I_5)\right]^{-1} \tag{4.51}$$

Substituting Equations (2.43), (4.28), and (4.48) into Equation (4.34) yields the following for region #4

$$G_4 = \left[\mathscr{F} 2K(A_4 I_1^2 + 2B_4 I_2)\right]^{-1} \tag{4.52}$$

Equations (2.40) and (4.49) are now substituted into (4.35) which yields

$${}^{1}\,\mathrm{d}\epsilon_{ij}^{I} = \frac{A_1 I_1 \delta_{ij} + 2B_1 \sigma_{ij}}{\mathscr{F} 2K(A_1 I_1^2 + 2B_1 I_2)} \left[A_1 I_1\,\mathrm{d}I_1 + B_1\,\mathrm{d}I_2\right] \tag{4.53}$$

Substituting Equations (2.41) and (4.50) into Equation (4.35) yields

$${}^{2}\,\mathrm{d}\epsilon_{ij}^{I} = \frac{A_2 I_1 \delta_{ij} + 2B_2 \sigma_{ij} + D_2(a_m a_i \sigma_{jm} + a_j a_n \sigma_{ni})}{\mathscr{F} 2K(A_2 I_1^2 + 2B_2 I_2 + 2D_2 I_5)} \left[A_2 I_1\,\mathrm{d}I_1 + B_2\,\mathrm{d}I_2 + D_2\,\mathrm{d}I_5\right] \tag{4.54}$$

Substituting Equations (2.42) and (4.51) into Equation (4.35) yields

$${}^{3}\,\mathrm{d}\epsilon_{ij}^{I} = \frac{A_3 I_1 \delta_{ij} + 2B_3 \sigma_{ij} + D_3(a_m a_i \sigma_{jm} + a_j a_n \sigma_{ni})}{\mathscr{F} 2K(A_3 I_1^2 + 2B_3 I_2 + 2D_3 I_5)} \left[A_3 I_1\,\mathrm{d}I_1 + B_3\,\mathrm{d}I_2 + D_3\,\mathrm{d}I_5\right] \tag{4.55}$$

Substituting Equations (2.43) and (4.52) into Equation (4.35) yields

$${}^{4}\,\mathrm{d}\epsilon_{ij}^{I} = \frac{A_4 I_1 \delta_{ij} + 2B_4 \sigma_{ij}}{\mathscr{F} 2K(A_4 I_1^2 + 2B_4 I_2)} \left[A_4 I_1\,\mathrm{d}I_1 + B_4\,\mathrm{d}I_2\right] \tag{4.56}$$

Equations (4.53) through (4.56) comprise the isotropic inelastic flow law for each region of the stress space. The form of $\mathscr{F}$ must be specified and this is done in the next section.

4.5 Uniaxial Formulation of $\mathscr{F}(K)$

For region #1 of the Haigh-Westergaard stress space substituting the incremental strain tensor defined in Equation (4.53) into the evolutionary law given by Equation (4.29) leads to

$$2K\,\mathrm{d}K = A_1 I_1\,\mathrm{d}I_1 + B_1\,\mathrm{d}I_2 \tag{4.57}$$

Substituting Equation (4.54) into Equation (4.29) for region #2 of the Haigh-Westergaard stress space yields

$$2K\,\mathrm{d}K = A_2 I_1\,\mathrm{d}I_1 + B_2\,\mathrm{d}I_2 + D_2\,\mathrm{d}I_5 \tag{4.58}$$

Substituting Equation (4.55) into Equation (4.29) for region #3 of the Haigh-Westergaard stress space yields

$$2K\,\mathrm{d}K = A_3 I_1\,\mathrm{d}I_1 + B_3\,\mathrm{d}I_2 + D_3\,\mathrm{d}I_5 \tag{4.59}$$

Substituting Equation (4.56) into Equation (4.29) for region #4 of the Haigh-Westergaard stress space yields

$$2K\,\mathrm{d}K = A_4 I_1\,\mathrm{d}I_1 + B_4\,\mathrm{d}I_2 \tag{4.60}$$

Even though the assumption is made that the material hardens isotropically and only one state variable is required, there are four incremental evolutionary equations governing the behavior of the inelastic state variable K.

Now consider a uniaxial tensile stress state where

$$\sigma_{ij} = \begin{bmatrix} \sigma_t & 0 & 0 \\ 0 & 0 & 0 \\ 0 & 0 & 0 \end{bmatrix} \tag{4.61}$$

The assumption is made that the stress state resides on the yield surface and the invariants for this stress state are

$$I_1 = \sigma_t \tag{4.62}$$

$$I_2 = \sigma_t^2 \tag{4.63}$$

The strain increment for a corresponding increment in the inelastic stress is

$${}^1\mathrm{d}\epsilon_{11}^I = \frac{1}{{}_t\mathscr{F}\ 2K(A_1 I_1^2 + 2B_1 I_2)} \frac{\partial f_1}{\partial \sigma_{11}} \frac{\partial f_1}{\partial \sigma_{kl}} \mathrm{d}\sigma_{kl} \tag{4.64}$$

where the scalar function $\mathscr{F}$ is denoted as ${}_t\mathscr{F}$ for this uniaxial tensile load application. Solving this expression for ${}_t\mathscr{F}$ yields

$$ {}_t\mathscr{F} = \frac{1}{2K(A_1 I_1^2 + 2B_1 I_2)} \frac{\partial f_1}{\partial \sigma_{11}} \frac{\partial f_1}{\partial \sigma_{kl}} \frac{\mathrm{d}\sigma_{kl}}{\mathrm{d}\epsilon_{11}^I} \tag{4.65} $$

Since σ_{11} is the only non-zero component of the stress tensor, for a uniaxial tension test, then

$$ {}_t\mathscr{F} = \frac{1}{2K(A_1 I_1^2 + 2B_1 I_2)} \frac{\partial f_1}{\partial \sigma_{11}} \frac{\partial f_1}{\partial \sigma_{11}} \frac{d\sigma_{11}}{d\epsilon_{11}^I} \tag{4.66} $$

Substitution of the invariants I_1 and I_2 from above into this last expression leads to

$$ {}_t\mathscr{F} = \frac{A_1 + 2B_1}{2K} \frac{d\sigma_{11}}{d\epsilon_{11}^I} \tag{4.67} $$

Here a total derivative of σ_{11} is taken with respect to ϵ_{11}^I. In essence the function ${}_t\mathscr{F}$ is dependent on two variables, i.e.,

$$ {}_t\mathscr{F} = {}_t\mathscr{F}(K, slope) \tag{4.68} $$

We wish to maintain this format for the functional dependence, but stipulate the dependence on a slope in terms of the total strain - a quantity that can be measured experimentally. The total strain can be decomposed into elastic and inelastic components, thus in a uniaxial tensile test

$$ (\epsilon_{11})^{tot} = (\epsilon_{11})^E + (\epsilon_{11})^I \tag{4.69} $$

On a differential basis the decomposition becomes

$$ (d\epsilon_{11})^{tot} = (d\epsilon_{11})^E + (d\epsilon_{11})^I \tag{4.70} $$

such that

$$ (d\epsilon_{11})^{tot} > (d\epsilon_{11})^I \tag{4.71} $$

Thus, if ${}_t\mathscr{F}$ is a function of a slope and that slope is determined using total strains then this quantity would slightly underestimate the theoretical slope found in the derivation of ${}_t\mathscr{F}$ above, i.e.,

$$\frac{d\sigma_{11}}{d\epsilon_{11}^{tot}} < \frac{d\sigma_{11}}{d\epsilon_{11}^{I}} \tag{4.72}$$

Using a slope in terms of a total strain will underestimate the functional value of ${}_t\mathscr{F}$. As will be seen momentarily this discrepancy will be minimized by regressing the data to find constants once a functional form is established for ${}_t\mathscr{F}$.

If the slope of the current stress and total strain curve is used to characterize $\mathscr{F}$ then this slope can be approximated through the use of the Ramberg–Osgood constitutive model where

$$\begin{aligned} \epsilon^{tot} &= \frac{\sigma}{E} + \alpha\left(\frac{\sigma_0}{E}\right)\left(\frac{\sigma}{\sigma_0}\right)^n \\ &= \frac{\sigma}{E} + C_1\left(\frac{\sigma}{\sigma_0}\right)^n \\ &= \frac{\sigma}{E} + C_2\sigma^n \end{aligned} \tag{4.73}$$

There are other non-linear uniaxial stress-strain models that can be utilized leading to other formulations for the scalar function ${}_t\mathscr{F}$. As an example Prager's [2007] model is used in the American Society of Mechanical Engineers (ASME) Boiler and Pressure Vessel Code. Prager's [2007] model is too detailed leading to a complex formulation for the slope of that constitutive model, thus the slope of the Ramberg-Osgood stress-strain curve is adopted for use here. This slope can be obtained by taking the differential of both sided of Equation (4.73), i.e.,

$$\begin{aligned} d\epsilon^{tot} &= \frac{1}{E}d\sigma + C_2 d(\sigma^n) \\ &= \frac{1}{E}d\sigma + nC_2\sigma^{n-1}d\sigma \\ &= \left(\frac{1}{E} + nC_2\sigma^{n-1}\right)d\sigma \end{aligned} \tag{4.74}$$

Thus

$$\frac{d\sigma}{d\epsilon^{tot}} = \frac{1}{\frac{1}{E} + nC_2\sigma^{n-1}} \tag{4.75}$$

How the constants n and C_2 are estimated from stress-total strain data is demonstrated momentarily. Moreover, the slope identified in Equation (4.75) can be readily computed given these constants and the current values of stress. At stresses that are beyond the initial threshold values where the stress-strain curve is nonlinear, the increment in total strain is predominantly inelastic, and the assumption is made that

$$\frac{d\sigma_{11}}{d\epsilon_{11}^{I}} \approx \frac{d\sigma_{11}}{d\epsilon_{11}^{tot}} \tag{4.76}$$

Such that

$${}_t\mathscr{F} = \frac{A_1 + 2B_1}{2K}\left(\frac{1}{\frac{1}{E} + nC_2\sigma^{n-1}}\right) \tag{4.77}$$

With Equation (4.77) a functional form for ${}_t\mathscr{F}$ has been established. As noted above other forms could be considered. Here the simplest formulation was adopted for convenience.

Now consider the case where a uniaxial compression stress is applied to a graphite material

$$\sigma_{ij} = \begin{bmatrix} \sigma_c & 0 & 0 \\ 0 & 0 & 0 \\ 0 & 0 & 0 \end{bmatrix} \tag{4.78}$$

The invariants for this stress state are

$$I_1 = \sigma_c \tag{4.79}$$

$$I_2 = \sigma_c^2 \tag{4.80}$$

Denoting the scalar function $\mathscr{F}$ as ${}_c\mathscr{F}$ then

$$ {}^4\mathrm{d}\epsilon_{11}^I = \frac{1}{{}_c\mathscr{F}\ 2K(A_4 I_1^2 + 2B_4 I_2)} \frac{\partial f_4}{\partial \sigma_{11}} \frac{\partial f_4}{\partial \sigma_{kl}} \mathrm{d}\sigma_{kl} \tag{4.81} $$

Solving for ${}_c\mathscr{F}$

$$ {}_c\mathscr{F} = \frac{1}{2K(A_4 I_1^2 + 2B_4 I_2)} \frac{\partial f_4}{\partial \sigma_{11}} \frac{\partial f_4}{\partial \sigma_{kl}} \frac{\mathrm{d}\sigma_{kl}}{\mathrm{d}\epsilon_{11}} \tag{4.82} $$

Since σ_{11} is the only non-zero component of the stress tensor, then

$$ {}_c\mathscr{F} = \frac{1}{2K(A_4 I_1^2 + 2B_4 I_2)} \frac{\partial f_4}{\partial \sigma_{11}} \frac{\partial f_4}{\partial \sigma_{11}} \frac{d\sigma_{11}}{d\epsilon_{11}^I} \tag{4.83} $$

which simplifies to

$$ {}_c\mathscr{F} = \frac{A_4 + 2B_4}{2K} \frac{d\sigma_{11}}{d\epsilon_{11}} \tag{4.84} $$

This equation for ${}_c\mathscr{F}$ is different than the corresponding equation for tension and this is consistent with the fact that for graphite, behavior in tension is different than behavior in compression. So at this point there are two sets of parameters for the selected functional dependence of $\mathscr{F}$, i.e.,

$$ \begin{aligned} n \rightarrow &\quad {}_t n \quad {}_c n \\ C_2 \rightarrow &\quad {}_t C_2 \quad {}_c C_2 \end{aligned} \tag{4.85} $$

To compute the constants for $\mathscr{F}$ attention is focused on the slope of a stress-strain curve. The discussion that follows applies to etiher tension of compression. Using total strain data the slope is numerically approximated using a central difference method, i.e.,

$$ \frac{d\sigma}{d\epsilon^{tot}} = \frac{\sigma_{i+1} - \sigma_{i-1}}{\epsilon_{i+1}^{tot} - \epsilon_{i-1}^{tot}} \tag{4.86} $$

and from Equation (4.75)

$$ \frac{\sigma_{i+1} - \sigma_{i-1}}{\epsilon_{i+1}^{tot} - \epsilon_{i-1}^{tot}} = \frac{1}{\frac{1}{E} + nC_2\sigma^{n-1}} \tag{4.87} $$

This last expression be linearized as follows:

$$ln\left(\frac{\epsilon_{i+1}^{tot}-\epsilon_{i-1}^{tot}}{\sigma_{i+1}-\sigma_{i-1}}-\frac{1}{E}\right)=(n-1)ln(\sigma_i)+ln(nC_2) \tag{4.88}$$

In Equation (4.88) σ is the current uniaxial stress value. This equation has the form

$$y=mx+b \tag{4.89}$$

where

$$\begin{aligned} y &= ln\left(\frac{\epsilon_{i+1}^{tot}-\epsilon_{i-1}^{tot}}{\sigma_{i+1}-\sigma_{i-1}}-\frac{1}{E}\right) \\ m &= n-1 \\ x &= ln(\sigma) \end{aligned} \tag{4.90}$$

and

$$b=ln(nC_2) \tag{4.91}$$

The values for the two constants are then determined as

$$\begin{aligned} n &= m+1 \\ C_2 &= \frac{exp(b)}{n} \end{aligned} \tag{4.92}$$

where m and b are obtained from regressing the tensile or compression data. Using the uniaxial tension and compression data provided by Bratton (2009) the constants ${}_tn$, ${}_tC_2$, ${}_cn$ and ${}_cC_2$ can be calculated by using linear regression. This is presented in the next chapter.

4.6 Equivalent Stress and Strain – Multiaxial $\mathscr{F}$

In the previous section a functional form for $\mathscr{F}$ was derived for uniaxial tension and another for uniaxial compression. Here equivalent stress and strain measures are developed in order to construct a complete multiaxial fomulation for $\mathscr{F}$. This effort incorporates the concept

of plastic work. In the multi-axial case plastic work is defined as

$$dW^p = \sigma_{ij} d\epsilon^I_{ij} \tag{4.93}$$

using tensor notation. Since work is a scalar, plastic work can also be defined using equivalent scalar expressions for stress and strain as follows

$$dW^p = \Sigma dE^I \tag{4.94}$$

Here Σ is a scalar measure of the multi-axial stress state and dE^I is a scalar measure of the multiaxial inelastic increment in strain. Defining these two scalar quantities is accomplished by first substituting Equation (4.30) into equatin (4.93). This yields the following relationship for plastic work

$$dW^p = d\lambda \; \sigma_{pq} \frac{\partial f}{\partial \sigma_{pq}} \tag{4.95}$$

Note that by taking the first derivative of the threshold function with respect to the Cauchy stress yields

$$\frac{\partial f}{\partial \sigma_{pq}} \sigma_{pq} = 2\tilde{f} \tag{4.96}$$

The form for $\tilde{f}$ is of the same form as f, but without the state variable. Mathematically this reuslts in

$$\tilde{f} = f + K^2 \tag{4.97}$$

and

$$\frac{\partial \tilde{f}}{\sigma_{ij}} = \frac{\partial f}{\sigma_{ij}} \tag{4.98}$$

Where in Region #1

$$\tilde{f}_1 = \frac{1}{2} A_1 I_1^2 + B_1 I_2 \tag{4.99}$$

in Region #2

$$\tilde{f}_2 = \frac{1}{2}A_2 I_1^2 + B_2 I_2 + D_2 I_5 \tag{4.100}$$

in Region #3

$$\tilde{f}_3 = \frac{1}{2}A_3 I_1^2 + B_3 I_2 + D_3 I_5 \tag{4.101}$$

and in Region #4

$$\tilde{f}_4 = \frac{1}{2}A_4 I_1^2 + B_4 I_2 \tag{4.102}$$

Inserting Equation (4.96) into Equation (4.95) leads to

$$\Sigma dE^I = 2\tilde{f}\ d\lambda \tag{4.103}$$

Moreover, squaring both sides of Equation (4.30) and solving for $d\lambda$ leads to

$$d\lambda = \left[d\epsilon_{ij}^I d\epsilon_{ij}^I\right]^{\frac{1}{2}} \left[\frac{\partial f}{\sigma_{mn}}\frac{\partial f}{\sigma_{mn}}\right]^{-\frac{1}{2}} \tag{4.104}$$

Substituting Equation (4.104) into Equation (4.103) yields

$$\Sigma dE^I = \left[2\tilde{f}(d\epsilon_{ij}^I d\epsilon_{ij}^I)^{\frac{1}{2}}\right] \left[\frac{\partial f}{\sigma_{mn}}\frac{\partial f}{\sigma_{mn}}\right]^{-\frac{1}{2}} \tag{4.105}$$

By collecting the strain-like terms an equivalent strain can be obtained from this last expression and is defined as

$$dE^I = \left[d\epsilon_{ij}^I d\epsilon_{ij}^I\right]^{\frac{1}{2}} \tag{4.106}$$

In addition, by collecting the remaining stress-like terms an equivalent stress can be defined as

$$\Sigma = 2\tilde{f}\left[\frac{\partial f}{\sigma_{ij}}\frac{\partial f}{\sigma_{ij}}\right]^{-\frac{1}{2}} \tag{4.107}$$

Using the definition of the threshold function f then four expressions are obtained for

the equivalent stress. Using Equation (4.99) then for Region #1

$$2\tilde{f}_1 = A_1 I_1^2 + 2B_1 I_2 \tag{4.108}$$

which leads to

$$\frac{\partial f_1}{\sigma_{ij}} \frac{\partial f_1}{\sigma_{ij}} = A_1^2 I_1^2 + 4A_1 B_1 I_1^2 + 4B_1^2 I_2 \tag{4.109}$$

and the equivalent stress for region #1 is

$${}_1\Sigma = \frac{A_1 I_1^2 + 2B_1 I_2}{\sqrt{A_1^2 I_1^2 + 4A_1 B_1 I_1^2 + 4B_1^2 I_2}} \tag{4.110}$$

For Region #2 with

$$2\tilde{f}_2 = A_2 I_1^2 + 2B_2 I_2 + 2D_2 I_5 \tag{4.111}$$

then

$$\frac{\partial f_2}{\sigma_{ij}} \frac{\partial f_2}{\sigma_{ij}} = A_2^2 I_1^2 + 4A_2 B_2 I_1^2 + 4A_2 D_2 I_1 I_4 + 4B_2^2 I_2 + 8B_2 D_2 I_5 + 4D_2^2 I_5 \tag{4.112}$$

and the equivalent stress for Region #2 is

$${}_2\Sigma = \frac{A_2 I_1^2 + 2B_2 I_2 + 2D_2 I_5}{\sqrt{A_2^2 I_1^2 + 4A_2 B_2 I_1^2 + 4A_2 D_2 I_1 I_4 + 4B_2^2 I_2 + 8B_2 D_2 I_5 + 4D_2^2 I_5}} \tag{4.113}$$

For Region #3 with

$$2\tilde{f}_3 = A_3 I_1^2 + 2B_3 I_2 + 2D_3 I_5 \tag{4.114}$$

then

$$\frac{\partial f_3}{\sigma_{ij}} \frac{\partial f_3}{\sigma_{ij}} = A_3^2 I_1^2 + 4A_3 B_3 I_1^2 + 4A_3 D_3 I_1 I_4 + 4B_3^2 I_2 + 8B_3 D_3 I_5 + 4D_3^2 I_5 \tag{4.115}$$

and the equivalent stress for Region #3 is

$$ {}_3\Sigma = \frac{A_3 I_1^2 + 2B_3 I_2 + 2D_3 I_5}{\sqrt{A_3^2 I_1^2 + 4A_3 B_3 I_1^2 + 4A_3 D_3 I_1 I_4 + 4B_3^2 I_2 + 8B_3 D_3 I_5 + 4D_3^2 I_5}} \tag{4.116} $$

Finally for Region #4 with

$$ 2\tilde{f}_4 = A_4 I_1^2 + 2B_4 I_2 \tag{4.117} $$

then

$$ \frac{\partial f_4}{\sigma_{ij}} \frac{\partial f_4}{\sigma_{ij}} = A_4^2 I_1^2 + 4A_4 B_4 I_1^2 + 4B_4^2 I_2 \tag{4.118} $$

and the equivalent stress for Region #4 is

$$ {}_4\Sigma = \frac{A_4 I_1^2 + 2B_4 I_2}{\sqrt{A_4^2 I_1^2 + 4A_4 B_4 I_1^2 + 4B_4^2 I_2}} \tag{4.119} $$

With a complete formulation for an equivalent stress and equivalent strain in hand the next step is the derivation of a mulitaxial formulation for the $\mathscr{F}$ function. Equation (4.34) is used as the starting point for the derivation. Partial derivatives of the threshold function f with respect to the state variable K and a similar derivative of f with respect to the Cauchy stress σ_{pq} along with Equation (4.28) transforms Equation (4.34) into the following format

$$ G = \left[2K \; 2\tilde{f} \; \mathscr{F}\right]^{-1} \tag{4.120} $$

Where $\tilde{f}$ is defined by Equations (4.99) through (4.102) base on the region of the stress space. Substituting this expression for G into Equation (4.35) yields the following general expression for the increment in inelastic strain

$$ d\epsilon_{ij}^I = \left(\frac{1}{2K}\right)\left(\frac{1}{2\tilde{f}}\right)\left(\frac{1}{\mathscr{F}}\right)\frac{\partial f}{\partial \sigma_{km}}\frac{\partial f}{\partial \sigma_{ij}} d\sigma_{km} \tag{4.121} $$

Multiplying this expression by $d\epsilon_{ij}$ yields

$$d\epsilon_{ij}^{I} d\epsilon_{ij}^{I} = \frac{1}{4K^2\ 4\tilde{f}^2\ \mathscr{F}^2} \frac{\partial f}{\partial \sigma_{ij}} \frac{\partial f}{\partial \sigma_{ij}} \frac{\partial f}{\partial \sigma_{km}} \frac{\partial f}{\partial \sigma_{km}} d\sigma_{pq} d\sigma_{pq} \tag{4.122}$$

Solving for $\mathscr{F}$ leads to

$$\mathscr{F} = \left(\frac{1}{2K}\right)\left(\frac{1}{2\tilde{f}}\right)\left[\frac{\partial f}{\partial \sigma_{ij}} \frac{\partial f}{\partial \sigma_{ij}}\right]\left[\frac{d\sigma_{pq} d\sigma_{pq}}{d\epsilon_{kl}^{I} d\epsilon_{kl}^{I}}\right]^{\frac{1}{2}} \tag{4.123}$$

This last equation is expressed in terms of tensor quantities. Using the definition of an equivalent stress and equivalent inelastic strain derived earlier this last equation can be expressed as

$$\mathscr{F} = \frac{2\tilde{f}}{2K\Sigma^2} \frac{dS}{dE^I} \tag{4.124}$$

Where

$$dS = (d\sigma_{ij} d\sigma_{ij})^{\frac{1}{2}} \tag{4.125}$$

Adopting this perspective for anisotropy will greatly simlify the equation for $\mathscr{F}$ later.

Now, Equation (4.123) is specilaized to uniaxial tensile conditions and compared to the uniaxial formulation given in the previous section, i.e. the functional for of $\mathscr{F}$ given in Equation (4.67). Here we start with the stress state for a uniaxial tensile test.

$$\sigma_{ij} = \begin{bmatrix} \sigma_t & 0 & 0 \\ 0 & 0 & 0 \\ 0 & 0 & 0 \end{bmatrix} \tag{4.126}$$

This stress state lies in Region #1 and the associated invariants are

$$\begin{aligned} I_1 &= \sigma_t \\ I_2 &= \sigma_t^2 \end{aligned} \tag{4.127}$$

Substituting these invariants along with the definition of the threshold function from Equation (4.41) into Equation (4.107) for the equivalent stress in Region #1 yields

$$\Sigma = \sigma_t \tag{4.128}$$

For the uniaxial tensile test case f is

$$\tilde{f}_1 = \frac{1}{2} A_1 \sigma_t^2 + B_1 \sigma_t^2 \tag{4.129}$$

the partial of f with respect to the stress tensor is

$$\frac{\partial f_1}{\partial \sigma_{ij}} = A_1 \sigma_t \delta_{ij} + 2 B_1 \sigma_{ij} \tag{4.130}$$

the strain tensor simplifies to

$$\frac{1}{d\epsilon_{ij}} = \frac{1}{d\epsilon_{11}} \tag{4.131}$$

and with

$$\begin{aligned} dS &= (d\sigma_{ij} d\sigma_{ij})^{\frac{1}{2}} \\ &= (d\sigma_{11} d\sigma_{11})^{\frac{1}{2}} \\ &= d(\sigma_t) \end{aligned} \tag{4.132}$$

Then

$$\mathscr{F} = \frac{A_1 + 2B_1}{2K} \frac{d\sigma_t}{d\epsilon_{11}} \tag{4.133}$$

This is the same formulation found in Equation (4.67) for the uniaxial load case.

4.7 Summary of Isotropic Constitutive Equations

In this section the isotropic constitutive model is summarized by stress region. Keep in mind that for region #1

$$\sigma_1 \geq \sigma_2 \geq \sigma_3 \geq 0 \tag{4.134}$$

which results in

$$\begin{aligned} {}^1\,\mathrm{d}\epsilon_{ij}^I &= \frac{(A_1 I_1 \delta_{ij} + 2B_1\sigma_{ij})(A_1 I_1 \delta_{km} + 2B_1\sigma_{km})}{\mathscr{F} 2K(A_1 I_1^2 + 2B_1 I_2)}\,\mathrm{d}\sigma_{km} \\ 2K\,\mathrm{d}K &= A_1 I_1\,\mathrm{d}I_1 + B_1\,\mathrm{d}I_2 \end{aligned} \qquad \begin{cases} f_1 = \dfrac{1}{2}A_1 I_1^2 + B_1 I_2 - K^2 = 0 \\ \text{and} \\ \dfrac{\partial f_1}{\partial \sigma_{ij}} d\sigma_{ij} = [A_1 I_1 \delta_{ij} + 2B_1\sigma_{ij}]d\sigma_{ij} > 0 \end{cases}$$

or

$$\begin{aligned} {}^1\mathrm{d}\epsilon_{ij}^I &= 0 \\ \mathrm{d}K &= 0 \end{aligned} \qquad \begin{cases} f_1 = \dfrac{1}{2}A_1 I_1^2 + B_1 I_2 - K^2 < 0 \\ \text{or} \\ f_1 = \dfrac{1}{2}A_1 I_1^2 + B_1 I_2 - K^2 = 0 \quad \text{and} \\ \dfrac{\partial f_1}{\partial \sigma_{ij}} d\sigma_{ij} = [A_1 I_1 \delta_{ij} + 2B_1\sigma_{ij}]d\sigma_{ij} < 0 \end{cases} \tag{4.135}$$

For region #2

$$\sigma_1 \geq \sigma_2 \geq 0 \geq \sigma_3 \tag{4.136}$$

which results in

$$\begin{aligned} {}^2\,\mathrm{d}\epsilon_{ij}^I &= \frac{(A_2 I_1 \delta_{ij} + 2B_2\sigma_{ij} + D_2(a_m a_i \sigma_{jm} + a_j a_n \sigma_{ni}))}{\mathscr{F} 2K(A_2 I_1^2 + 2B_2 I_2 + 2D_2 I_5)} \big[A_2 I_1 \delta_{km} \\ &\qquad + 2B_2\sigma_{km} + D_2(a_n a_k \sigma_{mn} + a_m a_n \sigma_{nk})\big]\,\mathrm{d}\sigma_{km} \\ 2K\,\mathrm{d}K &= A_2 I_1\,\mathrm{d}I_1 + B_2\,\mathrm{d}I_2 + D_2\,\mathrm{d}I_5 \end{aligned} \qquad \begin{cases} f_2 = \dfrac{1}{2}A_2 I_1^2 + B_2 I_2 + D_2 I_5 - K^2 = 0 \\ \text{and} \\ \dfrac{\partial f_2}{\partial \sigma_{ij}} d\sigma_{ij} = \big[A_2 I_1 \delta_{ij} + 2B_2\sigma_{ij} + D_2(a_k a_i \sigma_{jk} \\ \qquad + a_j a_m \sigma_{mi})\big]\sigma_{ij} > 0 \end{cases}$$

or

$$\begin{aligned} {}^2\mathrm{d}\epsilon_{ij}^I &= 0 \\ \mathrm{d}K &= 0 \end{aligned} \qquad \begin{cases} f_2 = \dfrac{1}{2}A_2 I_1^2 + B_2 I_2 + D_2 I_5 - K^2 < 0 \\ \text{or} \\ f_2 = \dfrac{1}{2}A_2 I_1^2 + B_2 I_2 + D_2 I_5 - K^2 = 0 \quad \text{and} \\ \dfrac{\partial f_2}{\partial \sigma_{ij}} d\sigma_{ij} = \big[A_2 I_1 \delta_{ij} + 2B_2\sigma_{ij} + D_2(a_k a_i \sigma_{jk} + a_j a_m \sigma_{mi})\big] d\sigma_{ij} < 0 \end{cases} \tag{4.137}$$

For region #3

$$\sigma_1 \geq 0 \geq \sigma_2 \geq \sigma_3 \tag{4.138}$$

which results in

$$\begin{aligned}
{}^3\,\mathrm{d}\epsilon_{ij}^I &= \frac{A_3 I_1 \delta_{ij} + 2B_3\sigma_{ij} + D_3(a_m a_i \sigma_{jm} + a_j a_n \sigma_{ni})}{\mathscr{F} 2K(A_3 I_1^2 + 2B_3 I_2 + 2D_3 I_5)}\big[A_3 I_1 \delta_{km} \\
&\qquad + 2B_3\sigma_{km} + D_3(a_n a_k \sigma_{mn} + a_m a_n \sigma_{nk})\big]\,\mathrm{d}\sigma_{km} \\
2K\,\mathrm{d}K &= A_3 I_1\,\mathrm{d}I_1 + B_3\,\mathrm{d}I_2 + D_3\,\mathrm{d}I_5
\end{aligned}
\qquad
\begin{cases}
f_3 = \dfrac{1}{2}A_3 I_1^2 + B_3 I_2 + D_3 I_5 - K^2 = 0 \\
\text{and} \\
\dfrac{\partial f_3}{\partial \sigma_{ij}} d\sigma_{ij} = \big[A_3 I_1 \delta_{ij} + 2B_3\sigma_{ij} + D_3(a_k a_i \sigma_{jk} \\
\qquad + a_j a_m \sigma_{mi})\big] d\sigma_{ij} > 0
\end{cases}$$

or

$$\begin{aligned}
{}^3\mathrm{d}\epsilon_{ij}^I &= 0 \\
\mathrm{d}K &= 0
\end{aligned}
\qquad
\begin{cases}
f_3 = \dfrac{1}{2}A_3 I_1^2 + B_3 I_2 + D_3 I_5 - K^2 < 0 \\
\text{or} \\
f_3 = \dfrac{1}{2}A_3 I_1^2 + B_3 I_2 + D_3 I_5 - K^2 = 0 \quad \text{and} \\
\dfrac{\partial f_3}{\partial \sigma_{ij}} d\sigma_{ij} = \big[A_3 I_1 \delta_{ij} + 2B_3\sigma_{ij} + D_3(a_k a_i \sigma_{jk} \\
\qquad + a_j a_m \sigma_{mi})\big] d\sigma_{ij} < 0
\end{cases} \tag{4.139}$$

Finally for region #4

$$0 \geq \sigma_! \geq \sigma_2 \geq \sigma_3 \tag{4.140}$$

and here the constitutive model takes on the following formulation

$$\begin{aligned} {}^4\,\mathrm{d}\epsilon^I_{ij} &= \frac{(A_4 I_1 \delta_{ij} + 2B_4\sigma_{ij})(A_4 I_1 \delta_{km} + 2B_4\sigma_{km})}{\mathscr{F} 2K(A_4 I_1^2 + 2B_4 I_2)}\,\mathrm{d}\sigma_{km} \\ 2K\,\mathrm{d}K &= A_4 I_1\,\mathrm{d}I_1 + B_4\,\mathrm{d}I_2 \end{aligned} \qquad \begin{cases} f_4 = \dfrac{1}{2}A_4 I_1^2 + B_4 I_2 - K^2 = 0 \\ \text{and} \\ \dfrac{\partial f_4}{\partial \sigma_{ij}} d\sigma_{ij} = [A_4 I_1 \delta_{ij} + 2B_4] d\sigma_{ij} > 0 \end{cases}$$

or

$$\begin{aligned} {}^4\mathrm{d}\epsilon^I_{ij} &= 0 \\ \mathrm{d}K &= 0 \end{aligned} \qquad \begin{cases} f_4 = \dfrac{1}{2}A_4 I_1^2 + B_4 I_2 - K^2 < 0 \\ \text{or} \\ f_4 = \dfrac{1}{2}A_4 I_1^2 + B_4 I_2 - K^2 = 0 \quad \text{and} \\ \dfrac{\partial f_4}{\partial \sigma_{ij}} d\sigma_{ij} = [A_4 I_1 \delta_{ij} + 2B_4 \sigma_{ij}] d\sigma_{ij} < 0 \end{cases} \tag{4.141}$$

4.8 Anisotropic Flow Rule

Once again the flow law is derived from the threshold potential function by way of the derivative following of the threshold function

$$d\epsilon_{ij}^{I} = d\lambda \frac{\partial f}{\partial \sigma_{ij}} \tag{4.142}$$

where $d\lambda$ is the scalar quantity that defines the length of the gradient vector. For anisotropy Equation (4.142) represents a flow rule that embodies the concept of normality, and by using the threshold function in this equation an associated flow rule is explicitly adopted. The gradient defines the normal to the threshold surface and this normal defines the direction of the increment of the inelastic strain vector.

$$f = f(\sigma_{ij}, a_i a_j, d_i d_j, K) \tag{4.143}$$

Recall the a_i is a vector associated with the direction of the principle stresses and the d_i vector is associated with the preferred material direction for transverse isotropy.

The gradients to the threshold surface are given in Equations (3.33), (3.46), (3.55),and (3.60). These functions account for the different material behavior in tension and compression as well as the directional properties of certain types of graphite. The threshold surface is once again divided into four piecewise continuous functions based on principle stresses as follows.

$$\text{Region}\#1 \qquad \sigma_1 \geq \sigma_2 \geq \sigma_3 \geq 0 \tag{4.144}$$

$$\text{Region}\#2 \qquad \sigma_1 \geq \sigma_2 \geq 0 \geq \sigma_3 \tag{4.145}$$

$$\text{Region}\#3 \qquad \sigma_1 \geq 0 \geq \sigma_2 \geq \sigma_3 \tag{4.146}$$

$$\text{Region}\#4 \qquad 0 \geq \sigma_1 \geq \sigma_2 \geq \sigma_3 \tag{4.147}$$

The subscript on the function denotes which region of the stress space the function in valid. Thus for region #1

$$f_1 = \frac{1}{2}A_1 I_1^2 + B_1 I_2 + E_1 I_1 I_6 + F_1 I_7 - K^2 \tag{4.148}$$

The threshold function defined for region #2 is

$$f_2 = \frac{1}{2}A_2 I_1^2 + B_2 I_2 + D_2 I_5 + E_2 I_1 I_6 + F_2 I_7 + H_2 I_9 - K^2 \tag{4.149}$$

The threshold function defined for region #3 is

$$f_3 = \frac{1}{2}A_3 I_1^2 + B_3 I_2 + D_3 I_5 + E_3 I_1 I_6 + F_3 I_7 + H_3 I_9 - K^2 \tag{4.150}$$

and the threshold function defined for region #4 is

$$f_4 = \frac{1}{2}A_4 I_1^2 + B_4 I_2 + E_4 I_1 I_6 + F_4 I_7 - K^2 \tag{4.151}$$

The derivative of the threshold function in region #1 with respect to the inelastic state variable is

$$\frac{\partial f_1}{\partial K} = -2K \tag{4.152}$$

Since isotropic hardening was assumed then similar derivatives with respect to K for region #2, region #3 and region #4 can be formulated, i.e.,

$$\frac{\partial f_2}{\partial K} = -2K \tag{4.153}$$

$$\frac{\partial f_3}{\partial K} = -2K \tag{4.154}$$

and

$$\frac{\partial f_4}{\partial K} = -2K \tag{4.155}$$

respectively

Substituting Equations (3.61), (4.28), and (4.152) into Equation (4.34) yields the following for region #1

$$G_1 = \left[\mathscr{F} 2K(A_1 I_1^2 + 2B_1 I_2 + 2E_1 I_1 I_6 + 2F_1 I_7)\right]^{-1} \tag{4.156}$$

Substituting Equations (3.62), (4.28), and (4.153), and into Equation (4.34) yields the following for region #2

$$G_2 = \left[\mathscr{F} 2K(A_2 I_1^2 + 2B_2 I_2 + 2D_2 I_5 + 2E_2 I_1 I_6 + 2F_2 I_7 + 2H_2 I_9)\right]^{-1} \tag{4.157}$$

Substituting Equations (3.63), (4.28), and (4.154) into Equation (4.34) yields the following for region #3

$$G_3 = \left[\mathscr{F} 2K(A_3 I_1^2 + 2B_3 I_2 + 2D_3 I_5 + 2E_3 I_1 I_6 + 2F_3 I_7 + 2H_3 2I_9)\right]^{-1} \tag{4.158}$$

Substituting Equations (3.64), (4.28), and (4.155) into Equation (4.34) yields the following for region #4

$$G_4 = \left[\mathscr{F} 2K(A_4 I_1^2 + 2B_4 I_2 + 2E_4 I_1 I_6 + 2F_4 I_7)\right]^{-1} \tag{4.159}$$

The formulations for the scalar function $\mathscr{F}$ has yet to be determined.

Now we concentrate on the incremental strain relationship from Equation (4.35). Equations (3.61) and (4.156) are substituted into (4.35) such that

$$
\begin{aligned}
{}^{1}\,\mathrm{d}\epsilon_{ij}^{I} = & \frac{(A_1 I_1 + E_1 I_6)\delta_{ij} + 2B_1\sigma_{ij} + E_1 I_1 d_i d_j + F_1(d_p d_j \sigma_{ip} + d_j d_q \sigma_{qi})}{\mathscr{F} 2K(A_1 I_1^2 + 2B_1 I_2 + 2E_1 I_1 I_6 + 2F_1 I_7)}\Big[\\
& (A_1 I_1 + E_1 I_6)\,\mathrm{d}I_1 + B_1\,\mathrm{d}I_2 + E_1 I_1\,\mathrm{d}I_6 + F_1\,\mathrm{d}I_7\Big]
\end{aligned}
\tag{4.160}
$$

Substituting Equations (3.62) and (4.157) into Equation (4.35) yields

$$
\begin{aligned}
{}^{2}\,\mathrm{d}\epsilon_{ij}^{I} = & \frac{1}{\mathscr{F} 2K(A_2 I_1^2 + 2B_2 I_2 + 2D_2 I_5 + 2E_2 I_1 I_6 + 2F_2 I_7 + 2H_2 I_9)}\Big[\\
& (A_2 I_1 + E_1 I_6)\,\mathrm{d}I_1 + B_2\,\mathrm{d}I_2 + D_2\,\mathrm{d}I_5 + E_2 I_1\,\mathrm{d}I_6 + F_2\,\mathrm{d}I_7 + H_2\,\mathrm{d}I_9\Big]\Big[\\
& (A_2 I_1 + E_2 I_6)\delta_{ij} + 2B_2\sigma_{ij} + D_2(a_m a_i \sigma_{jm} + a_j a_n \sigma_{ni}) + E_2 I_1 d_i d_j + \\
& F_2(d_k d_j \sigma_{ik} + d_j d_m \sigma_{mi}) + \frac{1}{2} H_2(a_m a_n d_n d_i \sigma_{jm} + a_j a_n d_n d_k \sigma_{kj} + \\
& \quad a_i a_n d_n d_m \sigma_{jm} + a_k a_n d_n d_j \sigma_{ki})\Big]
\end{aligned}
\tag{4.161}
$$

Substituting Equations (3.63) and (4.158) into Equation (4.35) yields

$$
\begin{aligned}
{}^{3}\,\mathrm{d}\epsilon_{ij}^{I} = & \frac{1}{\mathscr{F} 2K(A_3 I_1^2 + 2B_3 I_2 + 2D_3 I_5 + 2E_3 I_1 I_6 + 2F_3 I_7 + 2H_3 I_9)}\Big[\\
& (A_3 I_1 + E_3 I_6)\,\mathrm{d}I_1 + B_3\,\mathrm{d}I_2 + D_3\,\mathrm{d}I_5 + E_3 I_1\,\mathrm{d}I_6 + F_3\,\mathrm{d}I_7 + H_3\,\mathrm{d}I_9\Big]\Big[\\
& (A_3 I_1 + E_3 I_6)\delta_{ij} + 2B_3\sigma_{ij} + D_3(a_m a_i \sigma_{jm} + a_j a_n \sigma_{ni}) + E_3 I_1 d_i d_j + \\
& F_3(d_k d_j \sigma_{ik} d_j d_m \sigma_{mi}) + \frac{1}{2} H_3(a_m a_n d_n d_i \sigma_{jm} + a_j a_n d_n d_k \sigma_{kj} + \\
& \quad a_i a_n d_n d_m \sigma_{jm} + a_k a_n d_n d_j \sigma_{ki})\Big]
\end{aligned}
\tag{4.162}
$$

Substituting Equations (3.64) and (4.159) into Equation (4.35) yields

$$
\begin{aligned}
{}^{4}\,\mathrm{d}\epsilon_{ij}^{I} = & \frac{(A_4 I_1 + E_4 I_6)\delta_{ij} + 2B_4\sigma_{ij} + E_4 I_1 d_i d_j + F_4(d_p d_j \sigma_{ip} + d_j d_q \sigma_{qi})}{\mathscr{F} 2K(A_4 I_1^2 + 2B_4 I_2 + 2E_4 I_1 I_6 + 2F_4 I_7)}\Big[\\
& (A_4 I_1 + E_4 I_6)\,\mathrm{d}I_1 + B_4\,\mathrm{d}I_2 + E_4 I_1\,\mathrm{d}I_6 + F_4\,\mathrm{d}I_7\Big]
\end{aligned}
\tag{4.163}
$$

Equations (4.160) through (4.163) comprise the inelastic flow law for each region of the stress space.

4.9 The Scalar Function $\mathscr{F}(K)$ for Anisotropy

Modeling inelastic stress-strain behavior by substituting the incremental strain Equation (4.160) into the evolutionary law Equation (4.29) for region #1 leads to the following expression

$$2K\,\mathrm{d}K = (A_1 I_1 + E_1 I_6)\,\mathrm{d}I_1 + B_1\,\mathrm{d}I_2 + E_1 I_1\,\mathrm{d}I_6 + F_1\,\mathrm{d}I_7 \tag{4.164}$$

Substituting Equation (4.161) into the evolutionary law Equation (4.29) for region #2 yields

$$2K\,\mathrm{d}K = (A_2 I_1 + E_2 I_6)\,\mathrm{d}I_1 + B_2\,\mathrm{d}I_2 + D_2\,\mathrm{d}I_5 + E_2 I_1\,\mathrm{d}I_6 + F_2\,\mathrm{d}I_7 + H_2\,\mathrm{d}I_9 \tag{4.165}$$

Substituting Equation (4.162) into the evolutionary law Equation (4.29) for region #3 yields

$$2K\,\mathrm{d}K = (A_3 I_1 + E_3 I_6)\,\mathrm{d}I_1 + B_3\,\mathrm{d}I_2 + D_3\,\mathrm{d}I_5 + E_3 I_1\,\mathrm{d}I_6 + F_2\,\mathrm{d}I_7 + H_2\,\mathrm{d}I_9 \tag{4.166}$$

Substituting Equation (4.163) into the evolutionary law Equation (4.29) for region #4 yields

$$2K\,\mathrm{d}K = A_4 I_1\,\mathrm{d}I_1 + B_4\,\mathrm{d}I_2 + E_4 I_1\,\mathrm{d}I_6 + F_4\,\mathrm{d}I_7 \tag{4.167}$$

As was the case for isotropic graphite, for anisotropic graphite there are four separate incremental formulations for the isotropic state variable K. However, there is only one state variable, i.e., K and this is a scalar state variable. This state variable controls the size of the current threshold surface and this is consistent with the initial assumption that the only hardening mechanism is isotropic hardening.

Consider a uniaxial tensile stress is applied to an anisotropic graphite,

$$\sigma_{ij} = \begin{bmatrix} \sigma_t & 0 & 0 \\ 0 & 0 & 0 \\ 0 & 0 & 0 \end{bmatrix} \tag{4.168}$$

The invariants for this stress state are

$$I_1 = \sigma_t \tag{4.169}$$

$$I_2 = \sigma_t^2 \tag{4.170}$$

$$I_6 = d_1 d_1 \sigma_t \tag{4.171}$$

$$I_7 = d_1 d_1 \sigma_t^2 \tag{4.172}$$

The inelastic strain increment for this state of stress is

$${}^1\mathrm{d}\epsilon_{11}^I = \frac{1}{{}_t\mathscr{F} 2K(A_1 I_1^2 + 2B_1 I_2 + 2E_1 I_1 I_6 + 2F_1 I_7)} \frac{\partial f_1}{\partial \sigma_{11}} \frac{\partial f_1}{\partial \sigma_{kl}} \mathrm{d}\sigma_{kl} \tag{4.173}$$

Solving for ${}_t\mathscr{F}$ yields

$${}_t\mathscr{F} = \frac{1}{2K(A_1 I_1^2 + 2B_1 I_2 + 2E_1 I_1 I_6 + 2F_1 I_7)} \frac{\partial f_1}{\partial \sigma_{11}} \frac{\partial f_1}{\partial \sigma_{kl}} \frac{\mathrm{d}\sigma_{kl}}{\mathrm{d}\epsilon_{11}^I} \tag{4.174}$$

Since σ_{11} is the only non-zero component of the stress tensor, then

$${}_t\mathscr{F} = \frac{1}{2K(A_1 I_1^2 + 2B_1 I_2 + 2E_1 I_1 I_6 + 2F_1 I_7)} \frac{\partial f_1}{\partial \sigma_{11}} \frac{\partial f_1}{\partial \sigma_{11}} \frac{\mathrm{d}\sigma_{11}}{\mathrm{d}\epsilon_{11}^I} \tag{4.175}$$

Simplifying

$$ {}_t\mathscr{F} = \frac{1}{2K}(A_1 + 2B_1 + 2E_1 d_1 d_1 + 2F_1 d_1 d_1)\frac{d\sigma_{11}}{d\epsilon^I_{11}} \tag{4.176} $$

Once again the derivative of stress with respect to inelastic strain is approximated through the use of a Ramberg–Osgood uniaxial stress-strain law.

In a similar manner to a previous section, an effective stress and an effective strain measures are developed here. The effective stress in all regions is

$$ \Sigma = \frac{2\tilde{f}_\alpha}{\sqrt{\frac{\partial f_\alpha}{\partial \sigma_{ij}}\frac{\partial f_\alpha}{\partial \sigma_{ij}}}} \tag{4.177} $$

where for Region #1

$$
\begin{aligned}
2\tilde{f}_1 &= A_1 I_1^2 + 2B_1 I_2 + 2E_1 I_1 I_6 + 2F_1 I_7 \\
\frac{\partial f_1}{\partial \sigma_{ij}}\frac{\partial f_1}{\partial \sigma_{ij}} &= (3A_1^2 + E_1^2 + 2A_1 E_1 + 4A_1 B_1) I_1^2 + (6A_1 E_1 + 2E_1^2 + \\
&\quad 8B_1 E_1 + 3A_1 F_1 + 4E_1 F_1) I_1 I_6 + (3E_1^2 + 4E_1 F_1 + 2F_1^2) I_6^2 + \\
&\quad 4B_1^2 I_2 + (8B_1 F_1 + 2F_1^2) I_7
\end{aligned}
$$

for Region #2

$$
\begin{aligned}
2\tilde{f}_2 &= A_2 I_1^2 + 2B_2 I_2 + 2D_2 I_5 + 2E_2 I_1 I_6 + 2F_2 I_7 + 2H_2 I_9 \\
\frac{\partial f_2}{\partial \sigma_{ij}}\frac{\partial f_2}{\partial \sigma_{ij}} &= (3A_2^2 + 4A_2 B_2 + 2A_2 E_2 + E_2^2) I_1^2 + 4A_2 D_2 I_1 I_4 + 4B_2^2 I_2 + (6A_2 E_2 + \\
&\quad 4A_2 F_2 + B_2 E_2 + 2E_2^2 + 4E_2 F_2 + 2E_2 H_2 I_{11}^2) I_1 I_6 + (4A_2 H_2 + 4D_2 E_2 + \\
&\quad 2E_2 H_2) I_1 I_8 + (8B_2 D_2 + 2D_2^2 + 2D_2 H_2 I_{11}^2 + \frac{1}{2} H_2^2 I_{11}^2) I_5 + (8B_2 F_2 + 2F_2^2 + \\
&\quad 2F_2 H_2 I_{11}^2 + \frac{1}{2} H_2^2 I_{11}^2) I_7 + (8B_2 H_2 + 4D_2 F_2 + 2D_2 H_2 + 2F_2 H_2 + H_2^2 I_{11}^2) I_9 + \\
&\quad 2D_2^2 I_4^2 + (4D_2 E_2 + 2E_2 H_2) I_1 I_8 + (4D_2 E_2 + H_2^2 I_{11}^2) I_4 I_6 + 4D_2 H_2 I_4 I_8 + \\
&\quad (3E_2^2 + 4E_2 F_2 + 2F_2^2) I_6^2 + (4E_2 H_2 + 4F_2 H_2) I_6 I_8 + H_2^2 I_8^2 + 4D_2 F_2 I_{10}^2
\end{aligned}
$$

for Region #3

$$
\begin{aligned}
2\tilde{f}_3 &= A_3 I_1^2 + 2B_3 I_2 + 2D_3 I_5 + 2E_3 I_1 I_6 + 2F_3 I_7 + 2H_3 I_9 \\
\frac{\partial f_3}{\partial \sigma_{ij}} \frac{\partial f_3}{\partial \sigma_{ij}} &= (3A_3^2 + 4A_3 B_3 + 2A_3 E_3 + E_3^2) I_1^2 + 4A_3 D_3 I_1 I_4 + 4B_3^2 I_2 + (6A_3 E_3 + \\
&\quad 4A_3 F_3 + B_3 E_3 + 2E_3^2 + 4E_3 F_3 + 2E_3 H_3 I_{11}^2) I_1 I_6 + (4A_3 H_3 + 4D_3 E_3 + \\
&\quad 2E_3 H_3) I_1 I_8 + (8B_3 D_3 + 2D_3^2 + 2D_3 H_3 I_{11}^2 + \frac{1}{2} H_3^2 I_{11}^2) I_5 + (8B_3 F_3 + 2F_3^2 + \\
&\quad 2F_3 H_3 I_{11}^2 + \frac{1}{2} H_3^2 I_{11}^2) I_7 + (8B_3 H_3 + 4D_3 F_3 + 2D_3 H_3 + 2F_3 H_3 + H_3^2 I_{11}^2) I_9 + \\
&\quad 2D_3^2 I_4^2 + (4D_3 E_3 + 2E_3 H_3) I_1 I_8 + (4D_3 E_3 + H_3^2 I_{11}^2) I_4 I_6 + 4D_3 H_3 I_4 I_8 + \\
&\quad (3E_3^2 + 4E_3 F_3 + 2F_3^2) I_6^2 + (4E_3 H_3 + 4F_3 H_3) I_6 I_8 + H_3^2 I_8^2 + 4D_3 F_3 I_{10}^2
\end{aligned}
$$

and for Region #4

$$
\begin{aligned}
2\tilde{f}_4 &= A_4 I_1^2 + 2B_4 I_2 + 2E_4 I_1 I_6 + 2F_4 I_7 \\
\frac{\partial f_4}{\partial \sigma_{ij}} \frac{\partial f_4}{\partial \sigma_{ij}} &= (3A_4^2 + E_4^2 + 2A_4 E_4 + 4A_4 B_4) I_1^2 + (6A_4 E_4 + 2E_4^2 + \\
&\quad 8B_4 E_4 + 3A_4 F_4 + 4E_4 F_4) I_1 I_6 + (3E_4^2 + 4E_4 F_4 + 2F_4^2) I_6^2 + \\
&\quad 4B_4^2 I_2 + (8B_4 F_4 + 2F_4^2) I_7
\end{aligned}
$$

In the effective stress equations for Region #2 and Region #3 there are two new invariant terms I_{10} and I_{11}. These terms are defined as

$$I_{10} = a_i d_j \sigma_{ji} \tag{4.178}$$

and

$$I_{11} = a_i d_i \tag{4.179}$$

4.10 Summary of Anisotropic Constitutive Equations

In summary Region #1

$$
\begin{aligned}
{}^{1}\,\mathrm{d}\epsilon_{ij}^{I} &= \frac{(A_1 I_1 + E_1 I_6)\delta_{ij} + 2B_1\sigma_{ij} + E_1 I_1 d_i d_j + F_1(d_p d_j \sigma_{ip} + d_i d_q \sigma_{qj})}{\mathscr{F} 2K(A_1 I_1^2 + 2B_1 I_2 + 2E_1 I_1 I_6 + 2F_1 I_7)} \Big[(A_1 I_1 \\
&\quad + E_1 I_6)\,\mathrm{d}I_1 + B_1\,\mathrm{d}I_2 + E_1 I_1\,\mathrm{d}I_6 + F_1\,\mathrm{d}I_7\Big] \\
2K\,\mathrm{d}K &= (A_1 I_1 + E_1 I_6)\,\mathrm{d}I_1 + B_1\,\mathrm{d}I_2 + E_1 I_1\,\mathrm{d}I_6 + F_1\,\mathrm{d}I_7
\end{aligned}
\qquad
\begin{cases}
f_1 = \dfrac{1}{2}A_1 I_1^2 + B_1 I_2 + E_1 I_1 I_6 \\
\qquad + F_1 I_7 - K^2 = 0 \\
\text{and} \\
\dfrac{\partial f_1}{\partial \sigma_{ij}} d\sigma_{ij} = [(A_1 I_1 + E_1 I_6)\delta_{ij} + 2B_1\sigma_{ij} \\
\qquad + E_1 I_1 d_i d_j + F_1(d_k d_i \sigma_{jk} \\
\qquad + d_j d_m \sigma_{mi})] d\sigma_{ij} > 0
\end{cases}
$$

or

$$
\begin{aligned}
{}^{1}\mathrm{d}\epsilon_{ij}^{I} &= 0 \\
\mathrm{d}K &= 0
\end{aligned}
\qquad
\begin{cases}
f_1 = \dfrac{1}{2}A_1 I_1^2 + B_1 I_2 + E_1 I_1 I_6 + F_1 I_7 - K^2 < 0 \\
\text{or} \\
f_1 = \dfrac{1}{2}A_1 I_1^2 + B_1 I_2 + E_1 I_1 I_6 + F_1 I_7 - K^2 = 0 \quad \text{and} \\
\dfrac{\partial f_1}{\partial \sigma_{ij}} d\sigma_{ij} = [(A_1 I_1 + E_1 I_6)\delta_{ij} + 2B_1\sigma_{ij} \\
\qquad + E_1 I_1 d_i d_j + F_1(d_k d_i \sigma_{jk} + d_j d_m \sigma_{mi})] d\sigma_{ij} < 0
\end{cases}
\tag{4.180}
$$

Region #2

$$
\begin{aligned}
{}^{2}\,\mathrm{d}\epsilon_{ij}^{I} =& \frac{1}{\mathscr{F}2K(A_2I_1^2 + 2B_2I_2 + 2D_2I_5 + 2E_2I_1I_6 + 2F_2I_7 + 2H_2I_9)}\Big[(A_2I_1 \\
&+ E_2I_6)\,\mathrm{d}I_1 + B_2\,\mathrm{d}I_2 + D_2\,\mathrm{d}I_5 + E_2I_1\,\mathrm{d}I_6 + F_2\,\mathrm{d}I_7 + H_2\,\mathrm{d}I_9\Big]\Big[(A_2I_1 \\
&+ E_2I_6)\delta_{ij} + 2B_2\sigma_{ij} + D_2(a_m a_i \sigma_{jm} + a_j a_n \sigma_{ni}) + E_2I_1 d_i d_j \\
&+ F_2(d_k d_j \sigma_{ik} + d_i d_m \sigma_{mj}) + \frac{1}{2}H_2(a_p a_q d_q d_i \sigma_{jp} + a_j a_q d_q d_r \sigma_{ri} \\
&+ a_i a_n d_n d_m \sigma_{jm} + a_k a_n d_n d_j \sigma_{ki})\Big] \\
2K\,\mathrm{d}K =& (A_2I_1 + E_2I_6)\,\mathrm{d}I_1 + B_2\,\mathrm{d}I_2 + D_2\,\mathrm{d}I_5 \\
&+ E_2I_1\,\mathrm{d}I_6 + F_2\,\mathrm{d}I_7 + H_2\,\mathrm{d}I_9
\end{aligned}
$$

$$
\begin{cases}
f_2 = \dfrac{1}{2}A_2I_1^2 + B_2I_2 + D_2I_5 + E_2I_1I_6 \\
\qquad + F_2I_7 + H_2I_9 - K^2 = 0 \\
\text{and} \\
\dfrac{\partial f_2}{\partial \sigma_{ij}}d\sigma_{ij} = \big[(A_2I_1 + E_2I_6)\delta_{ij} + 2B_2\sigma_{ij} \\
\qquad + D_2(a_k a_i \sigma_{jk} + a_j a_m \sigma_{mi}) + E_2I_1 d_i d_j \\
\qquad + F_2(d_k d_i \sigma_{jk} + d_j d_m \sigma_{mi}) \\
\qquad + \dfrac{1}{2}H_2(a_p a_q d_q d_i \sigma_{jp} + a_j a_q d_q d_r \sigma_{ri} \\
\qquad + a_i a_n d_n d_m \sigma_{jm} + a_k a_n d_n d_j \sigma_{ki})\big]d\sigma_{ij} > 0
\end{cases}
$$

or

$$
\begin{aligned}
&{}^{2}\mathrm{d}\epsilon_{ij}^{I}=0\\
&\mathrm{d}K=0
\end{aligned}
\quad
\begin{cases}
f_2=\dfrac{1}{2}A_2I_1^2+B_2I_2+D_2I_5+E_2I_1I_6+F_2I_7+H_2I_9-K^2<0\\
\text{or}\\
f_2=\dfrac{1}{2}A_2I_1^2+B_2I_2+D_2I_5+E_2I_1I_6+F_2I_7+H_2I_9-K^2=0 \quad \text{and}\\
\dfrac{\partial f_2}{\partial\sigma_{ij}}d\sigma_{ij}=\big[(A_2I_1+E_2I_6)\delta_{ij}+2B_2\sigma_{ij}+D_2(a_ka_i\sigma_{jk}+a_ja_m\sigma_{mi})+E_2I_1d_id_j\\
\qquad +F_2(d_kd_i\sigma_{jk}+d_jd_m\sigma_{mi})+\dfrac{1}{2}H_2(a_pa_qd_qd_i\sigma_{jp}+a_ja_qd_qd_r\sigma_{ri}+a_ia_nd_nd_m\sigma_{jm}+a_ka_nd_nd_j\sigma_{ki})\big]d\sigma_{ij}<0
\end{cases}
\tag{4.181}
$$

Region #3

$$
\begin{aligned}
{}^{3}\,\mathrm{d}\epsilon_{ij}^{I} =& \frac{1}{\mathscr{F}2K(A_3I_1^2 + 2B_3I_2 + 2D_3I_5 + 2E_3I_1I_6 + 2F_3I_7 + 2H_3I_9)}\Big[(A_3I_1 \\
&+ E_3I_6)\,\mathrm{d}I_1 + B_3\,\mathrm{d}I_2 + D_3\,\mathrm{d}I_5 + E_3I_1\,\mathrm{d}I_6 + F_3\,\mathrm{d}I_7 + H_3\,\mathrm{d}I_9\Big]\Big[(A_3I_1 \\
&+ E_3I_6)\delta_{ij} + 2B_3\sigma_{ij} + D_3(a_ma_i\sigma_{jm} + a_ja_n\sigma_{ni}) + E_3I_1d_id_j \\
&+ F_3(d_kd_j\sigma_{ik} + d_id_m\sigma_{mj}) + \frac{1}{2}H_3(a_pa_qd_qd_i\sigma_{jp} + a_ja_qd_qd_r\sigma_{ri} \\
&+ a_ia_nd_nd_m\sigma_{jm} + a_ka_nd_nd_j\sigma_{ki})\Big] \\
2K\,\mathrm{d}K =& (A_3I_1 + E_3I_6)\,\mathrm{d}I_1 + B_3\,\mathrm{d}I_2 + D_3\,\mathrm{d}I_5 \\
&+ E_3I_1\,\mathrm{d}I_6 + F_2\,\mathrm{d}I_7 + H_2\,\mathrm{d}I_9
\end{aligned}
$$

$$
\begin{cases}
f_3 = \dfrac{1}{2}A_3I_1^2 + B_3I_2 + D_3I_5 + E_3I_1I_6 \\
\qquad + F_3I_7 + H_3I_9 - K^2 = 0 \\
\text{and} \\
\dfrac{\partial f_3}{\partial \sigma_{ij}}d\sigma_{ij} = \big[(A_3I_1 + E_3I_6)\delta_{ij} + 2B_3\sigma_{ij} \\
\qquad + D_3(a_ka_i\sigma_{jk} + a_ja_m\sigma_{mi}) + E_3I_1d_id_j \\
\qquad + F_3(d_kd_i\sigma_{jk} + d_jd_m\sigma_{mi}) \\
\qquad + \dfrac{1}{2}H_3(a_pa_qd_qd_i\sigma_{jp} + a_ja_qd_qd_r\sigma_{ri} \\
\qquad + a_ia_nd_nd_m\sigma_{jm} + a_ka_nd_nd_j\sigma_{ki})\big]d\sigma_{ij} > 0
\end{cases}
$$

or

$$
\begin{aligned}
{}^{3}\mathrm{d}\epsilon_{ij}^{I} = 0 \\
\mathrm{d}K = 0
\end{aligned}
\quad
\begin{cases}
f_3 = \frac{1}{2}A_3 I_1^2 + B_3 I_2 + D_3 I_5 + E_3 I_1 I_6 + F_3 I_7 + H_3 I_9 - K^2 < 0 \\
\text{or} \\
f_3 = \frac{1}{2}A_3 I_1^2 + B_3 I_2 + D_3 I_5 + E_3 I_1 I_6 + F_3 I_7 + H_3 I_9 - K^2 = 0 \quad \text{and} \\
\frac{\partial f_3}{\partial \sigma_{ij}} d\sigma_{ij} = \big[(A_3 I_1 + E_3 I_6)\delta_{ij} + 2B_3\sigma_{ij} + D_3(a_k a_i \sigma_{jk} + a_j a_m \sigma_{mi}) + E_3 I_1 d_i d_j \\
\qquad + F_3(d_k d_i \sigma_{jk} + d_j d_m \sigma_{mi}) + \frac{1}{2}H_3(a_p a_q d_q d_i \sigma_{jp} + a_j a_q d_q d_r \sigma_{ri} + a_i a_n d_n d_m \sigma_{jm} + a_k a_n d_n d_j \sigma_{ki})\big] d\sigma_{ij} < 0
\end{cases}
\tag{4.182}
$$

Region #4

$$
{}^{4}\,\mathrm{d}\epsilon_{ij}^{I} = \frac{(A_4 I_1 + E_4 I_6)\delta_{ij} + 2B_4\sigma_{ij} + E_4 I_1 d_i d_j + F_4(d_p d_j \sigma_{ip} + d_i d_q \sigma_{qj})}{\mathscr{F} 2K(A_4 I_1^2 + 2B_4 I_2 + 2E_4 I_1 I_6 + 2F_4 I_7)} \Big[(A_4 I_1 + E_4 I_6)\,\mathrm{d}I_1 + B_4\,\mathrm{d}I_2 + E_4 I_1\,\mathrm{d}I_6 + F_4\,\mathrm{d}I_7\Big]
$$

$$
2K\,\mathrm{d}K = A_4 I_1\,\mathrm{d}I_1 + B_4\,\mathrm{d}I_2 + E_4 I_1\,\mathrm{d}I_6 + F_4\,\mathrm{d}I_7
$$

$$
\begin{cases}
f_4 = \frac{1}{2}A_4 I_1^2 + B_4 I_2 + E_4 I_1 I_6 + F_4 I_7 = 0 \\
\text{and} \\
\frac{\partial f_4}{\partial \sigma_{ij}} d\sigma_{ij} = [(A_4 I_1 + E_4 I_6)\delta_{ij} + 2B_4\sigma_{ij} \\
\qquad + E_4 I_1 d_i d_j + F_4(d_k d_i \sigma_{jk} \\
\qquad + d_j d_m \sigma_{mi}) > 0
\end{cases}
$$

or

$$
\begin{array}{l}
{}^{4}\mathrm{d}\epsilon_{ij}^{I} = 0 \\
\mathrm{d}K = 0
\end{array}
\quad
\begin{cases}
f_4 = \dfrac{1}{2}A_4 I_1^2 + B_4 I_2 + E_4 I_1 I_6 + F_4 I_7 < 0 \\
\text{or} \\
f_4 = \dfrac{1}{2}A_4 I_1^2 + B_4 I_2 + E_4 I_1 I_6 + F_4 I_7 = 0 \quad \text{and} \\
\dfrac{\partial f_4}{\partial \sigma_{ij}} d\sigma_{ij} = [(A_4 I_1 + E_4 I_6)\delta_{ij} + 2B_4 \sigma_{ij} + E_4 I_1 d_i d_j \\
\qquad\qquad + F_4(d_k d_i \sigma_{jk} + d_j d_m \sigma_{mi}) < 0
\end{cases}
\tag{4.183}
$$

With the anisotropic formulation of the incremental inelastic stress-strain relationship in hand the next step is exercising the relationships with simple structural applications. This is done in the following chapter.

CHAPTER V

Characterization and Applications

5.1 Introduction - Elasticity

The inelastic constitutive model outlined in the previous chapters is exercised here under isothermal conditions for both isotropic and transversly isotropic nuclear-grade graphites. In order to make use of the inelastic constitutive model an elastic constitutive must also be defined. For isotropic elasticity two material constants have to be stipulated. These constants are Young's Modulus and Poison's ratio. For transversely isotropic elastic materials four material constants are required. These four parameters are Young's Modulus in the preferred material direction, Young's Modulus in the plane of isotropy, Poison's ratio across the preferred material direction and Poison's ratio in the plane of isotropy. Using index notation the elastic constitutive model for either isotropic or transversely isotropic materials is represented by the following expression

$$\epsilon^{E}_{kl} = \gamma_{ijkl}\sigma_{ij} \tag{5.1}$$

This index expression represents the following matrix formulation for isotropic materials

$$\begin{bmatrix} \epsilon_{11} \\ \epsilon_{22} \\ \epsilon_{33} \\ \epsilon_{12} \\ \epsilon_{13} \\ \epsilon_{23} \end{bmatrix} = \begin{bmatrix} 1/E & -\nu/E & -\nu/E & 0 & 0 & 0 \\ -\nu/E & 1/E & -\nu/E & 0 & 0 & 0 \\ -\nu/E & -\nu/E & 1/E & 0 & 0 & 0 \\ 0 & 0 & 0 & 1/G & 0 & 0 \\ 0 & 0 & 0 & 0 & 1/G & 0 \\ 0 & 0 & 0 & 0 & 0 & 1/G \end{bmatrix} \begin{bmatrix} \sigma_{11} \\ \sigma_{22} \\ \sigma_{33} \\ \sigma_{12} \\ \sigma_{13} \\ \sigma_{23} \end{bmatrix} \tag{5.2}$$

Here E, G, and ν are Young's modulus, the shear modulus and Poisson's ratio respectively. For transverse isotropy the matrix formulation is

$$\begin{bmatrix} \epsilon_{11} \\ \epsilon_{22} \\ \epsilon_{33} \\ \epsilon_{12} \\ \epsilon_{13} \\ \epsilon_{23} \end{bmatrix} = \begin{bmatrix} 1/E' & -\nu'/E' & -\nu/E & 0 & 0 & 0 \\ -\nu'/E' & 1/E' & -\nu/E & 0 & 0 & 0 \\ -\nu/E' & -\nu/E' & 1/E & 0 & 0 & 0 \\ 0 & 0 & 0 & 1/G' & 0 & 0 \\ 0 & 0 & 0 & 0 & 1/G' & 0 \\ 0 & 0 & 0 & 0 & 0 & 1/G \end{bmatrix} \begin{bmatrix} \sigma_{11} \\ \sigma_{22} \\ \sigma_{33} \\ \sigma_{12} \\ \sigma_{13} \\ \sigma_{23} \end{bmatrix} \tag{5.3}$$

The matrix formulation in Equation 5.3 is associated with the following preferred material direction

$$d_i = [0, 0, 1] \tag{5.4}$$

where E', G', and ν' are Young's modulus in the preferred direction, the shear modulus across the preferred direction, and Poisson's ratio across the preferred direction.

Four nuclear grade graphites with manufacturer's designations of 2114, G110, H451, and AGOT are used in the applications presented in this chapter. The elastic material constants for these four graphites are listed in Table I.. The graphite designated as G110 is isotropic so $E' = E$, $G' = G$ and $\nu' = \nu$ for this grade of graphite.

Table I.: Elastic Constants

Graphite Designation	$E(GPa)$	$E'(GPa)$	$G(GPa)$	$G'(GPa)$	ν	ν'
2114	16	7	9	3	0.4	0.25
G110	10	NA	6	NA	0.4	NA
H451	9	8	5	1	0.4	0.25
AGOT	11	5	6	2	0.4	0.25

Tensile and compression data from Bratton (2009) for the different graphite grades just mentioned are presented graphically in Figure 33. Bratton's (2009) stress-strain data for each graphite type can be found in Appendix 1, and the elastic constants above were obtained from that stress-strain data. The elastic constants in the table above were extracted from the data using ASTM C749-13. Note that ASTM C1259-15 can be used as an alternative method when dynamic test data is available. It is important to realize that the elastic behavior for graphite is the same in tension and compression. The inelastic behaviors are quite different in tension and compression. None of the stress-strain data emanating from the origin for the graphites identified above exhibit bilinear behavior (see Figure 33) which would indicate a different elastic response in tension when compared with compression.

The discussion here will keep the issue of the preferred direction of the material basic in order to highlight fundamental aspects of the inelastic constitutive model. If the coordinate axes for a given stress analysis do not align with the preferred material direction of a transversely isotropic material then the fourth order tensor of elastic material constants identified in Equation 5.1 would be transformed as follows

$$\gamma_{pqrw} = \alpha_{pi}\alpha_{qj}\alpha_{rl}\alpha_{wk}\gamma_{ijkl} \tag{5.5}$$

Here α_{ij} is the transformation matrix of direction cosines for the angles between the preferred material direction (which is perpendicular to the plane of isotropy) and the given coordinate axes used in the stress analysis. Furthermore, the preferred direction of the material can change from point to point in a component, i.e., a field of preferred directions can

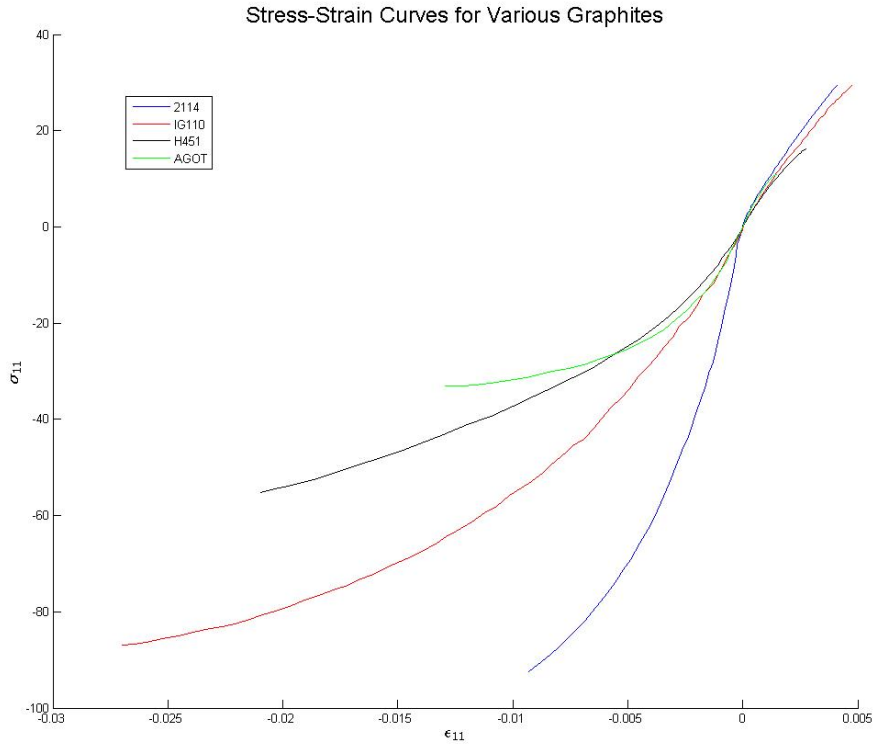

Figure 33: Stress-strain curves for various grades of nuclear graphite. (Bratton (2009))

exist in a material whereby

$$d_i = d_i(x_j) \tag{5.6}$$

This is a complication that is recognized and can be accommodated by the transversely isotropic constitutive model presented herein. This issue will not be pursued further for the sake of simplicity. This topic is left as future work if and when the anisotropic version of the inelastic constitutive model is incorporated into a finite element algorithm.

5.2 Inelastic Material Constants

With the elastic constitutive model characterized the next step is to establish values for the isotropic and anisotropic threshold stresses. The threshold stresses σ_t, σ_c, and τ_i (threshold shear stress) are necessary for an isotropic material. For a transversely isotropic material the isotropic threshold stress values are needed and the threshold stresses σ_{st}, σ_{sc}, and τ_s

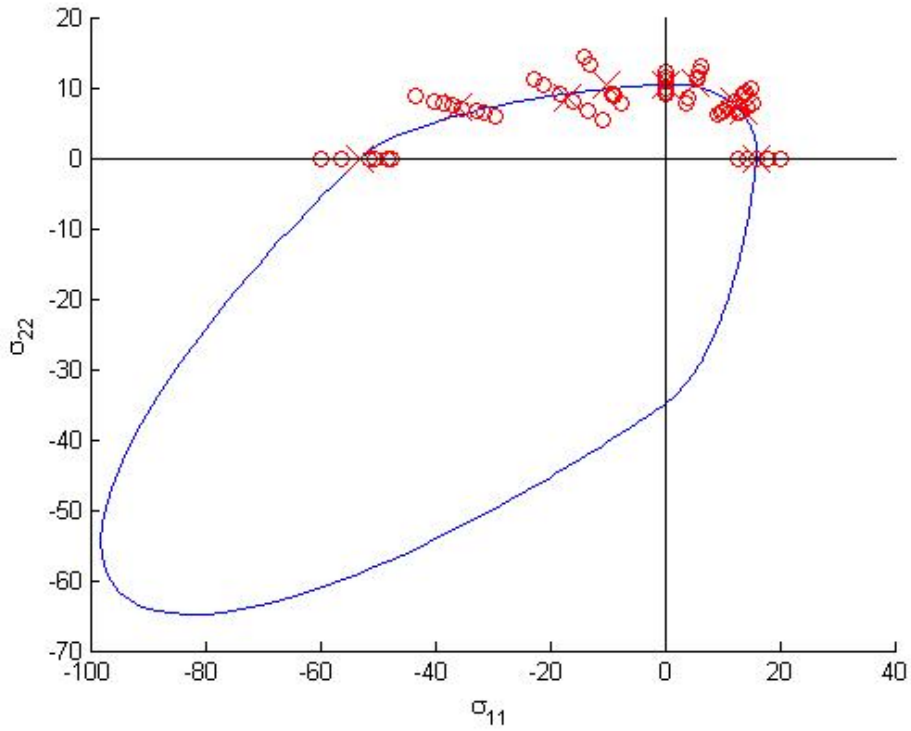

Figure 34: H451 failure data from Burchell (2007) fitted with an anisotropic threshold surface. Strees in MPa.sz

must be established. In addition to the threshold stresses a second set of material parameters are needed for inelasticity. These parameters quantify the degree of nonlinearity associated with the inelastic segment of the stress-strain curve. These are the parameters associated with the scalar function $\mathscr{F}$. In the isotropic case there are four material parameters associated with the scalar function $\mathscr{F}$, i.e., ${}_cn$ and ${}_cC_2$ for compression and ${}_tn$ and ${}_tC_2$ for tension.

In the next section uniaxial test predictions (tension and compression) are made using the constitutive model (elastic and inelastic) and compared with uniaxial test data (tension and compression). In order to make the comparison threshold stresses have been characterized for H451 graphite using Bratton's (2009) stress-strain data in conjunction with Burchell's (2007) failure data. Bratton's (2009) stress-strain data in Figure **??** for H451 corresponds to a uniaxial tension test and a separate compression test conducted in the preferred material direction of each material. The tensile test data and compression test

Table II.: Threshold Stresses (MPa) in the Preferred Direction by Graphite Type

Graphite Type	σ_{st}	σ_{sc}	τ_i
2114	2.248	3.712	1.67
G110	1.309	4.169	1.18
H451	2.2	11	1.31
AGOT	1.108	2.089	0.86

data are superimposed and the threshold stresses σ_{st} and σ_{sc} are obtained directly from this data. Data for tension in the plane of isotropy, compression in the plane of isotropy, and both torsional load paths relative to the preferred material direction are not available for H451 and must be inferred using failure data. The average failure stresses corresponding to the threshold stresses σ_t, σ_{st}, σ_{sc}, and τ_s for H451 were obtained by Burchell (2007) and the failure data appears in Figure 34. The assumption is made here that the failure surface defined by Burchell's (2007) data is concentric with the threshold surface of the material. Ratios between failure stresses are calculated and applied to the requisite threshold stresses, given that threshold stresses σ_{st} and σ_{sc} are known. This yields the threshold stresses σ_t and τ_i. The threshold stresses for the 2114 and AGOT can be obtained in a similar manner. Again G110 is isotropic, therefore $\sigma_t = \sigma_{st}$, $\sigma_c = \sigma_{sc}$ and $\tau_i = \tau_s$. Threshold stress values for the four nuclear graphites are summarized in Table II..

The data provided by Bratton (2009) contains numerical stress-strain data pairs for the four graphites under consideration. Using the parameter estimation scheme outlined in the previous chapter the tensile and compressive values for n and C_2 associated with the scalar function $\mathscr{F}$ for these four graphites are listed in Table III..

Table III.: Constants for the Scalar Function $\mathscr{F}$

Graphite Designation	${}_tn$	${}_tC_2$	${}_cn$	${}_cC_2$
2114	1.4342	1.744E-05	4.7835	1.532E-12
AGOT	2.824	4.323E-07	4.6151	9.286E-10
G110	1.6359	6.919E-06	2.7697	7.352E-08
H451	2.3975	8.729E-07	2.7442	2.157E-07

5.3 Comparison: Stress-Strain Predictions with Data

Characterizing the elastic and inelastic models is a large effort requiring an extensive data base. Once the models are assembled and characterized the next step is examining how they function under various applied boundary conditions. Following this scenario the constitutive models (elastic and inelastic) are initially used to predict very simple uniaxial tension and compression behavior after characterization. Model predictions for these simple load paths are displayed in this section for all four graphites previously mentioned. In a perfect world one would use an extended data base to characterize all model parameters and then, for example, make a comparison to stress-strain data from torsional tests or thin wall pressure vessel tests - test data that was not used in the characterization process. While failure data exists for nuclear grade graphite subject to torsion and pressure vessel test loads, stress-strain data for these two types of tests is not available. So initially, information available from uniaxial data and failure data obtained under mutliaxial states of stress are used to characterize model parameters. Predictions are then presented for the entire uniaxial stress-strain curves, tension and compression, and test data is overlain on the curves for comparison purposes.

Three threshold stress values are required in order to make model predictions under uniaxial loads for isotropic graphites, i.e., σ_t, σ_c, and τ_i. In order to make uniaxial predictions for transversely isotropic graphites loaded in tension or compression the threshold stress σ_{st}, σ_{sc}, and τ_s are required. The threshold stress values in and across the preferred direction for all four graphites are listed in Table II., keeping in mind that G110 is isotropic.

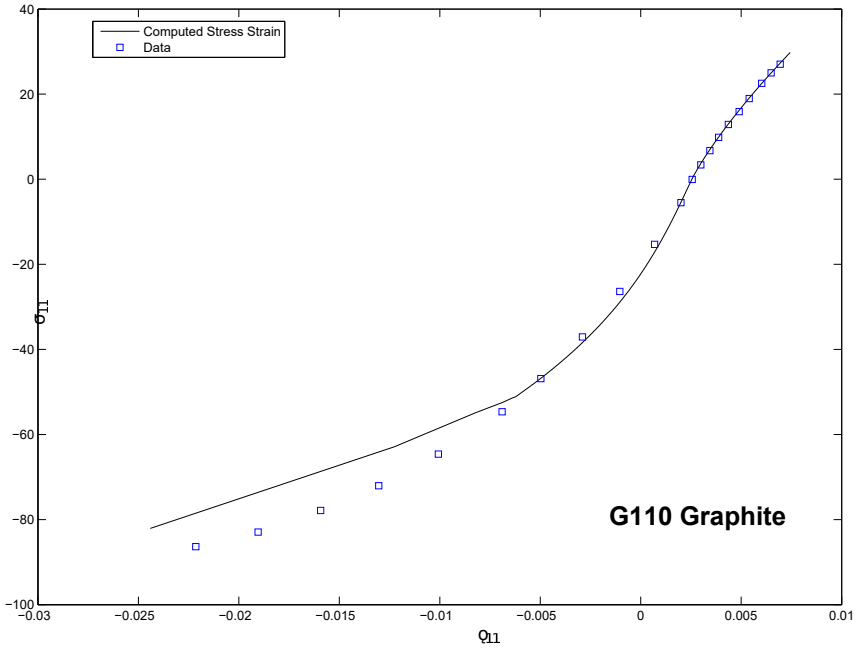

Figure 35: Predicted Stress-strain behavior for G110 Graphite with data for simple tension and compression. All stresses are in MPa. Data is courtesy of Braton (2009)

With the threshold stresses for G110 in Table II., the inelastic model parameter values in Table III., and the elastic constants in Table I., the elastic and inelastic constitutive models were utilized to create the stress-strain curve (tension and compression) depicted in Figure 35. The solid line represents load paths in both tension and compression. These load paths were modeled assuming that the material was in the virgin state at the beginning of either load path, i.e., the material has not hardened. Selected stress-strain data pairs that are fairly well spaced out from Bratton (2009) are included in this Figure 35 for comparison purposes. The model apparently tracks the tensile data well, but as inelastic strains accumulate in the compressive regime there is a loss in fidelity in the comparison to the data.

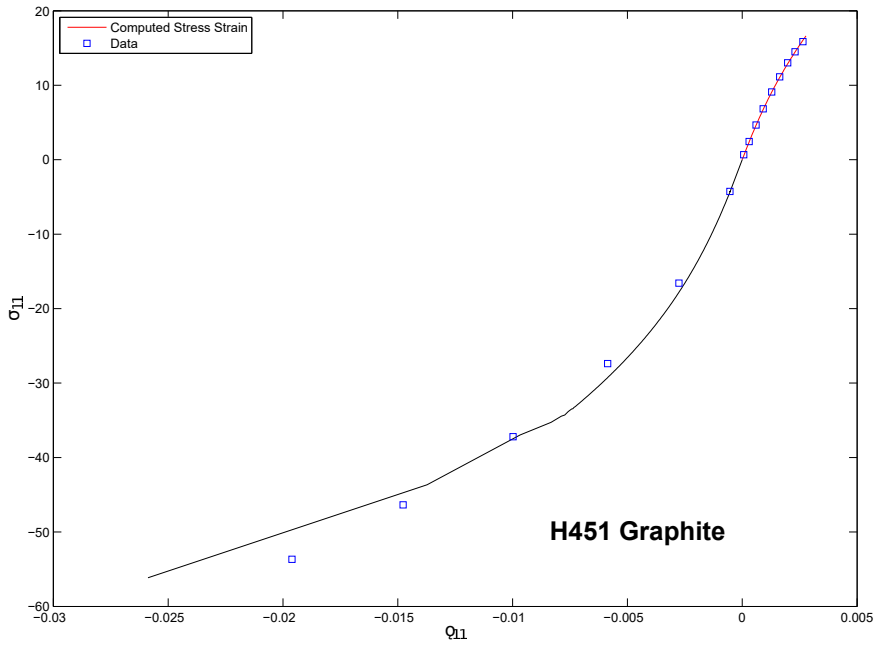

Figure 36: Predicted Stress-strain behavior for H451 Graphite with date for simple tension and compression. All stresses are in MPa. Data is courtesy of Braton (2009)

With the threshold stresses for H451 in Table II., the inelastic model parameter values in Table III., and the elastic constants in Table I., the elastic and inelastic constitutive models were utilized to create the stress-strain curve (tension and compression) depicted in Figure 36. Once again, the solid line represents load paths in both tension and compression, and these load paths were modeled assuming that the material was in the virgin state at the beginning of either load path, i.e., the material has not hardened. Selected stress-strain data pairs that are fairly well spaced out from Bratton (2009) are included in this Figure 36 for comparison purposes. Based on visual inspection there is good correlation with Bratton's (2009) tensile data and fairly good correlation with the compression data.

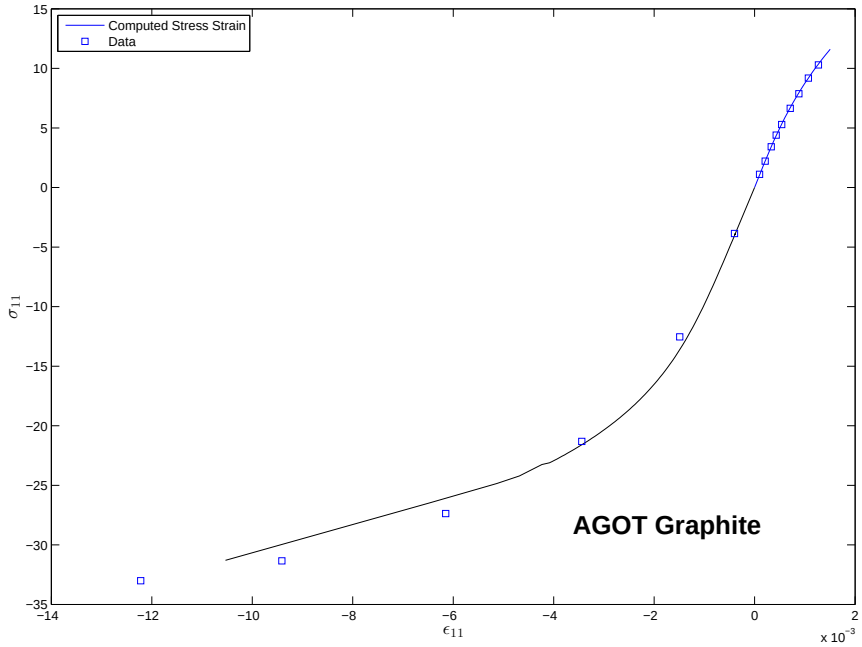

Figure 37: Predicted Stress-strain behavior for AGOT Graphite with data for simple tension and compression. All stresses are in MPa. Data is courtesy of Braton (2009)

With the threshold stresses for AGOT in Table II., the inelastic model parameter values in Table III., and the elastic constants in Table I., the elastic and inelastic constitutive models were utilized to create the stress-strain curve (tension and compression) depicted in Figure 37. Once again, the solid line represents load paths in both tension and compression, and these load paths were modeled assuming that the material was in the virgin state at the beginning of either load path, i.e., the material has not hardened. Selected stress-strain data pairs from Bratton (2009) are included in this Figure 37 for comparison purposes. Again, there seems to be good correlation in the tensile regime and relatively good correlation in the compressive region of the curve.

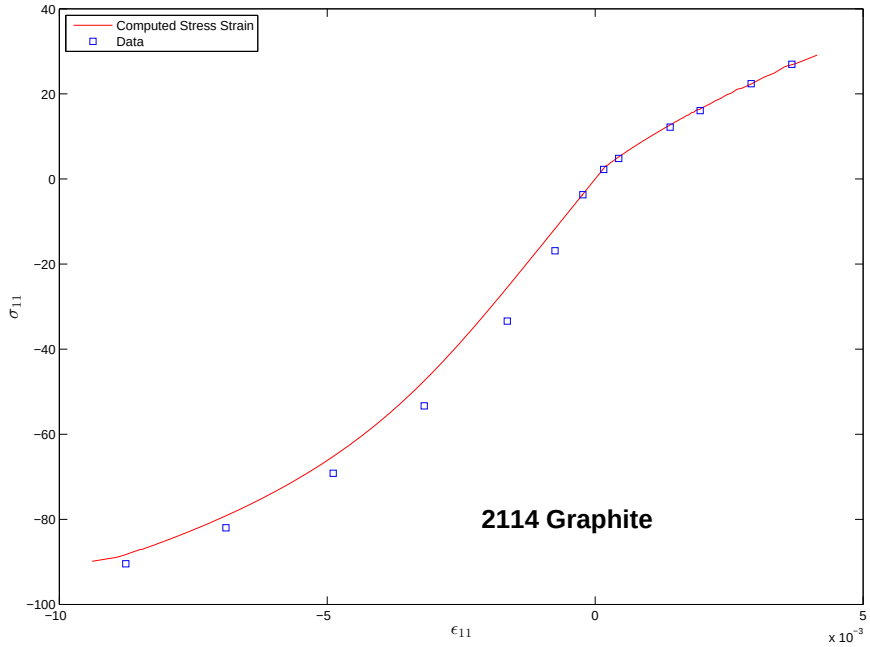

Figure 38: Predicted Stress-strain behavior for 2114 Graphite with data for simple tension and compression. All stresses in MPa. Data is courtesy of Braton (2009)

Finally, with the threshold stresses for 2114 in Table II., the inelastic model parameter values in Table III., and the elastic constants in Table I., the elastic and inelastic constitutive models were utilized to create the stress-strain curve (tension and compression) depicted in Figure 38. Again, the solid line represents load paths in both tension and compression, and these load paths were modeled assuming that the material was in the virgin state at the beginning of either load path, i.e., the material has not hardened. Selected stress-strain pairs from the Bratton (2009) data are included in Figure 38 for comparison purposes. There appears to be good correlation on the tensile portion of the curve. However, on the compression segment of the curve there is a tendency to overestimate the strain at a given level of stress.

Overall the model tends to drift a bit relative to the compression data for each graphite. Several issues could explain this drift. First, in this work it was assumed that graphite hardens isotropically both in tension and compression. These materials may harden differently

in compression than they do in tension. In addition, the assumed functional form for ${}_c\mathscr{F}$ may be optimized in the sense that some weighted function can be used to better correlate with compressive data. This issue is reserved for future efforts.

5.4 Strain Controlled Behavior Over One Cycle

In this section predictions for cyclic stress-strain behavior is examined for both isotropic and transversely isotropic material. One can fatigue a material under load control or displacement control. Results here represent analyses performed under total strain control where

$$\epsilon_{total} = \epsilon_{elastic} + \epsilon_{inelastic} \tag{5.7}$$

The material is subjected to a total uniaxial tensile strain of 0.004. Subsequent to achieving this total tensile strain limit the load is reversed until a 0.01 total strain limit is achieved in compression. Figure 39 depicts the stress-strain curve for H451 graphite subjected to this total strain cycle. Initially all materials are assumed to be in a virgin state before loads are applied. Within several strain cycles the stress-strain curve flattens out becoming a straight line with little hysteresis and a slope equal to the elastic Young's modulus. In essence, after a limited number of cycles the response becomes elastic as the material hardens isotropically as the fixed strain cycle is completely encompassed within the expanding threshold surface.

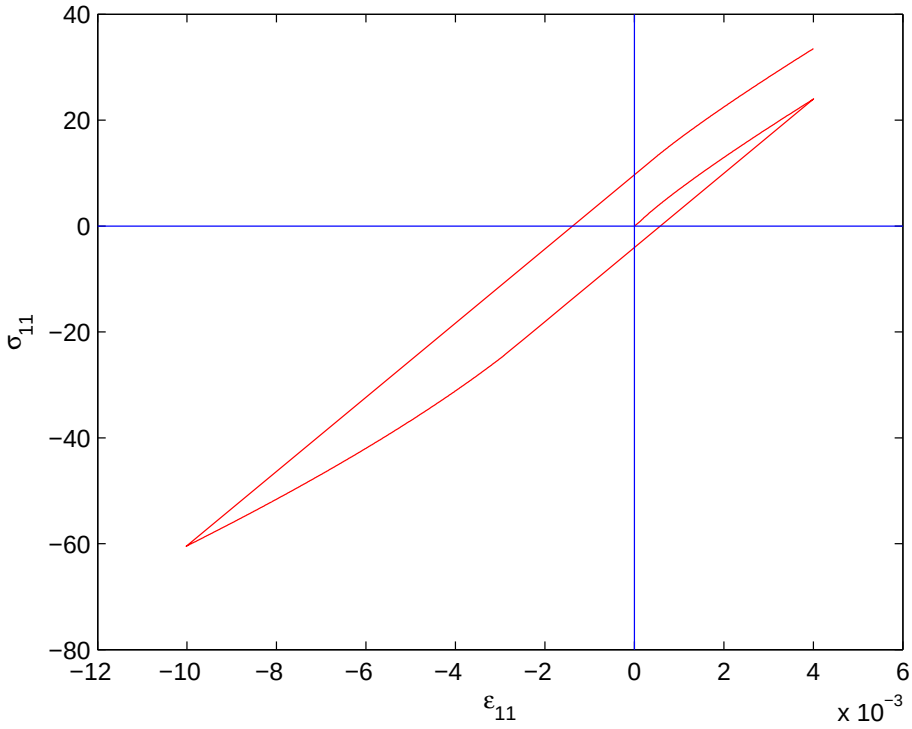

Figure 39: Hysteresis loop for isotropic H451 Graphite using isotropic hardening. All stresses in MPa

Next the model's predictive capabilities are examined under the assumption of anisotropy with varying orientations of the preferred material direction. Figure 40 depict single hysteresis loops for H451 associated with preferred material direction vectors d_i = (1, 0, 0), d_i = (1/2, 1/2, 0) and d_i = (0, 1, 0). As expected the model is stiffer when the preferred direction of the material is oriented to the load direction, i.e., when $d_i = (1, 0, 0)$. As a result, the stress response with this orientation is higher in tension and compression relative to the other preferred directions due to the increased stiffness. Again, if this hysteresis loop is continued for several more cycles the result would be a linear stress-strain relationship as the threshold surface grows to include the stresses generated at these strain limits.

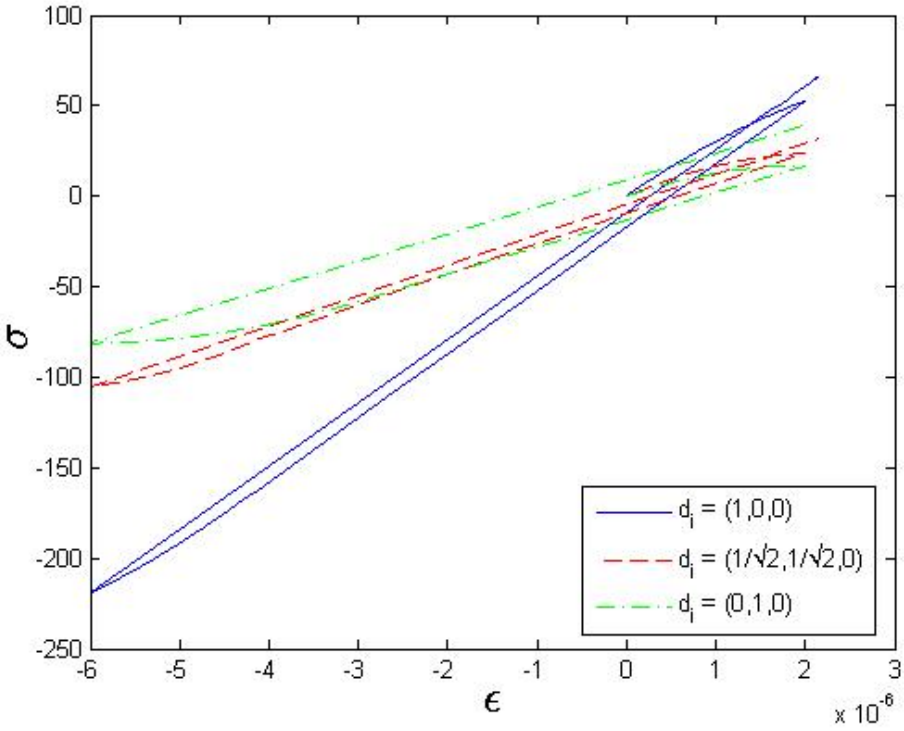

Figure 40: Hysteresis loop for anisotropic H451 Graphite depicting varying preferred material directions with isotropic hardening. All stresses in MPa

5.5 The Inelastic Response of Isotropic H451

In this section the model's ability to predict inelastic deformation is exercised under various combinations of uniaxial, torsional and pressure vessel load paths applied to isotropic H451. Conceptually it has been presumed that the material hardens isotropically for all load paths. Thus the geometry associated with the virgin threshold surface and the increment in inelastic strain vector obtained from the normality assumption holds along the entire length of the load path traversed. The material used in these analyses is H451 graphite. Specific material parameters (elastic and inelastic) for both isotropic and anisotropic versions of H451 graphite are shown in Table IV.. Here stress values are specified in units of MPa.

Table IV.: H451 Material Parameters (stress in units of MPa)

H451	E_{11}	E_{22}	ν_{12}	ν_{23}	G_{12}	σ_{st}	σ_{sc}	τ_s	σ_t	σ_c	τ_i
Isotropic	8070	–	0.4	–	4600	2.2	11.0	2.1	–	–	–
Anisotropic	8070	3500	0.4	0.25	4600	2.2	11.0	2.1	1.67	7.27	1.6

5.5.1 Torsional Load Path - Isotropic H451

Torsional loading is the first elastic-inelastic load path examined. This load path is representative of a thin-wall tube subjected to a torque. Here an *r* (associates with x_1), θ (associates with x_2) and *z* (associates with x_3) coordinate system is utilized. Figure 41 depicts a virgin threshold surface along with a torsional load path and the resultant increment in inelastic strain vector associated with this load path. The normality of the increment in inelastic strain vector to the threshold flow surface requires that the vector will have not only a shear strain components but a normal strain components as well. Thus in a thin-wall tube fabricated from graphite (see Burchell's (2007) work) subjected to a torsional load, radial, circumferential and axial normal strains should be expected, not just torsional strains. The direction cosines associated with the components of the increment in inelastic strain under torsional loading are $(0.1214, 0.1214, 0.1214, 0, 0, 0.9852)$. Here direction cosine values correspond to the total strain components $(\epsilon_{11}, \epsilon_{22}, \epsilon_{33}, \epsilon_{23}, \epsilon_{13}, \epsilon_{12})$. The normal increments in inelastic strains ($d\epsilon_{11}, d\epsilon_{22}$, and $d\epsilon_{33}$) will be slight in comparison to the increments in inelastic shear strain. In comparison, if only a uniaxial load is applied to the tube (either in tension or compression) only increments in inelastic axial strains are predicted by the model. For a J_2 model where a material behaves the same in tension and compression, a torsional load path produces only shear strains. This is depicted graphically in Figure 42.

Stress-strain curves for an H451 graphite subjected to a torsional load path are presented in Figure 43. Again these curves represent the response of a thin walled tube being subjected to a torque. The strain components ϵ_{33} (axial) and ϵ_{12} are plotted versus the applied torsional stress. The ϵ_{11} (radial) and ϵ_{22} (circumferential) strains are identical to the

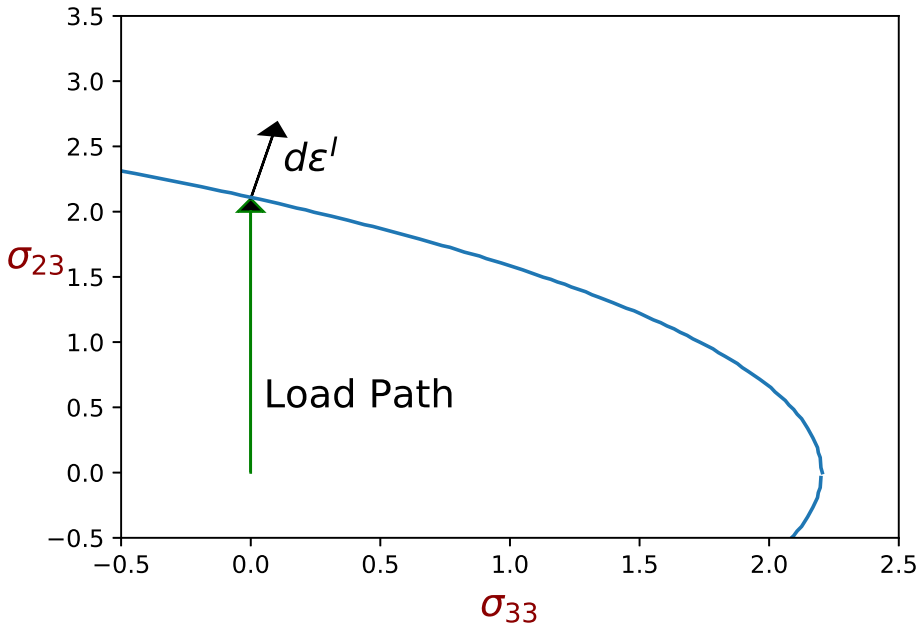

Figure 41: Threshold surface for isotropic H451 Graphite with a torsional load path showing the incremental strain direction. Stresses in MPa.

ϵ_{33} strain response. The stress state at the end of the load path is

$$\sigma_{ij} = \begin{bmatrix} 0 & 0 & 0 \\ 0 & 0 & 4.3 \\ 0 & 4.3 & 0 \end{bmatrix} \tag{5.8}$$

which corresponds to the following total strains at the end of the load path

$$\epsilon_{ij} = \begin{bmatrix} 0.17 & 0 & 0 \\ 0 & 0.17 & 1.38 \\ 0 & 1.38 & 0.17 \end{bmatrix} \times 10^{-3} \tag{5.9}$$

This assumes there are no restraints (i.e., boundary conditions) on the tube other than the applied torque.

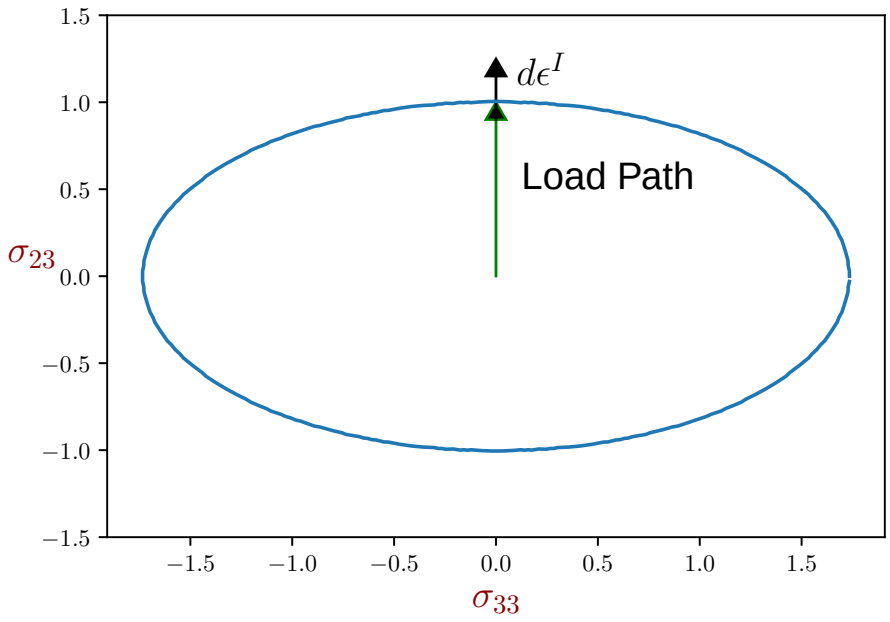

Figure 42: J_2 (Von Mises) threshhold surface shown with a torsional load path. Stress in MPa.

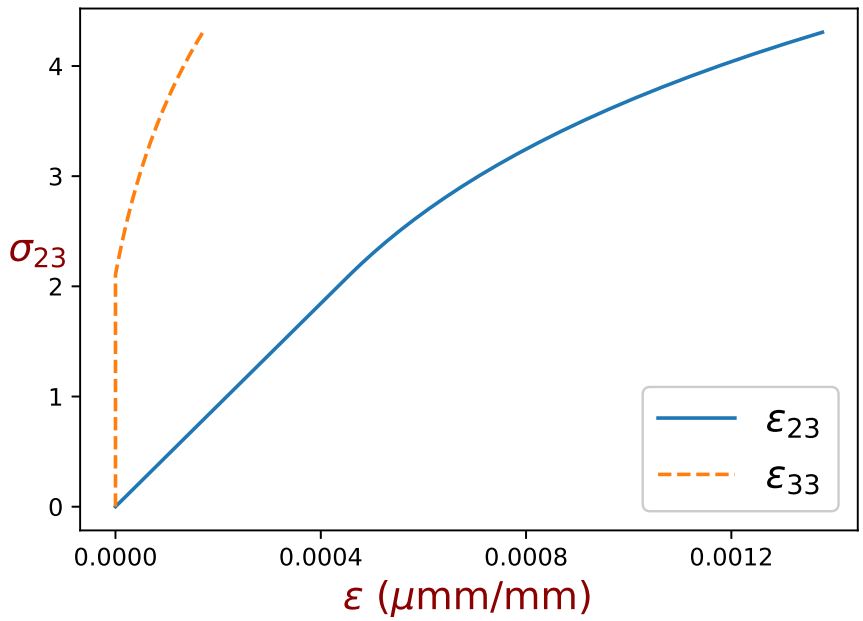

Figure 43: Predicted stress-strain curves for a tube fabricated from isotropic H451 graphite subjected to a torque 41. Stress in MPa.

5.5.2 Pressure Vessel Load Path - Isotropic H451

The next elastic-inelastic load path considered represents a thin-wall tube subjected to an internal pressure. The stress matrix for this load path is identified as

$$\sigma_{ij} = \begin{bmatrix} 0 & 0 & 0 \\ 0 & 2\sigma & 0 \\ 0 & 0 & \sigma \end{bmatrix} \tag{5.10}$$

Here ϵ_{22} corresponds to a circumferential strain and ϵ_{33} is a longitudinal strain. For a J_2 model associated with a material that has identical inelastic behavior in tension and compression only increments in inelastic strain associated with ϵ_{22} (i.e., the circumferential direction) would be predicted. The J_2 model predicts zero inelastic strain in the ϵ_{33} direction (see Figure 45). For isotropic H451 the pressure vessel load path generates increments in all three normal inelastic strain components. The ϵ_{22} and ϵ_{33} components of the inelastic strain vector are depicted graphically in Figure 44. Here the pressure vessel load path is projected onto a virgin threshold surface for an isotropic H451 graphite material. Although in this figure only the ϵ_{22} and ϵ_{33} components of the increment in inelastic strain vector appear, the entire increment of the inelastic strain rate vector has direction cosines $(-0.03, 0.90, 0.43, 0, 0, 0)$. A contraction in the radial direction corresponds to a thinning of the pressure vessel wall. For this load path the final stress state is

$$\sigma_{ij} = \begin{bmatrix} 0 & 0 & 0 \\ 0 & 6.14 & 0 \\ 0 & 0 & 3.07 \end{bmatrix} \tag{5.11}$$

Figure 46 shows the stress-strain curves for a thin wall tube fabricated from isotropic H451 material and subjected to a pressure vessel load path. The final accumulated strains associ-

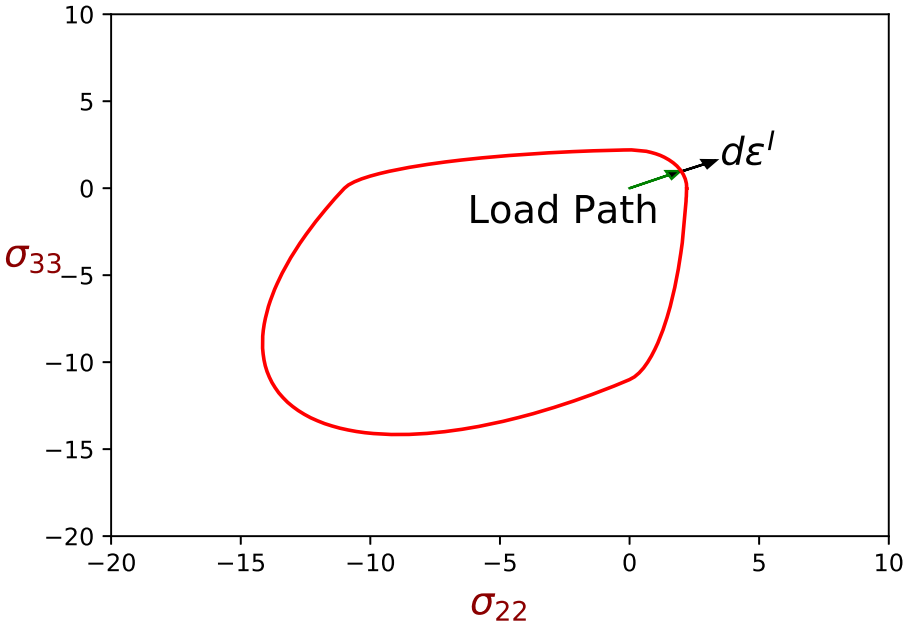

Figure 44: Threshhold surface for isotropic H451 shown with a pressure vessel load path and the corresponding increment in inelastic strain vector. Stress in MPa.

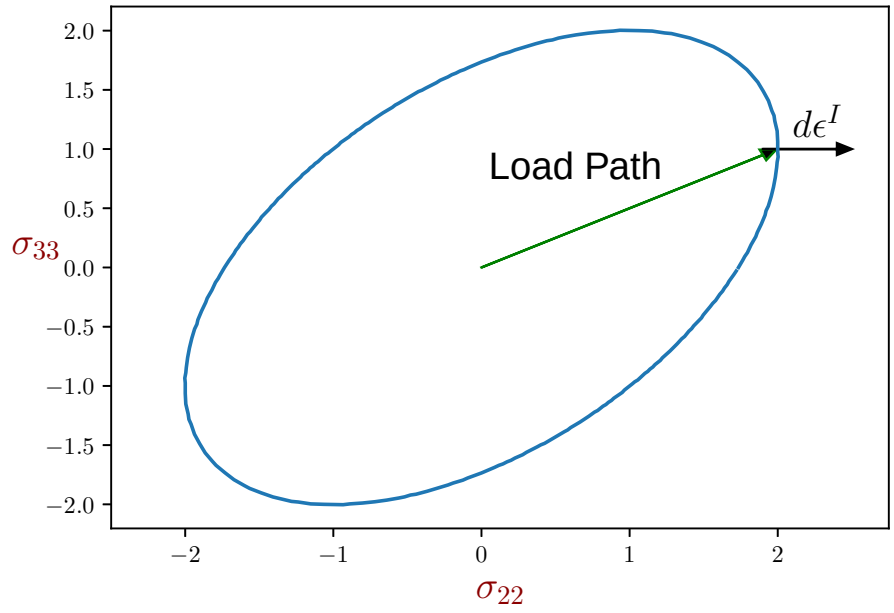

Figure 45: J_2 (Von Mises) threshhold surface shown with a pressure vessel load path. Stress in MPa.

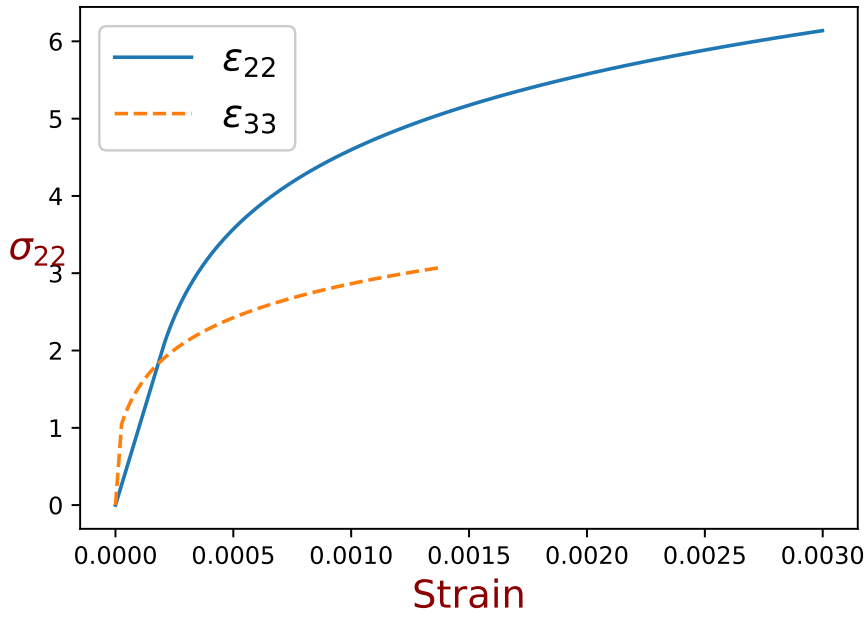

Figure 46: Predicted circumferential and longitudinal stress-strain behavior for pressure vessel load path 44 as a function of circumferential strain and longitudinal strain. The material is isotropic H451 graphite. Stress in MPa.

ated with this stress state are

$$\epsilon_{ij} = \begin{bmatrix} -0.00026 & 0 & 0 \\ 0 & 0.0030 & 0 \\ 0 & 0 & 0.0013 \end{bmatrix} \tag{5.12}$$

5.5.3 A Non-proportional Load Path - Isotropic H451

The third elastic-inelastic load path represents a uniaxial stress (σ_{11}) followed by the application of a shear stress (σ_{12}), i.e., a non-proportional load path. This load path lies completely within the elastic range for the initial uniaxial segment. This segment starts at a zero stress and increases to a value of 2.2 MPa. While holding the uniaxial stress at 2.2 MPa a shear stress is applied in the subsequent load segment. The shear stress is similarly increased from a value of zero to a value of 2.2 MPA. Given how the load path is imposed

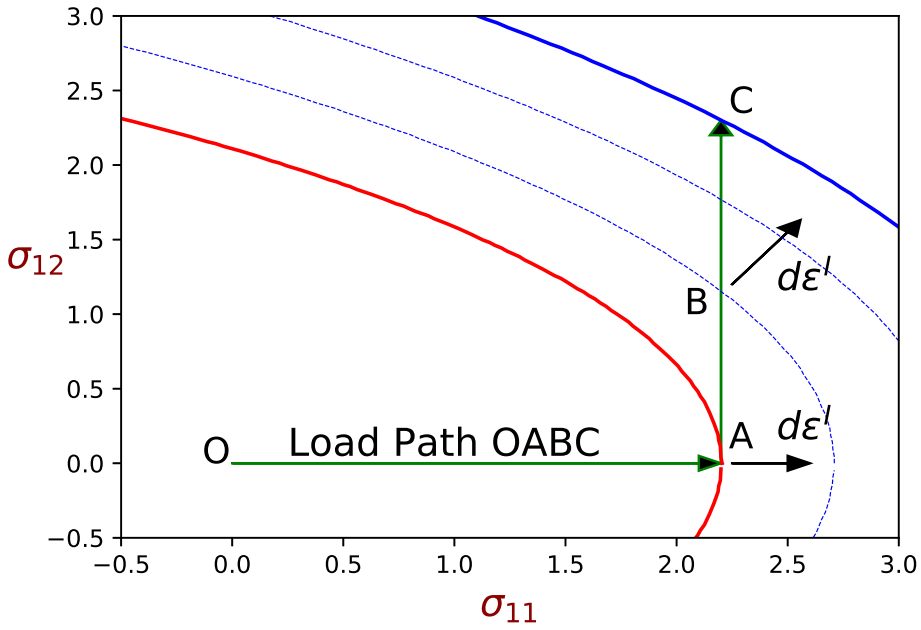

Figure 47: Non-proportional load path with initial, subsequent and final threshold surfaces using isotropic H451. Stress in MPa.

inelastic strains are only accrued along the second segment of the load path for isotropic H451. In the next section a load path with similar end point stress values is examined with a proportional load path and final strain states will be compared to the non-proportional strains cited in this section. The load path is depicted graphically in Figure 47. In this figure the inner threshold surface is a virgin threshold surface, and the outer threshold surface represents the material after it has hardened isotropically. Given the attending geometry of the inelastic threshold surface and the increment in inelastic strain vector we expect and obtain inelastic strains in both the ϵ_{11} and ϵ_{12} directions under the application of the σ_{12} stress in segment AB of the load path.

Figure 48 supports this expectation with an σ_{11} and ϵ_{11} stress-strain curve over the entire load path. The first portion of this stress-strain curve response is elastic and corresponds to segment OA of the load path. The plateau region in this stress-strain curve represents the inelastic response developed from applying a shear stress in the second segment of the load path. The increase in axial strain under the application of a shear stress while the

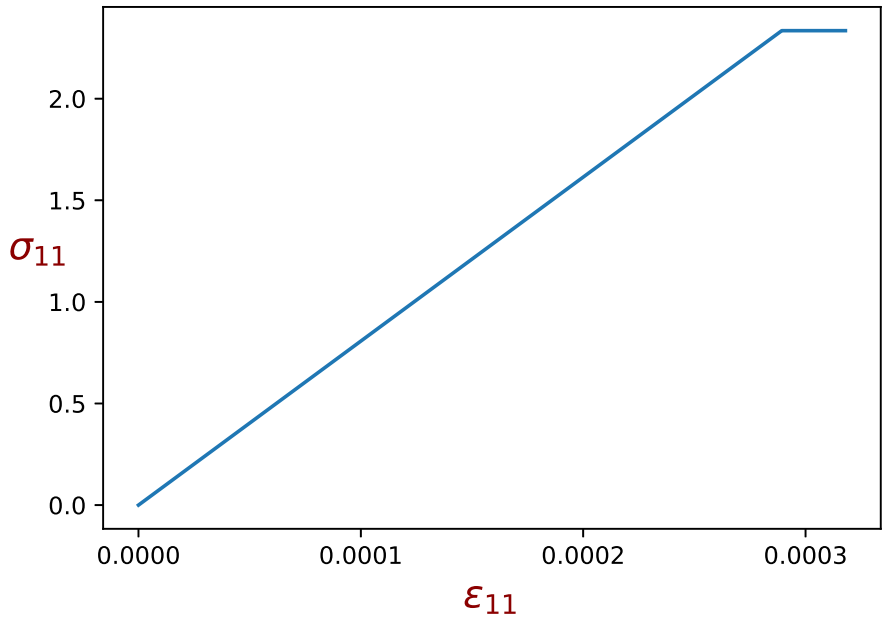

Figure 48: The σ_{11}-ϵ_{11} stress-strain curve for the non-proportional load path OABC 47 - isotropic H451 graphite. Stress in MPa.

uniaxial stress is held constant is the result of the normality condition built into the model. In addition, compressive ϵ_{22} and ϵ_{33} strains are predicted.

Figure 49 depicts the σ_{12} and ϵ_{12} stress-strain curve for the entire load path (OAB). Elastic shear strains are not accumulated along segment OA of the load path. However, along segment AB of this load path shear strains are accumulated. The material response is entirely inelastic along segment AB and as a result the shear stress-strain curve in Figure 49 is non-linear with an increasing rate of inelastic shear strain being accumulated as the increment in the inelastic strain vector rotates as shown in Figure 47.

The final stress state is

$$\sigma_{ij} = \begin{bmatrix} 2.2 & 2.2 & 0 \\ 2.2 & 0 & 0 \\ 0 & 0 & 0 \end{bmatrix} \tag{5.13}$$

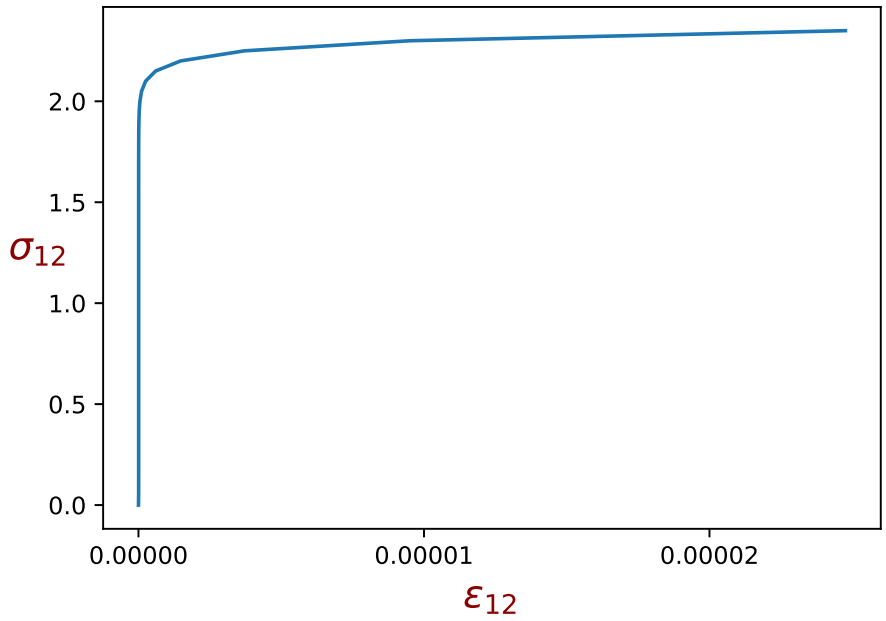

Figure 49: The σ_{12}-ϵ_{12} stress-strain curve for the non-proportional load path OABC 47 - isotropic H451 graphite. Stress in MPa.

The final accumulated strains are

$$\epsilon_{ij} = \begin{bmatrix} 0.318 & 0.025 & 0 \\ 0.025 & -0.113 & 0 \\ 0 & 0 & -0.116 \end{bmatrix} \times 10^{-3} \tag{5.14}$$

5.5.4 A Proportional Load Path - Isotropic H451

In a previous section results from a pressure vessel load path were presented. That load path can be considered a proportional load path. In this section the analytical results for a second elastic-inelastic proportional load path are presented. For this proportional load path a normal stress and a shear stress are concurrently applied in a 1:1 ratio to an isotropic H451 graphite. This load path with its one-to-one slope is identified by line segment OA in Figure 50. Again the inner threshold surface is a virgin threshold surface, and the outer threshold surface at the end of the load path represents the material after it has hardened

isotropically. At the end of the load path the final stress state is identical to the stress state identified for the non-proportional load path where the uniaxial and torsional stress components were applied sequentially. As expected the final accumulated strains for the proportional load path are different from the accumulated strains for the non-proportional load path with identical stress components at the end of the load path. Clearly the final strain state of the material is path dependent.

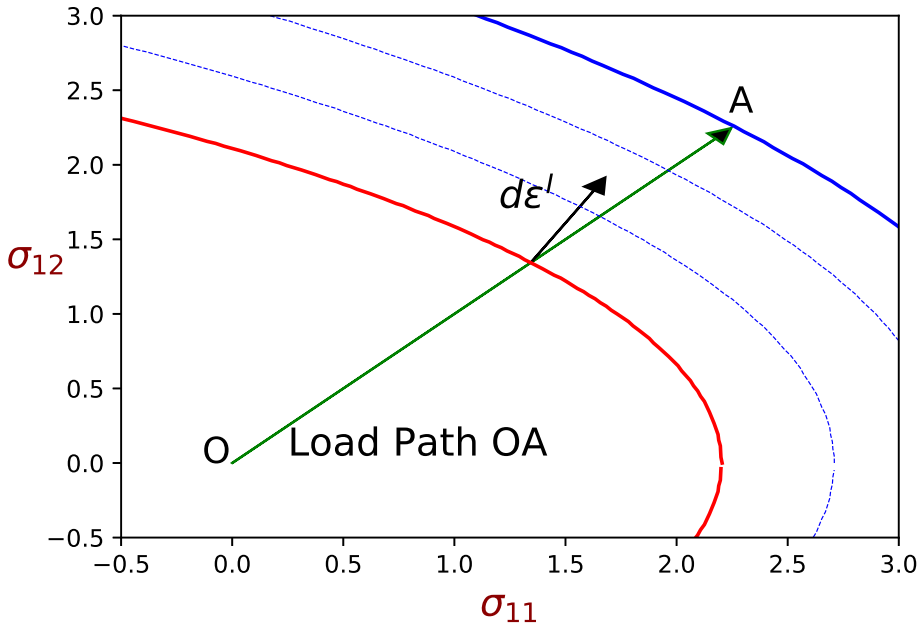

Figure 50: Proportional load path with initial, subsequent and final threshhold surfaces using isotropic H451. Stress in MPa.

The $\sigma_{11} - \epsilon_{11}$ stress-strain curves are presented in Figure 51 for this load path. The linear segment of the curve represents the elastic response of the material up to the virgin threshold surface (load segment OA). Loads beyond point A on the virgin threshold surface causes the material to harden isotropically and the tensile stress-strain curve becomes nonlinear. Figure 52 depicts the same trends in the $\sigma_{12} - \epsilon_{12}$ stress-strain curve.

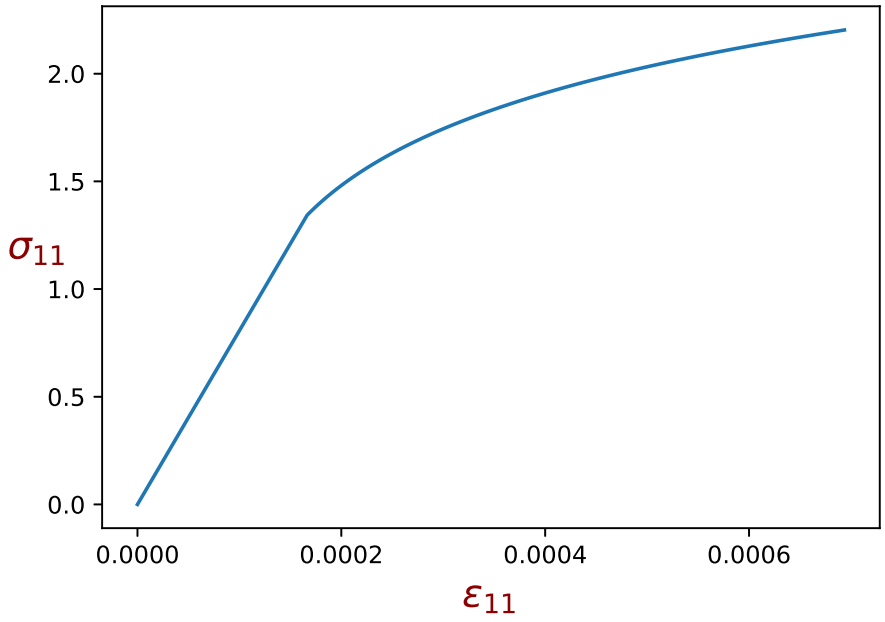

Figure 51: Tensile stress-strain curve for the proportional load path OA depicted in Figure 50 applied to isotropic H451 graphite. Stress in MPa.

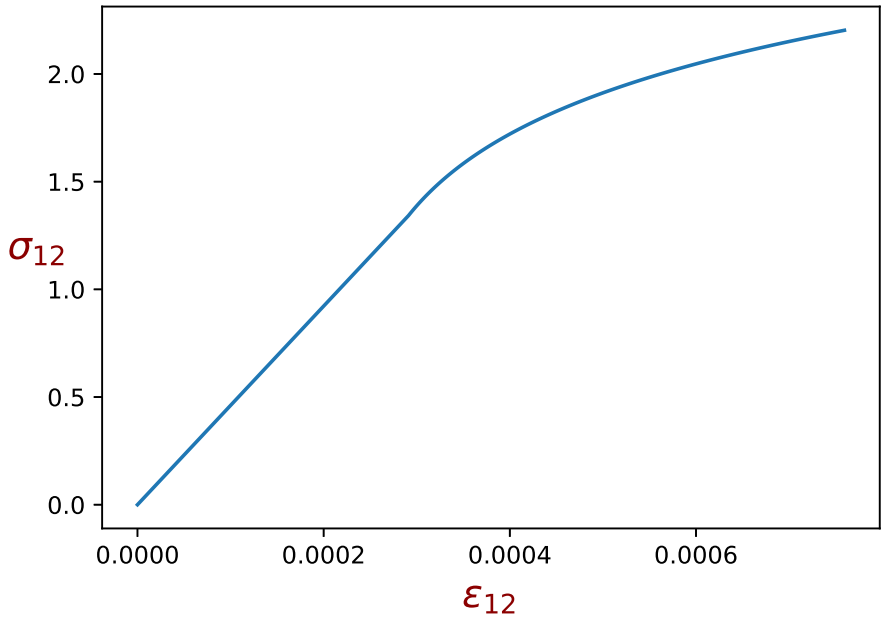

Figure 52: Torsional stress-strain curve for the proportional load path OA depicted in Figure 50 applied to isotropic H451 graphite. Stress in MPa.

The final stress state at the end of the load path is

$$\sigma_{ij} = \begin{bmatrix} 2.2 & 2.2 & 0 \\ 2.2 & 0 & 0 \\ 0 & 0 & 0 \end{bmatrix} \tag{5.15}$$

The corresponding final accumulated strains for this load path are

$$\epsilon_{ij} = \begin{bmatrix} 0.694 & 0.759 & 0 \\ 0.759 & -0.00762 & 0 \\ 0 & 0 & -0.0792 \end{bmatrix} \times 10^{-3} \tag{5.16}$$

As indicated in the discussion above the final strains are different than the strains accumulated along the non proportional load path.

5.6 The Inelastic Response of Anisotropic H451

The effect of combined shear and tensile total strains are examined in this section utilizing the material properties for anisotropic H451 graphite. Two load paths are examined. The first load path represents tensile and shear stresses applied sequentially. For the second load path these stresses are applied proportionally. Material properties for aniostropic H451 graphite can be found in Table IV. An assumed preferred material direction for both load paths is identified as $d_i = (0.707, 0.707, 0)$. These non-proportional and proportional load paths are identical to the load paths applied to isotropic H451 in an earlier section.

5.6.1 A Non-proportional Load Path - Anisotropic H451

Results for the elastic-inelastic load path representing a uniaxial stress (σ_{11}) followed by the application of a shear stress (σ_{12}), i.e., a non-proportional load path, are presented here. The load path is identical to the non-proportional load path applied to isotropic H451 presented in Section 5.5.3. The entire load path (OABCD) is identified in Figure 53. For this load

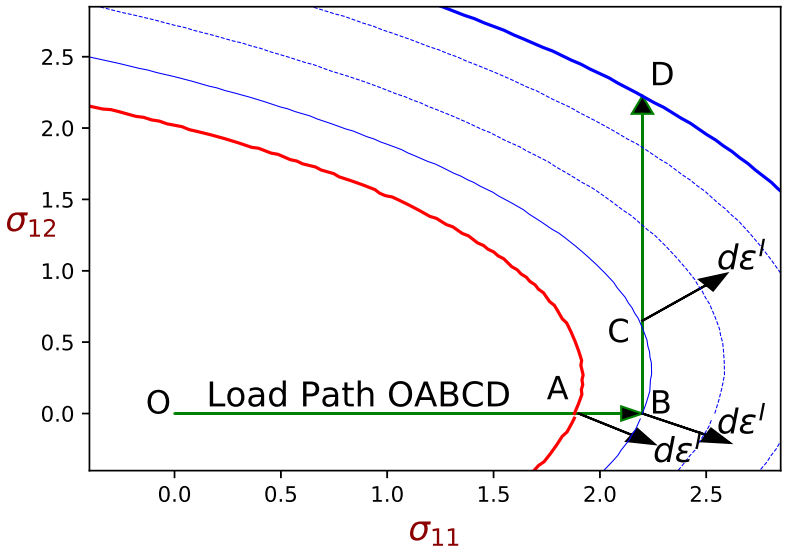

Figure 53: Non-proportional load path with initial, subsequent and final threshold surfaces for anisotropic H451 with a preferred material direction $d_i = (0.707, 0.707, 0)$. Stress in MPa.

path the preferred material direction is not aligned with the orientation of the uniaxial stress σ_{11}. This misalignment tends to rotate the threshold surface and subsequent surfaces in the counter clockwise direction (again, see Figure 53). The applied tensile stress associated with load segment OAB exceeds the inelastic threshold stress for anisotropic H451 at point A. Along load segment AB of the load path the material hardens isotropically. As a result of the rotated threshold surfaces (rotated counterclockwise relative to load segment OAB) negative inelastic shear strains are generated after the virgin threshold surface is attained.

At point B the tensile stress is held fixed at a value of 2.2 MPa and a shear stress is subsequently applied. This combined state of stress is applied along segment BCD. Along load segment BC the load path backs away from the current inelastic threshold surface and the material behaves elastically. At point C the material once again behaves inelastically. However, as indicated in Figure 53 the normality assumption rotates the increment in inelastic strain vector such that it the shear strain component of that vector changes sign at point C.

The normal component of the increment in inelastic strain vector remains positive

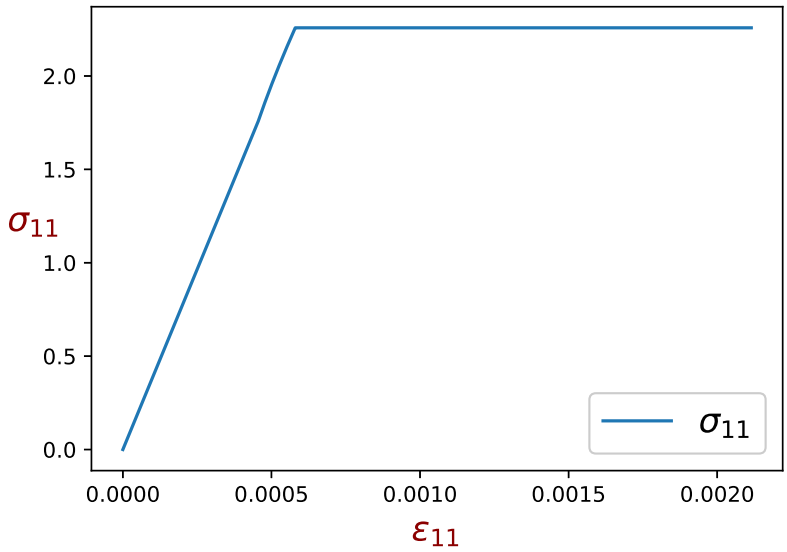

Figure 54: Tensile stress-strain curve for the non-proportional load path OABCD Figer 53 applied to anisotropic H451 with a preferred material direction $d_i = (0.707, 0.707, 0)$. Stress in MPa.

throughout the load path. Figure 54 shows that the tensile stress-strain curve is linear to point A on the load path and then becomes slightly non-linear until point B is attained on the load path. From point B onwards there is an increase in tensile strain without an increase in tensile stress along load segment BCD. This is captured in Figure 54 with the plateau region of the stress-strain curve

Predictions for the combined applied normal stress and shear stress segment of the load path for shear strain are complicated and need a bit of explanation. First due to the rotation of the preferred material direction the accumulation of shear strain under the application of a normal stress is due to to material anisotropy. As noted earlier when the load path transitions into the inelastic region we continue to expect a negative inelastic shear strain. As the load path changes direction at point B and shear stress is applied, the load path is elastic to point C. Therefore along load path BC the strains elastic. Along load segment CD the strains are again inelastic. From the normality condition these inelastic strains are expected to be positive. This is shown in Figure 55.

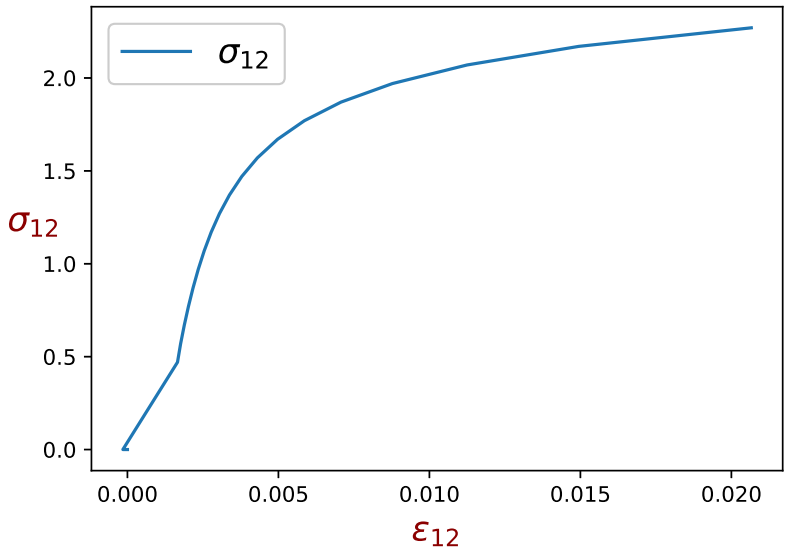

Figure 55: Shear stress-strain curve for the non-proportional load path OABCD in Figure 53 applied to anisotropic H451 with a preferred material direction $d_i = (0.707, 0.707, 0)$. Stress in MPa.

The final stress state is

$$\sigma_{ij} = \begin{bmatrix} 2.2 & 2.2 & 0 \\ 2.2 & 0 & 0 \\ 0 & 0 & 0 \end{bmatrix} \tag{5.17}$$

and the final accumulated strains are

$$\epsilon_{ij} = \begin{bmatrix} 21.5 & 20.6 & 0 \\ 20.6 & 2.4 & 0 \\ 0 & 0 & -0.80 \end{bmatrix} \times 10^{-3} \tag{5.18}$$

5.6.2 Proportional Loading - Anisotropic H451

Results for the elastic-inelastic load path representing the application of a uniaxial stress (σ_{11}) and a shear stress (σ_{12}) in 1:1 proportion are presented here. The load path is identical to the proportional load path applied to isotropic H451 presented in Section 5.5.4. The entire load path (OAB) is identified in Figure 56. For this load path the preferred material direction is not aligned with the orientation of the uniaxial stress σ_{11} since

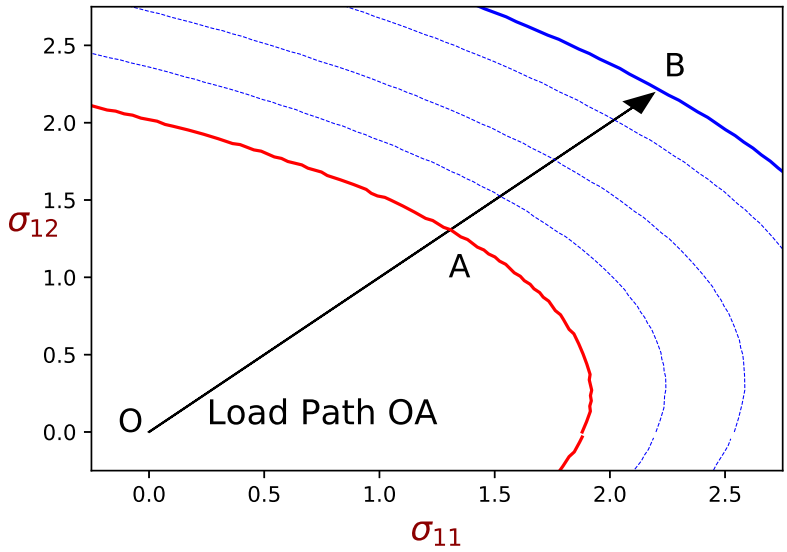

Figure 56: Proportional load path with initial, subsequent, and final threshold surfaces for anisotropic H451 graphite with a preferred material direction $d_i = (0.707, 0.707, 0)$. Stress in MPa.

$d_i = (0.707, 0.707, 0)$. This misalignment again rotates the threshold surface and subsequent surfaces in the counter clockwise direction (again, see Figure 56). The applied proportional stress associated with load segment OAB exceeds the inelastic threshold stress for anisotropic H451 at point A. Along load segment AB of the load path the material hardens isotropically. For this load path both the tensile and shear strain components of the increment in inelastic strain vector are positive. This is easily seen as a result of the normality condition in Figure 56.

The $\sigma_{11} - \epsilon_{11}$ stress-strain curves are presented in Figure 57 for this load path. The linear segment of the curve represents the elastic response of the material up to the virgin threshold surface (load segment OA). Loads beyond point A on the virgin threshold surface causes the material to harden isotropically and the tensile stress-strain curve becomes nonlinear. Figure 58 depicts the same trends in the $\sigma_{12} - \epsilon_{12}$ stress-strain curve.

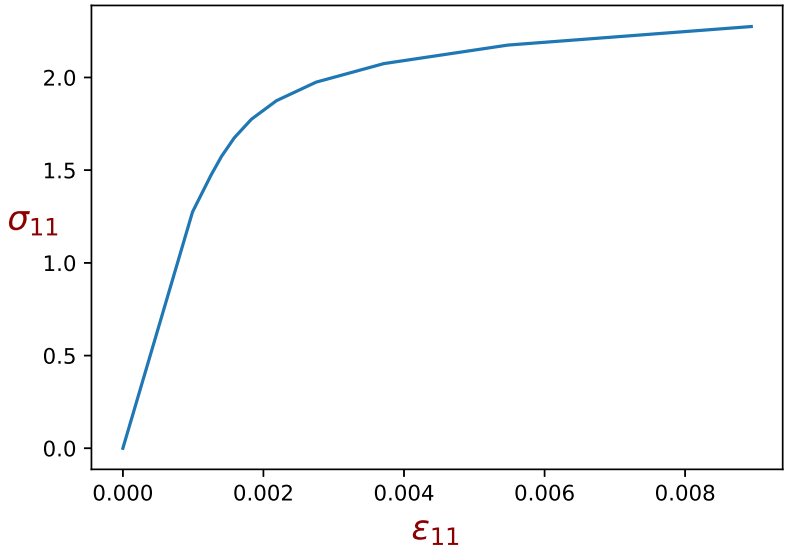

Figure 57: Tensile stress-strain for the proportional load path OAB, Figure 56 applied to anisotropic H451 with a preferred material direction $d_i = (0.707, 0.707, 0)$. Stress in MPa.

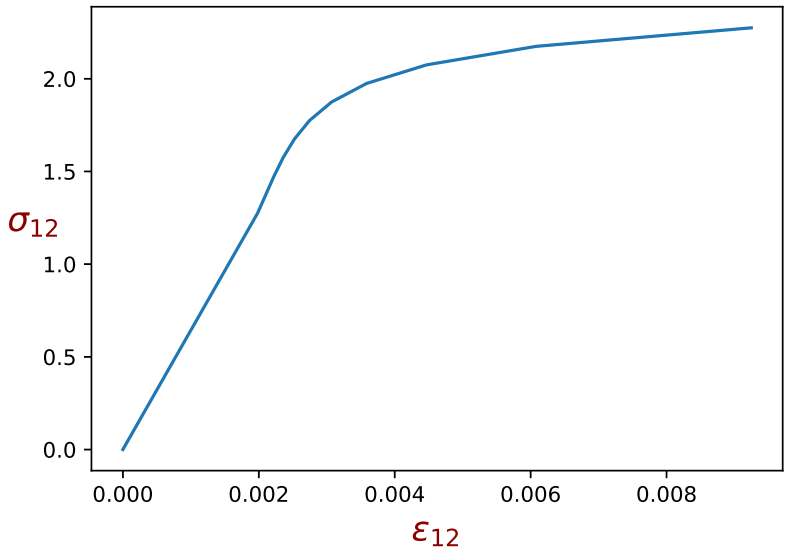

Figure 58: Shear stress-strain curve for the proportional load path OAB Figure 56 applied to anisotropic H451 with a preferred material direction $d_i = (0.707, 0.707, 0)$. Stress in MPa.

The final stress state is

$$\sigma_{ij} = \begin{bmatrix} 2.2 & 2.2 & 0 \\ 2.2 & 0 & 0 \\ 0 & 0 & 0 \end{bmatrix} \tag{5.19}$$

and the final accumulated strains are

$$\epsilon_{ij} = \begin{bmatrix} 8.94 & 9.25 & 0 \\ 9.25 & 1.32 & 0 \\ 0 & 0 & -0.364 \end{bmatrix} \times 10^{-3} \tag{5.20}$$

When compared to the final strain state for the non-proportional load path applied to anisotropic H451 the final strains are different for identical final stress states. Clear indication that the model captures path dependence.

CHAPTER VI

Conclusion and Future Work

This effort represents a multi-axial inelastic constitutive theory for isotropic and anisotropic nuclear grade graphite. The complete theory is derived from an inelastic threshold potential function. The potential nature is exhibited in the manner by which the flow and evolutionary laws are derived. The potential-normality structure of the theory dictates the direction of the increment in inelastic strain vector for each point is directed normal to the threshold surface. Thus the structure of the inelastic constitutive theory is tied to the concepts of potential functions and normality.

Tensorial invariant theory served as the primary structure in the development, where an integrity basis was derived for the anisotropic formulation. This structure reduces to the isotropic formulation under suitable choices of threshold stress values. A subset of the basis was adopted. Using the invariants that composed the basis insured that the inelastic threshold stress is form invariant.

Projections of equal to a constant value representing states of inelasticity illustrated the transversely isotropic nature of anisotropic graphite. Theoretical predictions of an isotropically hardening threshold surface homogeneously stressed and strained elements were presented and discussed. Predictions were generated that compared favorably to available data sets. The predictions demonstrates the model's ability to capture real world behavior as well as the flexibility in capturing the non-linear, inelastic behavior of transversely

isotropic nuclear graphite.

In the development of the theory the dependence of the scalar function was restricted such that members of the integrity basis are linear or quadratic in stress. In the adopted form of the polynomial, the linear members of the integrity basis were then multiplied by the first invariant to generate a polynomial quadratic in stress. Rational forms for the function, i..e., division by invariants, could have been adopted. However this leads to the possibility of singularities if a particular invariant became zero.

For simplicity the theory was developed assuming isotropic hardening. In the future the model should be extended to accommodate kinematic hardening. Finally, attention should be given to extending the concepts presented here to capture phenomenon such as creep, relaxation, recovery, as well as strain rate sensitivity. This can be accomplished by adopting concepts originally proposed by Duffy (1987) and Robinson (1978).

In addition, we recommend running multiaxial tests of the various grades of graphite. These tests should be used to verify the model presented in this work. Specifically, we would prefer that the tension-torsion test presented here be run. Then incorporating this model into a finite elemental analysis program would be the next step.

CHAPTER VII

REFERENCES

Bodner, S.R. and Partom, Y. 1975 "Consitutive Equatinos Elastic-Viscoplastic Strain-Hardening Materials", ASME Journal of applied Mechanics **42**

Burchell, Tim, Yahr, Terry, and Battiste, Rick, 2007 "Modeling the Multiaxial Strength of H-451 Nuclear Grade Graphite," Carbon, **45**, pp. 2570-2583

Bratton, R., private communication

Chaboche, J.L., 1977 "Viscoplastic Constitutive Equations for the Description of Cyclic and Anisotropic Behavior of Metals", Bulletin de L'Academie des Science, Serie des Science Techniques, **25**(1)

Chen, W.F. and Han, D.J., 1995 *Plasticity for Structural Engineers*, Gau Lih Book Co. Ltd., Taipei, Taiwan

Chow, C.L. and Yang, F., 1991 "On One-Parameter Description of Damage State for Brittle Material," Engineering Fracture Mechanics, **40**(2), pp.335-343

U.S.DOE Nuclear Energy Research Advisory Committee and the Generation IV International Forum, 2002 "A Technology Roadmap for Generation IV Nuclear Energy Systems," GIF-002-00, December

Duffy, S.F. 1987, "A Viscoplastic Constitutive Theory for Transversely Isotropic Metal Alloys," Ph.D. Dissertation, University of Akron

Eason, ED, Hall, GN, Marsden, BJ, and Heys, GB, 2008 "Development of a Young's Modulus Model for Gilsocarbon Graphites Irradiated in Inert Enviroments," Journal of Nuclear Materials, **381**, pp. 145-151

Green, A.E. and Mkrtichian, J.Z., 1977 "Elastic Solids with Different Moduli in Tension and Compression," Journal of Elasticity, **7**(4), pp. 369-386

Greenstreet, W.L., Smith, J.E., Yahr, G.T., and Valachovic, R.S., 1970 "The Mechanical Behavior of Artificial Graphites as Portrayed by Uniaxial Tests," Carbon **8**, pp.649-665

Hsieh, S.S., Ting, E.C., Chen, W.F., 1979 "An Elastic-Fracture Model for Concrete," Procedings $3^r d$ Engineering Mechanics Division Specialists Conference, Austin, TX, pp. 437–440.

James, Christopher, 2011 "An Isotropic Bi-Modulus Constitutive Model for Nuclear Grade Graphite," Procedings American Nuclear Society 2011 Anual Meeting, Hollywood, FL

Janosik, L.A. 1990, "A Viscoplastic Theory for Monolithic Ceramics," Master Thesis, Cleveland State University

Jones, R.M. and Nelson, A.R., 1976 "Material Models for Nonlinear Deformation of Graphite," AIAA Journal **14**(6) pp. 709-717

Lehknitskii, S.G., 1963 *Theory of Elasticity of an Anisotropic Elastic Body*, transalted by P. Fern, Holden-Day Inc., San Francisco

Mendelsohn 1968,

Moore, S.E., 1969, "An Anisotropic Elastic-Plastic Stress Analysis of a Thick-Walled Graphite Cylinder," Master Thesis, The University of Tennessee

Rivlin, R.S. and Smith, G.F., 1969 Orthogonal Intergrity Basis for N Symmetric Matrices, *Contributions to Mechanics*, ed. D. Abir, Pergamon Press, Oxford

Robinson, D.N., 1978 "A Unified Creep-Plasticity Model for Structural Metals at High Temperature", ORNL/TM 5986

Ottosen, N.S., 1977 "A Failure Criterion for Concrete," Journal Engineering Mechanics Division ASCE, **103**(EM4), pp. 527–535.

Saito, Shinzo, 2010 "Role of Nuclear Energy to a Future Society of Shortage of Energy Resources and Global Warming," Journal of Nuclear Materials **398**, pp 1-9

Seldin, E.J., 1966 "Stress-Strain Properties of Polycrystalline Graphites in Tension and Compression at Room Temperature," Carbon **4** pp.177-191

Southward, F.H., et. al., 2004 "Next Generation Nuclear Plant (NGNP) Project - Preliminary Assessment of Two Possible Designs," 14th Pacific Basin Nuclear Conference, March 21-25, 2004, Honolulu, Hawaii

Spencer, A.J.M., 1971 Theory of Invariants, *Contimuum Physics*, **1**, ed. A.C. Eringen, Academic Press, London

Tabeddor, F. 1979 A Survey of Constitutive Educations of Bimodulus Elastic Materials, B. F. Goodrich Company, Akron, Ohio

Tsai, S.W. and Wu, E., 1971 "A General Theory of Strength of Anisotropic Materials," Journal of Compostie Materials, **5** pp. 58-80

Vijavakumar, K. and Ashoka, J.G. 1990 "A Bilinear Constitutive Model for Isotropic Bimodulus Materials," Transactions of the ASME,**372** pp. 112

Vijayakumar, K. and Rao, K.P., 1987 "Stress-Strain relations fo Composites with Different Stiffness in Tension and Compression," Computational Mechanics, **2**, pp. 167-175

Weng, Tu-Lung, 1969, “Biaxial Fractures Strength and Mechanical Properties of Graphite-Base Refractory Composites,” AIAA Journal, **7**(5), pp. 850-858

Willam, K.J. and Warnke, E.P., 1974 “Constitutive Models for the Triaxial Behavior of Concrete,” Int. Assoc Bridge Struct. Proc, **19**, pp. 1-30

APPENDIX

Invariant I_9 Equivalence Proof

Here the original I_9 invariant will be manipulated to show that the updated version is equivalent. Starting with the original definition for I_9.

$$\begin{aligned} I_9 &= a_i a_j d_j d_k \sigma_{km} \sigma_{mi} \\ &= \frac{1}{2}(a_i a_j d_j d_k \sigma_{km} \sigma_{mi} + a_i a_j d_j d_k \sigma_{km} \sigma_{mi}) \\ &= \frac{1}{2}(a_i a_j d_j d_k \sigma_{km} \sigma_{mi} + a_b a_j d_j d_c \sigma_{km} \sigma_{mi} \delta_{bi} \delta_{ck}) \end{aligned} \tag{1}$$

The last step above change the index from a_i to a_b by adding the δ_{bi} term and also changed the d_k index to d_c by including the δ_{ck} term. The next set of steps are changing the indexes on the right portion of the I_9 invariant.

$$\begin{aligned} I_9 &= \frac{1}{2}(a_i a_j d_j d_k \sigma_{km} \sigma_{mi} + a_b a_j d_j d_c \sigma_{km} \sigma_{mi} \delta_{bi} \delta_{ck}) \\ &= \frac{1}{2}(a_i a_j d_j d_k \sigma_{km} \sigma_{mi} + a_b a_j d_j d_c \sigma_{em} \sigma_{mi} \delta_{bi} \delta_{ce}) \\ &= \frac{1}{2}(a_i a_j d_j d_k \sigma_{km} \sigma_{mi} + a_k a_j d_j d_c \sigma_{em} \sigma_{mi} \delta_{ki} \delta_{ce}) \\ &= \frac{1}{2}(a_i a_j d_j d_k \sigma_{km} \sigma_{mi} + a_k a_j d_j d_c \sigma_{em} \sigma_{mf} \delta_{kf} \delta_{ce}) \\ &= \frac{1}{2}(a_i a_j d_j d_k \sigma_{km} \sigma_{mi} + a_k a_j d_j d_i \sigma_{em} \sigma_{mf} \delta_{kf} \delta_{ie}) \end{aligned} \tag{2}$$

Finally the indexes will be contracted by removing the Kronecker deltas.

$$\begin{aligned} I_9 &= \frac{1}{2}(a_i a_j d_j d_k \sigma_{km} \sigma_{mi} + a_k a_j d_j d_i \sigma_{im} \sigma_{mf} \delta_{kf}) \\ &= \frac{1}{2}(a_i a_j d_j d_k \sigma_{km} \sigma_{mi} + a_k a_j d_j d_i \sigma_{im} \sigma_{mk}) \\ &= \frac{1}{2}(a_i a_j d_j d_k \sigma_{km} \sigma_{mi} + a_k a_j d_j d_i \sigma_{km} \sigma_{mi}) \end{aligned} \tag{3}$$

Tensile stress-strain data

Table V.: Tensile Stress (MPa) and Strain Data for various Graphites. Bratton (2009)

2114		AGOT		G110		H451	
Stress	Strain	Stress	Strain	Stress	Strain	Stress	Strain
0.691576069	1.40625E-05	0.03211	0	0.39834	0.00002746	0.18505	0.000010929
1.296705172	7.03126E-05	0.1124	4.63321E-06	0.85358	9.61098E-05	0.40694	3.82513E-05
2.247622552	0.00016	0.20874	1.38996E-05	1.30882	0.00015	0.66586	6.55738E-05
2.766304828	0.00021	0.28902	2.08494E-05	1.82097	0.00021	0.99865	0.00011
3.284987241	0.00027	0.35325	2.54826E-05	2.33311	0.00027	1.33151	0.00015
4.063010138	0.00034	0.43353	0.000034749	2.95907	0.00036	1.66431	0.00019
4.408799586	0.00037	0.56199	4.63321E-05	3.86956	0.00048	2.034	0.00025
4.841034138	0.00044	0.75467	6.25483E-05	4.72313	0.00058	2.44073	0.0003
6.224185931	0.0006	0.89918	8.10811E-05	5.4629	0.00069	2.88444	0.00036
7.693784483	0.0008	1.10792	9.72973E-05	6.03195	0.00076	3.36524	0.00042
9.509173793	0.00103	1.26848	0.00012	6.71482	0.00084	3.73494	0.00047
11.1516669	0.00127	1.50934	0.00014	7.51149	0.00093	4.21568	0.00053

Tensile Stress (MPa) and Strain Data for various Graphites. Bratton (2009) Continued

2114		AGOT		G110		H451	
Stress	Strain	Stress	Strain	Stress	Strain	Stress	Strain
12.18903048	0.0014	1.73413	0.00016	8.08054	0.00103	4.65931	0.0006
12.79416083	0.00149	2.03921	0.00019	8.64959	0.00111	5.10302	0.00066
13.65862993	0.00162	2.21583	0.00021	9.33246	0.00121	5.58369	0.00072
14.52310076	0.00174	2.47274	0.00023	9.8446	0.00129	5.99035	0.00078
15.30112476	0.00185	2.69754	0.00025	10.64128	0.00139	6.35998	0.00084
16.07914703	0.00196	2.93839	0.00028	11.21033	0.00147	6.84059	0.00091
17.37585366	0.00216	3.21135	0.0003	11.77938	0.00157	7.32119	0.00098
18.84545559	0.00237	3.42009	0.00033	12.51915	0.00168	7.76469	0.00106
20.22860655	0.00258	3.61277	0.00035	13.14511	0.0018	8.31916	0.00115
21.26597014	0.00274	3.80545	0.00037	13.65725	0.00187	8.68873	0.00121
22.3897831	0.00291	3.96602	0.00038	14.22631	0.00195	9.09526	0.00128
23.340694	0.00307	4.12659	0.0004	14.79536	0.00207	9.53883	0.00136
24.20516903	0.00321	4.39955	0.00043	15.47822	0.00218	9.94535	0.00143
24.98319131	0.00335	4.57618	0.00045	16.04727	0.00228	10.38885	0.0015
25.93410731	0.00349	4.7528	0.00047	16.67323	0.00239	10.72151	0.00156
26.97147931	0.00367	4.91337	0.00049	17.24228	0.00249	11.12797	0.00163

Tensile Stress (MPa) and Strain Data for various Graphites. Bratton (2009) Continued

2114		AGOT		G110		H451	
Stress	Strain	Stress	Strain	Stress	Strain	Stress	Strain
27.66304552	0.00379	5.08999	0.00051	17.86824	0.00259	11.4976	0.00169
28.35462014	0.0039	5.28268	0.00054	18.4942	0.0027	11.8302	0.00175
29.39198883	0.00409	5.55564	0.00057	18.89253	0.00279	12.23666	0.00183
		5.84466	0.0006	19.5754	0.00288	12.64306	0.00191
		6.08551	0.00064	20.31516	0.00299	13.01255	0.00198
		6.35848	0.00067	20.88422	0.00309	13.34507	0.00205
		6.6475	0.00071	21.73779	0.00324	13.56675	0.00209
		6.8723	0.00074	22.53447	0.00336	13.82534	0.00215
		7.08103	0.00077	23.16043	0.00349	14.12076	0.00222
		7.33794	0.0008	23.90019	0.00361	14.49012	0.0023
		7.61091	0.00084	24.35544	0.00368	14.82264	0.00237
		7.86782	0.00088	24.92449	0.00379	15.11799	0.00244
		8.15684	0.00092	25.32282	0.00386	15.33954	0.0025
		8.4298	0.00096	25.83497	0.00397	15.56102	0.00256
		8.68671	0.001	26.34712	0.00408	15.85624	0.00264

Tensile Stress (MPa) and Strain Data for various Graphites. Bratton (2009) Continued

2114		AGOT		G110		H451	
Stress	Strain	Stress	Strain	Stress	Strain	Stress	Strain
		8.92756	0.00103	26.80236	0.00419	16.15145	0.00273
		9.18447	0.00107	27.2007	0.00426		
		9.48955	0.00112	27.48522	0.00432		
		9.7304	0.00116	28.11118	0.00446		
		9.9552	0.0012	28.39571	0.00453		
		10.13182	0.00124	29.42	0.00476		
		10.29239	0.00127				
		10.46901	0.00132				
		10.67775	0.00137				
		10.8062	0.00143				
		10.87043	0.00146				

Compressive stress-strain data

Table VI.: Compressive Stress (MPa) and Strain Data for various Graphites. Bratton (2009)

2114		AGOT		G110		H451	
Stress	Strain	Stress	Strain	Stress	Strain	Stress	Strain
-0.674892069	-4.14013E-05	-0.31341	-3.04679E-05	-0.54383	0	-55.20001	-0.02097
-2.02467669	-0.00014	-1.0447	-9.14037E-05	-1.81275	-0.00014	-54.65454	-0.02053
-3.711907724	-0.00023	-2.08939	-0.00021	-4.16933	-0.00041	-53.67272	-0.01961
-5.736581103	-0.00029	-3.86538	-0.0004	-6.34464	-0.00069	-52.25453	-0.01852
-9.111042759	-0.00041	-5.43242	-0.00055	-7.97612	-0.00083	-51.05453	-0.0177
-11.13571945	-0.0005	-7.10394	-0.0007	-9.97015	-0.0011	-49.52727	-0.01672
-13.83528503	-0.0006	-8.87992	-0.00094	-11.60163	-0.00124	-48	-0.01575
-16.87230097	-0.00075	-10.76038	-0.00122	-13.95821	-0.00172	-46.36364	-0.01477
-20.58420497	-0.00091	-12.53636	-0.00149	-16.49606	-0.002	-45.16364	-0.01406
-23.9586611	-0.00108	-13.89447	-0.00174	-18.67137	-0.00234	-43.09091	-0.01303
-28.00801455	-0.0013	-15.35705	-0.00204	-20.6654	-0.00276	-41.12728	-0.012
-30.37013738	-0.00147	-17.34197	-0.00244	-22.8407	-0.00303	-39.27273	-0.01096

Compressive Stress (MPa) and Strain Data for various Graphites. Bratton (2009) Continued

2114		AGOT		G110		H451	
Stress	Strain	Stress	Strain	Stress	Strain	Stress	Strain
-33.40715586	-0.00164	-19.11795	-0.00289	-25.01601	-0.00345	-37.20002	-0.00998
-38.13139483	-0.00199	-21.31182	-0.00344	-27.37259	-0.00379	-35.23637	-0.00906
-43.53052938	-0.00238	-22.66992	-0.0039	-29.18534	-0.00414	-32.83637	-0.00803
-45.55520945	-0.00255	-24.23697	-0.00451	-31.17937	-0.00455	-31.30909	-0.00738
-48.92967069	-0.00284	-25.38614	-0.005	-33.53595	-0.0049	-29.45455	-0.00656
-53.31646352	-0.00319	-26.43083	-0.00555	-35.71126	-0.00531	-27.38183	-0.00586
-56.01603248	-0.00344	-27.37106	-0.00615	-37.52401	-0.00572	-25.3091	-0.00515
-59.053024	-0.00373	-28.6247	-0.00692	-39.88059	-0.00614	-23.56364	-0.00455
-62.76494476	-0.00412	-29.46045	-0.00759	-41.87462	-0.00648	-20.83636	-0.00379
-65.80195986	-0.00449	-30.08727	-0.00826	-44.04993	-0.0069	-18.54545	-0.0032
-69.17642103	-0.00489	-30.81856	-0.0089	-45.50013	-0.00738	-16.58182	-0.00276
-71.20109103	-0.00518	-31.34091	-0.00941	-46.76906	-0.00766	-12.76364	-0.00195
-73.90066676	-0.00555	-31.75879	-0.00996	-47.85672	-0.00793	-10.03636	-0.00146
-76.93769531	-0.00604	-32.17667	-0.01048	-49.48819	-0.00834	-8.07273	-0.00108
-79.97471041	-0.00654	-32.49007	-0.011	-51.11967	-0.00869	-6.32727	-0.00087

Compressive Stress (MPa) and Strain Data for various Graphites. Bratton (2009) Continued

2114		AGOT		G110		H451	
Stress	Strain	Stress	Strain	Stress	Strain	Stress	Strain
-81.99938041	-0.00689	-32.80348	-0.01164	-53.29497	-0.00931	-4.25455	-0.00054
-84.36149648	-0.00739	-33.01242	-0.01222	-55.83283	-0.01014	-2.50909	-0.00027
-85.71128772	-0.00768	-33.01242	-0.01264	-58.00813	-0.01069	-0.21818	1.97986E-07
-87.39851159	-0.00803	-33.11689	-0.01295	-59.45834	-0.01124		
-88.74830283	-0.00836			-61.27109	-0.01179		
-90.43550648	-0.00876			-63.26512	-0.01248		
-91.78531117	-0.00911			-64.35278	-0.0129		
-92.46018317	-0.00929			-65.80298	-0.01331		
				-67.61573	-0.014		
				-68.88466	-0.01462		
				-70.69741	-0.01545		
				-72.14761	-0.01607		
				-73.23527	-0.01662		
				-74.5042	-0.01717		
				-75.41058	-0.01779		

Compressive Stress (MPa) and Strain Data for various Graphites. Bratton (2009) Continued

2114		AGOT		G110		H451	
Stress	Strain	Stress	Strain	Stress	Strain	Stress	Strain
				-76.49823	-0.01834		
				-77.58588	-0.01903		
				-78.8548	-0.01972		
				-79.94246	-0.02034		
				-80.66756	-0.0209		
				-81.57394	-0.02145		
				-82.48032	-0.02207		
				-83.02414	-0.02262		
				-83.56797	-0.02317		
				-84.11179	-0.02372		
				-85.01817	-0.02455		
				-85.562	-0.02524		
				-86.28709	-0.02593		
				-86.64965	-0.02648		
				-87.0122	-0.02697		